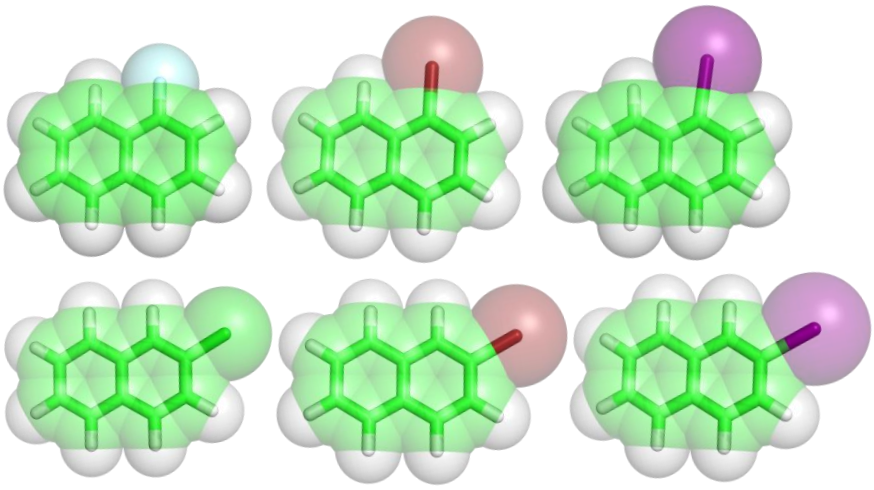

Thermodynamic Properties of Mono-Halogenated Naphthalenes

Filipe Miguel da Silva Ribeiro
MSc in Chemistry
Departamento de Química e Bioquímica
2013

Supervisors
Luís Manuel das Neves Belchior Faia dos Santos,
Associate Professor,
Faculdade de Ciências da Universidade do Porto

Manuel João dos Santos Monte,
Associate Professor,
Faculdade de Ciências da Universidade do Porto

U.PORTO

FACULDADE DE CIÊNCIAS
UNIVERSIDADE DO PORTO

Todas as correções determinadas pelo júri, e só essas, foram efetuadas.
O Presidente do Júri,

Porto, _____/_____/_____

Abstract

Vapor pressures of the condensed phases of 1-fluoronaphthalene, 1-bromonaphthalene, 1-iodonaphthalene, 2-chloronaphthalene, 2-bromonaphthalene and 2-iodonaphthalene, were measured by means of a static apparatus based on a MKS diaphragm capacitance manometer.

Based on the obtained results, the standard molar enthalpies, entropies and Gibbs energies of sublimation and vaporization, at T = 298.15 K, were derived, as well as, the phase diagram in the working (p,T) range.

A reasonable good correlation between the thermodynamic properties derived from the vapor–liquid and vapor-crystal data, and the size of the halogen atom was found.

The heat capacity, $C^0_{p,\mathrm{m}}$, and absolute entropy, S^0_{m}, on the gaseous phase, were estimated by statistical thermodynamics using the vibrational frequencies derived from quantum chemical (QC) calculations. A new Excel worksheet “ETHERMO.xls” for the calculation, by statistical thermodynamics, of the ideal gas, heat capacities and absolute entropies was developed, tested and used in this work. A comparative analysis of the different QC functionals, basis sets and computational methodologies was carried out. The homodesmic methodology applied to the statistical thermodynamics calculation, was found to be more efficient in the error cancelation than the one which uses corrective scaling factors in the vibrational frequencies. The computational study was extended to a comparative and differential analysis of the ideal gas properties between the studied compounds, considering the (1 and 2 position) isomerization effect and the nature of the halogen substituent.

Resumo

Neste trabalho, o método estático foi utilizado para medir pressões de vapor das fases condensadas dos seguintes compostos: 1-fluoronaftaleno; 1-bromonaftaleno; 1-iodonaftaleno; 2-cloronaftaleno; 2- bromonaftaleno; 2-iodonaftaleno.

Com base nos resultados obtidos, as entalpias, entropias e energias de Gibbs molares de sublimação e vaporização padrão, a T = 298.15 K, foram derivadas e os diagramas de fase (p,T) no intervalo de temperatura em estudo foram interpretados.

Foi encontrada uma boa correlação entre as propriedades termodinâmicas derivadas dos resultados obtidos e o tamanho do átomo de halogéneo.

A capacidade calorífica e a entropia absoluta da fase gasosa foram estimadas por meios de termodinâmica estatística, utilizando as frequências vibracionais derivadas de cálculos quânticos (CQ). Um novo ficheiro Excel "ETHERMO.xls" foi desenvolvido, testado e utilizado no cálculo das capacidades caloríficas e entropias absolutas do estado gasoso dos compostos estudados. Uma análise comparativa dos diferentes funcionais e diferentes conjuntos de bases foi explorada em detalhe. A metodologia homodésmica foi aplicada aos cálculos de termodinâmica estatística, e provou ser mais eficaz no cancelamento de erros do que a correcção das frequências vibracionais usando apenas “scaling factors”. O estudo computacional foi estendido de forma a fazer uma análise comparativa e diferencial das propriedades termodinâmicas dos compostos estudados em fase gasosa, em que foi explorada: a posição e a natureza do halogéneo substituído.

Acknowledgments

Começo por agradecer aos meus orientadores, Professor Luís Belchior Santos e Professor Manuel João Monte, pelo apoio, conhecimentos transmitidos, compreensão, confiança e paciência, durante todo o ano. Obrigado em especial, pela independência, autonomias de trabalho e dedicação que me mostraram durante este ano.

Também quero agradecer ao Professor André Melo, um dos melhores professores que tive na faculdade e que merece este meu agradecimento. Obrigado em especial, pelo apoio prestado na parte computacional e pelo incentivo transmitido ao longo destes anos.

Agora, um agradecimento especial a uma das pessoas que mais me marcou neste último ano e que ajudou a despertar a minha curiosidade por novas áreas da Química Física, a Marisa Rocha é um exemplo a seguir, e uma das pessoas mais aplicadas e motivadas que conheço. Sem ti, o percurso durante este ano de Tese não teria sido o mesmo. Obrigado Marisa pela amizade, apoio, sinceridade, sentido de humor, força, motivação e conhecimentos com que me presenteaste durante este curto ano.

Um agradecimento também à Rita Figueira, outra das pessoas que me apoiou este ano. Obrigado pela ajuda na integração no grupo, força, compreensão e ensinamentos.

Agradeço também a todos os meus amigos Químicos, e em especial à Isabel Barbosa, Ana Gomes, Cláudia Alves, Luís Fernandes, Carlos Figueiredo, Paul Costa, Paulo Serra, Tânia Oliveira, Diana Crista, Paulo Ferreira, Diana Pereira, Daniela Santos, Jorge Vigário, Ricardo Taveira, Rui Ferreira, Ana Rodrigues (Nana), Ana Lobo (Lobinho), Inês Vaz, Carlos Lima e Zé Carlos pelo apoio e amizade que demonstraram para comigo. Muito Obrigado Pessoal.

Agradeço a todo o Grupo de Química Física pela ajuda e apoio prestado.

Aos meus familiares, em especial aos meus pais, António e Aldevina, e aos meus irmãos Pedro e Diogo, por todo o apoio, amor, compreensão e paciência. Sem vocês não estaria aqui hoje e não seria quem sou. Obrigado.

Por fim, quero deixar um último agradecimento muito especial a uma das pessoas que mais me marcou na minha vida, o meu falecido avô António. Um grande Homem que partiu demasiado cedo. Espero, sinceramente, um dia ser como tu. Obrigado por tudo o que me ensinaste.

A ti dedico esta Tese.

Contents

Abstract III

Resumo IV

Acknowledgments V

Contents VII

List of Tables XI

List of Figures XV

Abbreviations XIX

Chapter 1. Introduction

1.1. State of art 3

1.1.1. Persistent Organic Pollutants 3

1.1.1.1. Introduction 3

1.1.1.2. Sources of POPs and their persistence in the environment 7

1.1.1.3. Physical chemical properties 7

Vapor pressure 8

Solubility 9

Influence of halogen atoms 9

1.1.1.4. Future challenges in POPs research 11

1.2. General introduction 12

1.2.1. Aim of the work 12

1.2.2. Nomenclature, constants, conversion factors, units and dimensions 14

References 17

Chapter 2. Studied Compounds

2.1. Studied compounds and literature data 21

2.1.1. 1-Halogenated naphthalenes 22

2.1.2. 2-Halogenated naphthalenes 25

2.2. Characterization of the compounds 28

2.2.1. Gas-Liquid chromatography 28

2.2.2. Fourier Transform Infrared spectroscopy 29

References 35

Chapter 3. Vapor Pressure Measurements

3.1. Introduction 39

3.1.1. Concepts 39

3.1.2. Vapor pressure equations 42

3.1.2.1. Clapeyron equation 42

3.1.2.2. Clausius-Clapeyron equation 44

3.1.2.3. Clarke-Glew equation 46

3.1.3. Thermodynamic properties calculations at T = 298.15 K 48

3.1.4. The arc method 51

3.2. The experimental set-up 52

3.2.1. The diaphragm capacitance manometers 54

3.2.2. Tubing 56

3.2.3. Sample cell 59

3.2.4. Vacuum system 60

3.2.5. Temperature control 61

3.2.6. Data acquisition and control 62

3.3. Experimental procedure 63

3.4. Experimental results 65

3.4.1. Results of 1-halogenated naphthalenes 65

3.4.1.1. Results for 1-fluoronaphthalene 65

3.4.1.2. Results for 1-bromonaphthalene 67

3.4.1.3. Results for 1-iodonaphthalene 69

3.4.2. Results of 2-halogenated naphthalenes 72

3.4.2.1. Results for 2-chloronaphthalene 72

3.4.2.2. Results for 2-bromonaphthalene 74

3.4.2.3. Results for 2-iodonaphthalene 76

References 81

Chapter 4. Statistical Thermodynamics

4.1. Quantum chemical calculations 85

4.1.1. Methods – particularities, advantages and disadvantages 86

4.1.2. Basis functions/functionals 87

4.1.3. Basis sets 87

4.2. Statistical Thermodynamics 89

Contributions from translation motion 91

Contributions from electronic motion 93

Contributions from rotational motion 94

Contributions from vibrational motion 97

4.2.1. Summary 101

4.3. Geometry optimization and vibrational frequency calculations 102

4.4. The isodesmic reactions 103

4.5. Computational Results 106

4.5.1. Results of 1-halogenated naphthalenes 106

4.5.1.1. Results for 1-fluoronaphthalene 106

4.5.1.2. Results for 1-chloronaphthalene 108

4.5.1.3. Results for 1-bromonaphthalene 110

4.5.1.4. Results for 1-iodonaphthalene 112

4.5.2. Results of 2-halogenated naphthalenes 114

4.5.2.1. Results for 2-fluoronaphthalene 114

4.5.2.2. Results for 2-chloronaphthalene 116

4.5.2.3. Results for 2-bromonaphthalene 118

4.5.2.4. Results for 2-iodonaphthalene 120

References 122

5. Discussion and Final Remarks

5.1. Experimental results 125

5.1.1. The influence of the size of the halogen atom 125

5.1.2. Estimative of thermodynamic properties of 1-chloronaphthalene 131

5.2. Statistical thermodynamics results 132

5.2.1. Calculation methodologies 132

5.2.2. Influence of Temperature 133

References 135

Supplementary Information

Attachment A - FTIR results 139

Attachment B - EThermo.xls, Worksheet File 150

Attachment C - Computational results 151

List of Tables

Table 1.1. Chemicals currently listed and under consideration for been considered as POPs under the Stockholm Convention. **5**

Table 1.2. CODATA recommended values, symbols and units for some physical constants. **14**

Table 1.3. Unit Names and SI units values. **15**

Table 1.4. Symbols, dimensions and SI units of some Physical Constants. **16**

Table 2.1. List of studied compounds in this work. Used abbreviation, molecular and structural formula. **21**

Table 2.2. Properties of 1-fluoronaphthalene: CAS number, molar mass, density, melting and boiling temperatures. **22**

Table 2.3. Properties of 1-bromonaphthalene: CAS number, molar mass, density, melting and boiling temperatures. **23**

Table 2.4. Literature data for 1-bromonaphthalene: thermodynamic properties, studied temperatures, $\Delta_{\text{trans}}H^0_{\text{m}}(T)$ and used methods. **23**

Table 2.5. Properties of 1-iodonaphthalene: CAS number, molar mass, density, melting and boiling temperatures. **24**

Table 2.6. Literature data for 1-iodonaphthalene: thermodynamic properties, studied temperatures, $\Delta_{\text{trans}}H^0_{\text{m}}(T)$ and used methods. **24**

Table 2.7. Properties of 2-chloronaphthalene: CAS number, molar mass, density, melting and boiling temperatures. **25**

Table 2.8. Literature data for 2-chloronaphthalene: thermodynamic properties, studied temperatures, $\Delta_{\text{trans}}H^0_{\text{m}}(T)$ and used methods. **25**

Table 2.9. Properties of 2-bromonaphthalene: CAS number, molar mass, density, melting and boiling temperatures. **26**

Table 2.10. Literature data for 2-bromonaphthalene: thermodynamic properties, studied temperatures, $\Delta_{\text{trans}}H^0_{\text{m}}(T)$ and used methods. **26**

Table 2.11. Properties of 2-iodonaphthalene: CAS number, molar mass, density, melting and boiling temperatures. **27**

Table 2.12. Literature data for 2-iodonaphthalene: thermodynamic properties, studied temperatures, $\Delta_{\text{trans}}H^0_{\text{m}}(T)$ and used methods. **27**

Table 2.13. Resume of the supplier information purities and measured purities by GC analysis in (%) of the studied compounds. **29**

Table 3.1. Vapor pressure results for 1-fluoronaphthalene.[a] **65**

Table 3.2. Vapor pressure results for 1-bromonaphthalene.[a] **67**

Table 3.3. Vapor pressure results for 1-iodonaphthalene.[a] **69**

Table 3.4. Standard (p^0 = 0.1 MPa) molar properties of vaporization derived from the fitting of the Clarke and Glew equation 3.18 to the experimental *p,T* results for 1-halogenated naphthalenes. **71**

Table 3.5. Absolute entropies derived from experimental and computational results for 1-halogenated naphthalenes. **71**

Table 3.6. Vapor pressure results for 2-chloronaphthalene.[a] **72**

Table 3.7. Vapor pressure results for 2-bromonaphthalene.[a] **74**

Table 3.8. Vapor pressure results for 2-iodonaphthalene.[a] **76**

Table 3.9. Standard (p^0 = 0.1 MPa) molar properties of sublimation derived from the fitting of the Clarke and Glew equation 3.18 to the experimental *p,T* results for 2-halogenated naphthalenes. **78**

Table 3.10. Standard (p^0 = 0.1 MPa) molar properties of vaporization derived from the fitting of the Clarke and Glew equation 3.18 to the experimental *p,T* results for 2-halogenated naphthalenes. **79**

Table 3.11. Standard (p^0 = 0.1 MPa) molar properties of fusion derived from the vaporization and sublimation results for 2-halogenated naphthalenes. **80**

Table 3.12. Absolute entropies derived from experimental and computational results for 2-halogenated naphthalenes. **80**

Table 4.1. Resume of the advantages and disadvantages of quantum chemical methods. **86**

Table 4.2. Resume of the different contributions (translational; electronic; rotational and vibrational). **101**

Table 4.3. Applied anharmonicity scaling factors for the correction of the vibrational frequencies for the different quantum chemical models. **102**

Table 4.4. Results of $C^0_{p,\mathrm{m}}$ (J.K^{-1}.mol^{-1}) using several models/basis sets for the molecules used in isodesmic reactions at *T* = 298.15 K. **104**

Table 4.5. Results of S^0_{m} (J.K^{-1}.mol^{-1}) using several models/basis sets for the molecules used in isodesmic reactions at *T* = 298.15 K. **105**

Table 4.6. Results for 1-fluoronaphthalene for $C^0_{v,\mathrm{m}}$, $C^0_{p,\mathrm{m}}$, S^0_{m} and $\Delta\Delta H$ at *T* = 298.15K. **106**

Table 4.7. Results of 1-chloronaphthalene for $C^0_{v,\mathrm{m}}$, $C^0_{p,\mathrm{m}}$, S^0_{m} and $\Delta\Delta H$ at *T* = 298.15K. **108**

Table 4.8. Results of 1-bromonaphthalene for $C^0_{v,\mathrm{m}}$, $C^0_{p,\mathrm{m}}$, S^0_{m} and $\Delta\Delta H$ at *T* = 298.15K. **110**

Table 4.9. Results of 1-iodonaphthalene for $C^0_{v,\mathrm{m}}$, $C^0_{p,\mathrm{m}}$, S^0_{m} and $\Delta\Delta H$ at *T* = 298.15K. **112**

Table 4.10. Results of 2-fluoronaphthalene for $C_{v,\mathrm{m}}^{0}$, $C_{p,\mathrm{m}}^{0}$, S_{m}^{0} and $\Delta\Delta H$ at T = 298.15K. **114**

Table 4.11. Results of 2-chloronaphthalene for $C_{v,\mathrm{m}}^{0}$, $C_{p,\mathrm{m}}^{0}$, S_{m}^{0} and $\Delta\Delta H$ at T = 298.15K. **116**

Table 4.12. Results of 2-bromonaphthalene for $C_{v,\mathrm{m}}^{0}$, $C_{p,\mathrm{m}}^{0}$, S_{m}^{0} and $\Delta\Delta H$ at T = 298.15K. **118**

Table 4.13. Results of 2-iodonaphthalene for $C_{v,\mathrm{m}}^{0}$, $C_{p,\mathrm{m}}^{0}$, S_{m}^{0} and $\Delta\Delta H$ at T = 298.15K. **120**

Table 5.1. Bondi radius and volume of the halogen atoms. **125**

Table 5.2. Thermodynamic properties of vaporization of the 1-halogenated naphthalene at T = 298.15 K. **131**

Table 6.1. Experimental IR spectral data and fundamental vibrational mode assignment, at T = 298.15 K, for 1-fluoronaphthalene. **139**

Table 6.2. Experimental IR spectral data and fundamental vibrational mode assignment, at T = 298.15 K, for 1-bromonaphthalene. **141**

Table 6.3. Experimental IR spectral data and fundamental vibrational mode assignment, at T = 298.15 K, for 1-iodonaphthalene. **143**

Table 6.4. Experimental IR spectral data and fundamental vibrational mode assignment, at T = 298.15 K, for 2-chloronaphthalene. **145**

Table 6.5. Experimental IR spectral data and fundamental vibrational mode assignment, at T = 298.15 K, for 2-bromonaphthalene. **147**

Table 6.6. Experimental IR spectral data and fundamental vibrational mode assignment, at T = 298.15 K, for 2-iodonaphthalene. **148**

Table 6.7. Results of $C_{v,\mathrm{m}}^{0}$ translational and rotational contributions fractions, using B3LYP/6-311++G(d,p) for the studied mono-halogenated naphthalenes at several temperatures. **151**

Table 6.8. Results of $C_{v,\mathrm{m}}^{0}$ vibrational contribution fraction, using B3LYP/6-311++G(d,p) for the studied mono-halogenated naphthalenes at several temperatures. **152**

Table 6.9. Results of S_{m}^{0} rotational contribution fraction, using B3LYP/6-311++G(d,p) for the studied mono-halogenated naphthalenes at several temperatures. **153**

Table 6.10. Results of S_{m}^{0} translational contribution fraction, using B3LYP/6-311++G(d,p) for the studied mono-halogenated naphthalenes at several temperatures. **153**

Table 6.11. Results of S_{m}^{0} vibrational contribution fraction, using B3LYP/6-311++G(d,p) for the studied mono-halogenated naphthalenes at several temperatures. **154**

Table 6.12. Results of $C_{p,\mathrm{m}}^{0}$ using B3LYP/6-311++G(d,p) for the studied mono-halogenated naphthalenes at several temperatures. **157**

Table 6.13. Results of S_{m}^{0} using B3LYP/6-311++G(d,p) for the studied mono-halogenated naphthalenes at several temperatures. **157**

List of Figures

Figure 1.1. Chemical structure of the studied mono-halogenated naphthalenes. **12**

Figure 2.1. Gas-liquid chromatography apparatus. **28**

Figure 2.2. Scheme of the ATR-FTIR principle. **31**

Figure 2.3. Graphical representation of a single reflection ATR. **31**

Figure 2.4. Spectrum BX-FTIR apparatus used in this work. **32**

Figure 2.5. FTIR spectra for 2-bromonaphthalene. $298.15 \leq T(K) \leq 343.15$ **33**

Figure 2.6. Peak high (at v=3056 cm^{-1}, aromatic C-H stretching) as a function of temperature for 2-bromonaphthalene. **34**

Figure 3.1. Schematic representation of a phase diagram of a pure substance presenting only one crystalline phase. **39**

Figure 3.2. Dependence of the chemical potential of crystal, liquid and gas phases on temperature at constant pressure. **40**

Figure 3.3. Dependence of the chemical potential of crystal, liquid and gas phases on temperature at constant pressure. **40**

Figure 3.4. Evaporation process - a schematic representation. **41**

Figure 3.5. Photo and Schematic representation of the measuring system. **53**

Figure 3.6. Schematic representation of the MKS Baratron capacitance manometer 631A . **54**

Figure 3.7. Schematic representation of the MKS Baratron capacitance manometer 631A. **55**

Figure 3.8. Schematic representation of the ConFlat DN16 CF connection. **56**

Figure 3.9. Schematic representation of the angle valves VAT 57. **57**

Figure 3.10. Schematic representation of the system that allows the control of all the two valves remotely. **58**

Figure 3.11. Schematic representation of the sample cell. **59**

Figure 3.12. Schematic representation of the double walled vessel used to thermostatize the sample cell. **60**

Figure 3.13. Schematic representation of the vaccum system. **61**

Figure 3.14. Image of the HP-VEE program used in the static apparatus. **62**

Figure 3.15. Graphic representation of ln(*p*/Pa) = *f* [1000 K/*T*] for 1-fluoronaphthalene. **66**

Figure 3.16. Graphic representation of the arc method [7] of the experimental results for 1-fluoronaphthalene. **66**

Figure 3.17. Graphic representation of ln(*p*/Pa) = *f* [1000 K/*T*] for 1-bromonaphthalene. **68**

Figure 3.18. Graphic representation of the arc method [7] of the experimental results for 1-bromonaphthalene. **68**

Figure 3.19. Graphic representation of ln(*p*/Pa) = *f* [1000 K/*T*] for 1-iodonaphthalene. **70**

Figure 3.20. Graphic representation of the arc method [7] of the experimental results for 1-iodonaphthalene. **70**

Figure 3.21. Graphic representation of ln(*p*/Pa) = *f* [1000 K/*T*] for 2-chloronaphthalene. **73**

Figure 3.22. Graphic representation of the arc method [7] of the experimental results for 2-chloronaphthalene. **73**

Figure 3.23. Graphic representation of ln(*p*/Pa) = *f* [1000 K/*T*] for 2-bromonaphthalene. **75**

Figure 3.24. Graphic representation of the arc method [7] of the experimental results for 2-bromonaphthalene. **75**

Figure 3.25. Graphic representation of ln(*p*/Pa) = *f* [1000 K/*T*] for 2-iodonaphthalene. **77**

Figure 3.26. Graphic representation of the arc method [7] of the experimental results for 2-iodonaphthalene. **77**

Figure 4.1. Scheme of the quantum chemical calculations typical “procedure”. **85**

Figure 4.2. Reaction scheme used in the isodesmic estimation procedure of the gaseous phase molar heat capacity and absolute entropy for mono-halogenated naphthalenes. **103**

Figure 4.3. Gaseous phase heat capacities results of 1- fluoronaphthalene using several basis sets . **107**

Figure 4.4. Gaseous phase absolute entropies results of 1- fluoronaphthalene using several basis sets. **107**

Figure 4.5. Gaseous phase heat capacities results of 1- chloronaphthalene using several basis sets. **109**

Figure 4.6. Gaseous phase absolute entropies results of 1- chloronaphthalene using several basis sets. **109**

Figure 4.7. Gaseous phase heat capacities results of 1- bromonaphthalene using several basis sets. **111**

Figure 4.8. Gaseous phase absolute entropies results of 1-bromonaphthalene using several basis sets. **111**

Figure 4.9. Gaseous phase heat capacities results of 1- iodonaphthalene using several basis sets. **112**

Figure 4.10. Gaseous phase absolute entropies results of 1- iodonaphthalene using several basis sets. **113**

Figure 4.11. Gaseous phase heat capacities results of 2- fluoronaphthalene using several basis sets. **115**

Figure 4.12. Gaseous phase absolute entropies results of 2-fluoronaphthalene using several basis sets. **115**

Figure 4.13. Gaseous phase heat capacities results of 2- chloronaphthalene using several basis sets. **117**

Figure 4.14. Gaseous phase absolute entropies results of 2-chloronaphthalene using several basis sets. **117**

Figure 4.15. Gaseous phase heat capacities results of 2- bromonaphthalene using several basis sets. **119**

Figure 4.16. Gaseous phase absolute entropies results of 2-bromonaphthalene using several basis sets. **119**

Figure 4.17. Gaseous phase heat capacities results of 2- iodonaphthalene using several basis sets. **121**

Figure 4.18. Gaseous phase absolute entropies results of 2-iodonaphthalene using several basis sets. **121**

Figure 5.1. Phase diagram of ln(*p*/Pa) = *f* [1000 K/*T*] for liquid 1- halogenated naphthalenes. **126**

Figure 5.2. Phase diagram of ln(*p*/Pa) = *f* [1000 K/*T*] for the liquid and solid 2- halogenated naphthalenes. **126**

Figure 5.3. Correlation between $\Delta_{\mathrm{l}}^{\mathrm{g}}G_{\mathrm{m}}^{0}(298.15\mathrm{K})$ and volume of the halogen atom for 1 and 2-halogenated naphthalenes. **127**

Figure 5.4. Correlation between $\Delta_{\mathrm{l}}^{\mathrm{g}}S_{\mathrm{m}}^{0}(298.15\mathrm{K})$ and volume of the halogen atom for 1 and 2-halogenated naphthalenes. **128**

Figure 5.5. Correlation between $\Delta_{\mathrm{l}}^{\mathrm{g}}H_{\mathrm{m}}^{0}(298.15\mathrm{K})$ and volume of the halogen atom for 1 and 2-halogenated naphthalenes. **129**

Figure 5.6. Phase diagram of ln(*p*/Pa) = *f* [1000 K/*T*] for 1 and 2- halogenated naphthalenes. **130**

Figure 5.7. Gaseous phase heat capacities results of 2-bromonaphthalene using several basis sets. **132**

Figure 5.8. Temperature dependence of the ideal gas isobaric (p^o=0.1 MPa) heat capacity. (B3LYP/6-311++G(d,p), scaling factor 0.9688). **134**

Figure 5.9. Temperature dependence of the ideal gas standard (p^o=0.1 MPa) molar absolute entropies. (B3LYP/6-311++G(d,p), scaling factor 0.9688). **134**

Figure 6.1. Experimental and Theoretical IR spectral data, at *T* = 298.15 K, for 1-fluoronaphthalene. **140**

Figure 6.2. Experimental and Theoretical IR spectral data, at *T* = 298.15 K, for 1-bromonaphthalene. **142**

Figure 6.3. Experimental and Theoretical IR spectral data, at *T* = 298.15 K, for 1-iodonaphthalene. **144**

Figure 6.4. Experimental and Theoretical IR spectral data, at *T* = 298.15 K, for 2-chloronaphthalene. **146**

Figure 6.5. FTIR spectra for 2-chloronaphthalene. $298.15 \le T(K) \le 343.15$ **146**

Figure 6.6. Experimental and Theoretical IR spectral data, at *T* = 298.15 K, for 2-bromonaphthalene. **147**

Figure 6.7. Experimental and Theoretical IR spectral data, at *T* = 298.15 K, for 2-iodonaphthalene. **149**

Figure 6.8. FTIR spectra for 2-iodonaphthalene. $298.15 \le T(K) \le 343.15$ **149**

Figure 6.9. EThermo file. **150**

Figure 6.10. Vibrational, rotational and translational fraction contributions for total $C_{v,\mathrm{m}}^{0}$ in function of T / K using B3LYP/6-311++G(d,p). **155**

Figure 6.11. Vibrational, rotational and translational fraction contributions for total S_{m}^{0} in function of T / K using B3LYP/6-311++G(d,p). **155**

Figure 6.12. Vibrational, rotational and translational fraction contributions for total $C^0_{v,\mathrm{m}}$ in function of T / K using B3LYP/6-311++G(d,p). **156**

Figure 6.13. Vibrational, rotational and translational fraction contributions for total S^0_{m} in function of T / K using B3LYP/6-311++G(d,p). **156**

Abbreviations

BFRs – Brominated Flame Retardants

CHLs – Chlordane

DDT – Dichlorodiphenyl-trichloroethane

FSAs – Fluorosilicic Acid Solutions

FTOHs – Fluorotelomer Alcohols

HCB – Hexachlorobenzene

MHNs – Mono-Halogenated Naphthalenes

PAHs – Polycyclic Aromatic Compounds

PBDEs – Polybrominated diphenyl ethers

PCBs – Polychlorinated biphenyls

PCDD/Fs – Polychlorinated dibenzo-p-dioxins and polychlorinated dibenzofurans

PCNs – Perfluorinated compounds and Polychlorinated Naphthalenes

PFCAs - Perfluoroalkyl Carboxylates

PFSAs – Perfluoroalkyl Sulfonates

PHNs – Poli-Halogenated Naphthalenes

POPRC – Persistent Organic Pollutants Review Committee

POPs – Persistent Organic Pollutants

UNEP – United Environment Programme

Chapter 1

Introduction

1.1. State of art

1.1.1. Persistent Organic Pollutants

1.1.1.1. Introduction

1.1.1.2. Sources of POPs and their persistence in the environment

1.1.1.3. Physical chemical properties

Vapor Pressure

Solubility

Influence of halogen atoms

1.1.1.4. Future challenges in POPs research

1.2. General introduction

1.2.1. Aim of the work

1.2.2. Nomenclature, constants, conversion factors, units and dimensions

References

1.1. State of art

1.1.1. Persistent Organic Pollutants

1.1.1.1. Introduction

Mono-halogenated naphthalenes belong to a group of diverse chemicals that are persistent in the environment and usually have several characteristics such as hydrophobicity, lipophilicity and high volatility. This group is referred as persistent organic pollutants (POPs). [1–3]. The features associated to POPs, makes them a threat to the environment as well as to the health of the living beings. Given to their resistance to metabolic degradation and to their lipophilicity, POPs are easily bioaccumulated in tissue and transported through food chains. The animals and humans exposure to these chemicals, causes a variety of health problems, such as reproductive abnormalities, birth defects, immune system dysfunction, neurological defects and cancer for example. [1–3] Despite of POPs being used, in the populated areas, in several processes, such as industry and agriculture, they are globally distributed and even found in remote environments such as the Arctic. Usually, the long-range transport via the atmosphere is the most likely way that these POPs can reach remote environments. However, the fact that they can exist in different phases, it is very difficult the tracing the movement of these compounds in the environment.

In the past few years, these compounds have received some attention by researchers because of their persistence, high bioaccumulation potential and harmful biological effects.

The importance of pursuing research in this kind of chemical compounds, in particular in their behaviour, sources, fate and environmental and health effects, is covered by the Stockholm Convention for which the host organization is the United Environment Programme (UNEP). Under the Stockholm Convention on POPs, 12 chlorinated chemical substances have been banned or severely restricted. These 12 compounds are listed in table 1.1 and include dioxins and furans (polychlorinated dibenzo-p-dioxins and polychlorinated dibenzofurans, PCDD/Fs), polychlorinated biphenyls (PCBs), hexachlorobenzene (HCB) and several organochlorines used as pesticides: dichlorodiphenyl-trichloroethane (DDT), chlordane (CHLs), toxaphene, dieldrin, aldrin, endrin, heptachlor and mirex.

These have been often referred as ‘legacy” POPs because of their long history of use and release into the environment.

The main goal of this Convention is “to protect human health and the environment from persistent organic pollutants”. [4] Additionally, it recognises the need for global action in respect to the facts that POPs are toxic, resistant to degradation, and bioaccumulative. For a chemical be considered as a persistent organic pollutant in the Convention, it must display the following characteristics:

- Persistence;
- Bioaccumulation;
- Potential for long-range environmental transport;
- Toxicity and Adverse effects.

Since 2008, 12 chemicals (table 1.1) were under consideration by POPs Review Committee (POPRC) to be included under the Convention.

Table 1.1. Chemicals currently listed and under consideration for been considered as POPs under the Stockholm Convention.

Currently listed	Under consideration
Aldrin	Chlordecone
(CAS: 309-00-2)	(CAS: 143-50-0)
Chlordane	Endosulfan
(CAS: 12789-03-6)	(CAS: 115-29-7)
DDT	Hexabromobiphenyl
(CAS: 50-29-3)	(CAS: 36355-1-8)
Dieldrin	Hexabromocyclododecane
(CAS: 60-57-1)	(CAS: 3194-55-6)
Endrin	α-Hexachlorocyclohexane
(CAS: 72-20-8)	(CAS: 319-84-6)
Heptachlor	β-Hexachlorocyclohexane
(CAS: 76-44-8)	(CAS: 319-85-7)
Hexachlorobenzene	Lindane
(CAS: 118-74-1)	(CAS: 58-89-9)
Mirex	Octabromodiphenyl ether
(CAS: 2385-85-5)	(CAS: 32536-52-0)
Polychlorinated biphenyls	Pentabromodiphenyl ether
	(CAS: 32534-81-9)
Polychlorinated dibenzo-p-dioxins	Pentachlorobenzene
	(CAS: 608-93-5)
Polychlorinated dibenzofurans	Perfluorooctane sulfonate
	(CAS: 29457-72-5)
Toxaphene	Short chain chlorinated paraffins
(CAS: 8001-35-2)	

However, there are numerous other chemical compounds used without any restriction, which are considered environmental contaminants and are often referred as “emerging” POPs. Basically, “emerging” POPs comprises the pollutants that have been recently discovered in the environment and are known to cause adverse effects in humans and wildlife.

The global environmental reports, indicates that, due to production and use restrictions of POPs, the emission sources of a number of “legacy” POPs (such as DDT and HCBs) in the last 20 years have moved from industrialized countries to less-developed country such as India and China. [5, 6]

Additionally, as a result of recent changes in global trade, there has been a shift in the manufacture of goods to developing countries with reduce labour costs and weaker environmental legislation. This will have implications for the global dispersion of “emerging” POPs like PBDEs. [5–7] Examples of “emerging” POPs include several types of halogenated compounds, such as brominated flame retardants (BFRs), polybrominated diphenyl ethers (PBDEs), perfluorinated compounds and polychlorinated naphthalenes (PCNs). Exposure to POPs comes mainly from the consumption of food products.

The research and understanding of the environmental processes, transport pathways, the impact of POPs in the environment and in health of the living beings requires sophisticated measurement techniques. An important research area is the one which explores the volatility of POPs, and consequently their capacity of spread via air and aquatic systems.

Since the beginning of Stockholm Convention, there has been substantial progress in the understanding of the impacts of POPs on the environment. At the same time, new issues and challenges have emerged along with the development of new thinking and strategies to tackle the problems. Understanding of the thermophysical properties of these compounds is essential for a correct evaluation of their dispersion as liquid and gaseous substances into the environment.

1.1.1.2. Sources of POPs and their persistence in the environment

Persistent Organic Pollutants have many sources. Some pesticides used in agriculture and pest control, industrial chemicals like PCBs present in capacitors and transformers, unintentionally produced compounds such as polycyclic aromatic hydrocarbons (PAHs), dioxins and furans, PBDEs, and even mono and poli-halogenated naphthalenes (MHNs and PHNs) which are used as flame retardants in consumer products. For perfluorinated compounds, their use in fire fighting foams might make them significant POPs. PAHs have many natural sources, but the most important anthropogenic sources are vehicles and combustion of firewood for cooking. Although, PAHs are often not included in the category of POPs, there are some researchers that consider them POPs. MHNs are persistent in the environment. Many of the unique physical chemical properties of this POPs group, which are beneficial from an industrial or commercial point of view, are the same properties that results in resistance and persistent environmental contaminants. For example, no degradation in other types of POPs such as PFSAs or PFCAs in environmental conditions, either abiotic or biotic, has been observed. [8] For example, PFCAs were detected in mg/L concentrations in groundwater at two military bases, 7 to 10 years after use. [9]

1.1.1.3. Physical chemical properties

Many of the organic pollutants, including POPs, that are of particular environmental concern, contain one or several halogen atoms, especially chlorine, and, to a lesser extent, fluorine, bromine and/or iodine. [10] The existence of halogenated compounds in the environment is primarily due to anthropogenic contributions.

There are several reasons for the still-vast industrial production of halogen-containing compounds. Not only because the substitution of carbon-bound hydrogen by halogens, which enhances the inertness of the molecule (and as consequence, its persistence in the environment), but also the presence of larger halogens (i.e., chlorine, bromine and iodine) leads to a higher hydrophobicity, increasing its tendency to partition into organic phases. [10]

Hence, one important aspect in the treatment of the partitioning of these kind of compounds in the environment is the quantitative description of how much a compound

likes or dislikes being in the gas phase as compared to other relevant condensed phases. To this treatment, a good knowledge of the physical chemical properties is crucial.

Vapor pressure

The vapor pressure of a compound is not only a measure of the maximum possible concentration of a compound in the gas phase at a given temperature, but it also provides an important quantitative information on the attractive forces among the compound's molecules in the condensed phase. Vapor pressure data may also be very useful for predicting equilibrium constants for the partitioning of organic compounds between the gas phase and other liquid or solid phases.

In the past years, the vapor pressures of fluorotelomer alcohols (FTOHs) have been reported in the literature. [11-15] However, the reported values are variable, differing by several orders of magnitude. Two studies [13, 16] in the literature have reported the vapor pressures of the fluorosilicic acid solutions (FSAs) and similar to the other POPs, reported values are variable. It is possible that some of the difficulties found in measuring vapor pressures of the FSAs are also applicable to the FTOHs and other POPs.

Several aspects can affect the vapor pressure of a halogenated pollutant, for example, the vapor pressures of the FTOHs are influenced by the length of the perfluoroalkyl chain, and the vapor pressures increases as length of the perfluoroalkyl chain decreases. In the case of mono and poli-halogenated naphthalenes the number of halogen atoms and the nature of the halogens are aspects to take into account. Increasing the number of halogen atoms or decreasing the size of the halogen atom, causes an increasing in the vapor pressure values. Despite of the high volatility of halogenated naphthalenes (e.g. 1-chloronaphthalene (T = 299.2 K; p = 8.43 Pa) [17]), the vapor pressure values are scarce, in which most of the cases the data presents high associated uncertainties and in some cases the data are inexistent (1-fluoronaphthalene).

Solubility

Solubility of POPs has also been studied in the past few years. Solubility studies are of great importance to understand how these compounds behave, transport and bioaccumulate in aquatic environments. Solubility fundamentally depends on the physical chemical properties of the solute and solvent, as well as on temperature, pressure and the pH of the solution.

Halogenated naphthalenes are usually lipophilic compounds with low K_{ow} and readily soluble in most organic solvents (e.g., diethyl ether, dichloromethane, hexane, toluene and isooctane.) The solubility in more polar solvents such as methanol is relatively low, but high enough for the use in liquid chromatography on analytical columns. [10] The lower the number of halogen atoms in the naphthalene ring, the higher the solubility in water. [10]

Influence of halogen atoms

The physical chemical properties of the halogenated compounds depends on the halogen. The unusual strength of the carbon–fluorine bond contributes to the thermal and chemical stability of poly- and perfluorinated chemicals. [18, 19] Although fluorine atoms are small, they are significantly larger than hydrogen atoms (van der Waal radii of 1.47 and 1.20 Å respectively). [18] As a result, perfluoroalkyl chains are less flexible than their hydrogen counterparts. [20] The fluorine atom has three pairs of nonbonding electrons in its outer electronic shell. In a perfluoroalkyl chain, these nonbonding electrons of the densely packed fluorine atoms act as a “coating” around the carbon backbone. This electron cloud sheath is an effective electrostatic and steric shield against any nucleophilic attack targeted against the central carbon atoms [18, 21] and also contributes to the chemical stability of PFCs.

Chlorine atom is the third element with highest electronegativity, and consequently a strong oxidizing agent. Chlorine is used in a wide range of industrial and consumer products, such as, solvents, disinfectants, agrochemicals, and pharmaceuticals, etc.

Chlorinated naphthalenes are very used (e.g. cable insulation, wood preservation, engine oil additives, capacitors, etc. [10]), not as pure materials, but as a mixture of several congeners.

They presents bioaccumulation index, and tends to increase with the degree of chlorination. In the case of mono chlorinated naphthalenes, it appears to be readily degradable by soil and water microorganisms under aerobic conditions.

With properties between those of chlorine and iodine, bromine is also very used industrially (as gasoline additive, pesticide etc. [22-24]). However, the high solubility of bromide ion has caused its accumulation in the oceans. Brominated naphthalenes are used as flame retardants in consumer products and in refractive index testing of oils. [25]

Iodine's relatively high atomic number, low toxicity, and ease of attachment to organic compounds have made it a part of many X-ray contrast materials in modern medicine. [26] Iodinated naphthalenes are the less volatile and the less toxic when compared with other halogenated naphthalenes, so, it is not a surprise that iodinated compounds are those which appear less in tables of halogenated pollutants.

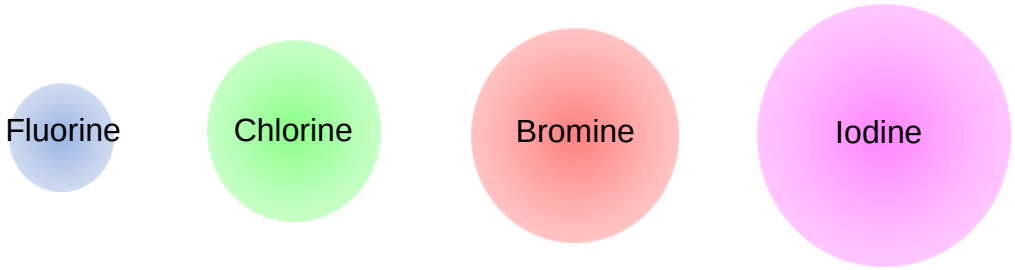

So, the properties of these type of compounds are important at an industrial level, but the knowledge of the transport and transformation processes in the atmosphere of these compounds, are essential and are among the key processes for the understand and evaluation of the distribution and fate of POPs in the environment.

1.1.1.4. Future challenges in POPs research

Scientists and policymakers needs to learn as much as possible from current knowledge related to the sources, fate, behaviour, and effects of those POPs listed (and even those not listed) and which have already been the subject of study for several decades. Such action is essential to prevent us from repeating the mistakes of the past. While good progress has been made on intensive research, there are some areas that can be the focus of research efforts in the next few years.

For example:

1. Understand the volatility of POPs and their behaviour in Nature;

2. Determine the bioavailability of pollutants other than PBDEs to humans, since it's also important to know how the other POPs can affect us (in a direct or indirect way);

3. Provide further understanding about the fate and partitioning of POPs in indoor and outdoor environments.

1.2. General introduction

1.2.1. Aim of the work

This study is focused on thermophysical properties of six mono-halogenated naphthalenes, depicted in figure 1.1.

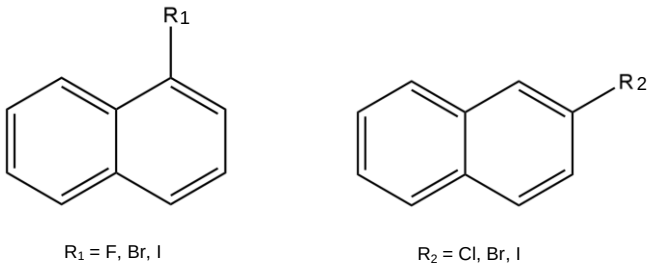

Figure 1.1. Chemical structure of the studied mono-halogenated naphthalenes.

The aim of this work is to evaluate the isomerization effect in the position 1 and 2 on the naphthalene ring, as well as to rationalize/correlate the volume of the halogen with some thermophysical properties.

This work can be subdivided in three main parts:

1- ***Vibrational spectra study***: Fourier transform infrared spectroscopy (FTIR) of the six halogenated naphthalenes and their temperature dependence were measured. The obtained results were analysed in order to evaluate the vibrational spectra dependence with the chemical nature and position of the halogen atom.

2- ***Thermodynamic study***: the vapor pressure of each studied compound was measured as a function of temperature using a Static apparatus. Based on the obtained results the thermodynamic properties of sublimation and vaporization, were derived.

3- ***Quantum Chemical Calculations***: the experimental study was supported by quantum chemical calculations. The heat capacity, $C^0_{p,\mathrm{m}}$, and absolute entropy, S^0_{m}, on the gaseous phase, were estimated by statistical thermodynamics using the vibrational frequencies derived by quantum chemical calculations using several based functionals and basis sets.

This dissertation is organized in five chapters according to the following structure:

- ***Chapter 1: Introduction***

A brief description of the motivation and aims of this work are given. The subdivision of the experimental and theoretical work and the structure/strategy of the thesis are also presented. Additionally, the state of art concerning the persistent organic pollutants is provided.

- ***Chapter 2: Studied Compounds***

A list of all the studied compounds and literature data is presented. The characterization of the studied compounds is presented and described in detail.

- ***Chapter 3: Vapor Pressure Measurements***

In this chapter, some theoretical concepts of thermodynamics are presented. The experimental techniques / methodologies used in the work are described in detail. The obtained experimental results and the derived thermodynamic properties of sublimation and vaporization are also presented.

- ***Chapter 4: Statistical thermodynamics***

The derived results for the heat capacities and absolute entropies, on the gaseous phase, using different functionals / basis sets are analysed. Also the results of the influence of temperature and fraction to the total contribution of partition functions are studied in detail and presented as supporting information.

- ***Chapter 5: Discussion and Final Remarks***

The obtained results along the thesis are presented and the combination of the experimental and theoretical results is analysed. A comparative and differential analysis between the six studied halogenated naphthalenes are presented based on the experimental and computational results and considering the isomerization effect (1 and 2 positions) and the chemical nature of the halogen substituent, and main conclusions are summarized.

1.2.2. Nomenclature, constants, units, conversion factors and dimensions

Nomenclature

The IUPAC nomenclature for inorganic and organic compounds were adopted, however in order to simplify the text, abbreviations of the name of compounds were defined.

Constants and units

The recommended (CODATA) [27] values for the physical constants used in this thesis are presented in table 1.2.

Table 1.2. CODATA recommended values, symbols and units for some physical constants.

Physical Constant	Symbol	Recommended Value	Unit
Speed of light in vacuum	c	299 792 458	$m.s^{-1}$
Planck Constant	h	6.626 068 76(52)	$x10^{-34}$ J.s
h/(2π)	$\hbar$	1.054 571 596(82)	$x10^{-34}$ J.s
Electron mass	m_e	9.109 381 88(72)	$x10^{-31}$ kg
Proton mass	m_p	1.672 621 58(13)	$x10^{-27}$ kg
Avogadro Constant	N_A	6.022 141 99(47)	$x10^{23}$ mol^{-1}
Molar gas Constant	R	8.314 462(15)	$J.K^{-1}.mol^{-1}$
Boltzmann Constant	k	1.380 650 3(24)	$x10^{-23}$ $J.K^{-1}$
Stefan-Boltzmann Constant	σ	5.670 400(40)	$x10^{-8}$ $W.m^{-2}.K^{-4}$
Bohr magneton	μ_B	9.274 008 99(37)	$x10^{-24}$ $J.T^{-1}$
Bohr radius	a_0	5.291 772 083(19)	$x10^{-11}$ m

Note: The digits in parentheses represent the 1σ uncertainty in the previous two quoted digits.

Conversion Factors

Unit conversion factors

In table 1.3 are presented the Unit conversion factors and their values in SI units.

Table 1.3. Unit Names and SI units values.

Unit name	Symbol	Value in SI units
angstrom	Å	10^{-10} m
atmosphere	atm	101.325 x 10^{3} Pa
atomic mass unit	U	1.660 540 x 10^{-27} kg
bar	bar	1 x 10^{5} Pa
calorie	cal	4.184 J
debye	D	3.335 641 x 10^{-30} C.m
electron volt	eV	160.2177 x 10^{-21} J
faraday	F	96.4853 x 10^{3} C
hartree	H	4.359 748 x 10^{-18} J
torr	Torr	133.3224 Pa

Dimensions

In table 1.4 are presented the symbols, dimensions and SI units of some of the physical constants used across this dissertation.

Table 1.4. Symbols, dimensions and SI units of some Physical Constants.

Physical Constant	Symbol	Dimensions	SI units
acceleration	a	$L.T^{-2}$	$m.s^{-2}$
angular momentum	L, J	$L^2.M.T^{-1}$	$m^2.kg.s^{-1}$
angular speed	ω	T^{-1}	$rad.s^{-1}$
area	A, S	L^2	m^2
Avogadro constant	N_A	N^{-1}	mol^{-1}
Bohr magneton	μ_B	$L^2.I$	$J.T^{-1}$
Boltzmann constant	k, k_B	$L^2.M.T^{-2}.\Theta^{-1}$	$J.K^{-1}$
capacitance	C	$L^{-2}.M^{-1}.T^4.I^2$	F
density	ρ	$L^{-3}.M$	$kg.m^{-3}$
energy	E, U	$L^2.M.T^{-2}$	J
energy density	u	$L^{-1}.M.T^{-2}$	$J.m^{-3}$
entropy	S	$L^2.M.T^{-2}.\Theta^{-1}$	$J.K^{-1}$
force	F	$L.M.T^{-2}$	N
frequency	υ, f	T^{-1}	Hz
gravitational constant	G	$L^3.M^{-1}.T^{-2}$	$m^3.kg^{-1}.s^{-2}$
hamiltonian	H	$L^2.M.T^{-2}$	J
heat capacity	C	$L^2.M.T^{-2}.\Theta^{-1}$	$J.K^{-1}$
length	L, l	L	m
mass	m, M	M	kg
molar gas constant	R	$L^2.M.T^{-2}.\Theta^{-1}.N^{-1}$	$J.K^{-1}.mol^{-1}$
moment of inertia	I	$L^2.M$	$kg.m^2$
Planck constant	h	$L^2.M.T^{-1}$	J.s
pressure	p, P	$L^{-1}.M.T^{-2}$	Pa
specific heat capacity	c	$L^2.T^{-2}.\Theta^{-1}$	$J.K^{-1}.kg^{-1}$
speed	u, υ , c	$L.T^{-1}$	$m.s^{-1}$
Stefan-Boltzmann constant	σ	$M.T^{-3}.\Theta^{-4}$	$W.m^{-2}.K^{-4}$
temperature	T	Θ	K
time	t	T	s
velocity	υ , u	$L.T^{-1}$	$m.s^{-1}$
volume	V, υ	L^3	m^3
weight	W	$L.M.T^{-2}$	N
work	W	$L^2.M.T^{-2}$	J

References

[1] Darnerud, P. O., *Environment International*, 29 (2003) 841–853.

[2] Legler, J.; Brouwer, A., *Environment International*, 29 (2003) 879–885.

[3] Santillo, D.; Johnston, P., *Environment International*, 29 (2003) 725–734.

[4] www.pops.int

[5] Lohmann, R.; Breivik, K.; Dachs, J.; Muir, D. C., *Environmental Pollution*, 150 (2007) 150–165.

[6] Tanabe, S., *Contamination by persistent toxic substances in the Asia-Pacific Region. In Persistent Organic Pollutants in Asia. Sources, Distributions Transport and Fate*, Elsevier Ltd, 2007, 773–817.

[7] Tanabe, S.; Ramu, K.; Isobe, T.; Takahashi, S., *Journal of Environmental Monitoring*, 10 (2008) 188–197.

[8] Oehme, M.; Mano, S.; Mikalsen, A., *Chemosphere*, 16 (1987) 102–114.

[9] Helm, P.; Bidleman, T.; Stern, G.; Koczanski, K., *Environmental Pollution*, 119 (2002) 69–78.

[10] Jaakko Paasivirta, *New types of Persistent Halogenated Compounds*, (2000), Springer.

[11] Stock, N. L.; Ellis, D. A.; Deleebeeck, L.; Muir, D. C. G.; Mabury, S. A., *Environ. Sci. Technol*., 38 (2004) 1693–1699.

[12] Kaiser, M. A.; Cobranchi, D. A.; Chai Kao, C.P.; Krusic, J.; Marchione, A. A.; Buck, R. C., *J. Chem. Eng. Data*, (2004) 912–916.

[13] Lei, Y. D.; Wania, F.; Mathers, D.; Mabury, S. A., *J. Chem. Eng. Data*, 49 (2004) 1013–1022.

[14] Krusic, P. J.; Marchione, A. A.; Davidson, F.; Kaiser, M. A.; Kao, C.P.C.; Richardson, R. E., et al. *J. Phys. Chem. A*, 109 (2005) 6232–6241.

[15] Cobranchi, D. P.; Botelho, M.W. B.; Buck, R. C.; Kaiser, M. A., *J. Chromatogr. A*, 1108 (2006) 248–251.

[16] Shoeib, M.; Harner, T.; Ikonomou, M.; Kannan, K., *Environ. Sci. Technol.*, 38 (2004) 1313–1320.

[17] S.P.Verevkin, *J.Chem.Thermodyn*., 35 (2003) 1237.

[18] Key, B. D.; Howell, R. D.; Criddle, C. S., *Environ. Sci. Technol.*, 31 (1991) 2445–2454.

[19] Fluoropolymer Manufacturers Group*. Detecting and quantifying low levels of fluoropolymer polymerization aids – a guidance document.* Society of the Plastic Industry, Inc., Washington, DC, (2003).

[20] Eaton, D. F.; Smart, B. E., *J. Am. Chem. Soc.*, 112 (1991) 2821–2823.

[21] Kirsch, P., *Modern Fluoroorganic Chemistry*. John Wiley & Sons Ltd, New York, (2004).

[22] Messenger, Belinda; Braun, Adolf, Pest Management Analysis and Planning Program, (2008).

[23] Decanio, Stephen J.; Norman, Catherine S., Contemporary Economic Policy, 23 (2008) 376.

[24] Alaeea, M.; Ariasb, P.; Sjödinc, A.; Bergman, Å., Environment International, 29 (2003) 683.

[25] http://www.ukmarinesac.org.uk/activities/water-quality/wq8_44.htm

[26] Thomson, K; Varma, D, "Safe use of radiographic contrast media". Australian Prescriber, 33 (2010) 19-22.

[27] http://www.codata.org/

Chapter 2

Studied Compounds

2.1. Studied compounds and literature data

2.1.1. 1-Halogenated naphthalenes

2.1.2. 2-Halogenated naphthalenes

2.2. Characterization of the compounds

2.2.1. Gas-liquid chromatography

2.2.2. Fourier Transform Infrared spectroscopy

References

2.1. Studied compounds and literature data

In this chapter some details about the studied compounds are presented. Table 2.1 presents the list of compounds, names, molecular formulas, structural formula and abbreviations used in this dissertation.

Table 2.1. List of studied compounds in this work. Used abbreviation, molecular and structural formula.

Compound	Used abbreviation	Molecular Formula	Structure
1-fluoronaphthalene	1-FNaph	$C_{10}H_7F$	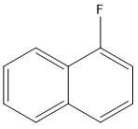
1-chloronaphthalene*	1-ClNaph	$C_{10}H_7Cl$	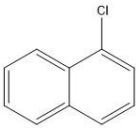
1-bromonaphthalene	1-BrNaph	$C_{10}H_7Br$	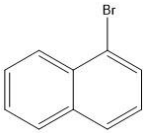
1-iodonaphthalene	1-INaph	$C_{10}H_7I$	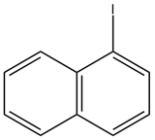
2-fluoronaphthalene*	2-FNaph	$C_{10}H_7F$	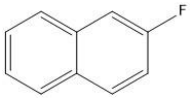
2-chloronapthalene	2-ClNaph	$C_{10}H_7Cl$	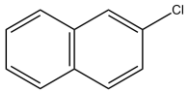
2-bromonaphthalene	2-BrNaph	$C_{10}H_7Br$	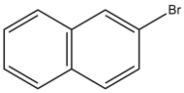
2-iodonaphthalene	2-INaph	$C_{10}H_7I$	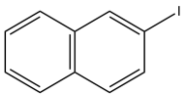

Note: * - compounds studied only computationally.

2.1.1. 1-Halogenated napthalenes

1-Fluoronaphthalene

Table 2.2. Properties of 1-fluoronaphthalene: CAS number, molar mass, density, melting and boiling temperatures. [1]

Structure	**Molecular Formula:** $C_{10}H_7F$
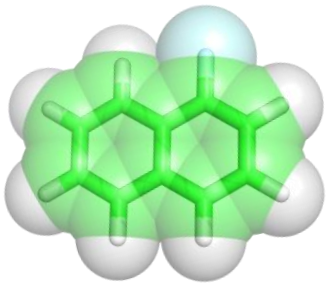	**CAS Number:** 321-38-0
	Molar Mass: 146.16 g/mol
	Density: 1132 kg/m^3
	Melting Temperature: 260 K
	Boiling Temperature: 488 K

Note: The melting and boiling temperature values at 1 atm.

For the 1-fluoronaphthalene, no data about the thermodynamic properties of phase transition was found in the literature.

1-Bromonaphthalene

Table 2.3. Properties of 1-bromonaphthalene: CAS number, molar mass, density, melting and boiling temperatures. [1]

Structure	**Molecular Formula:** $C_{10}H_7Br$
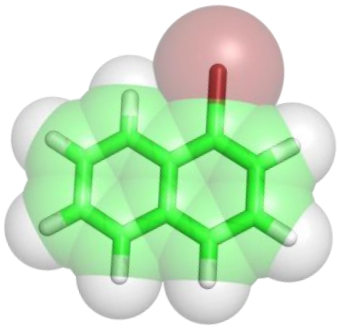	**CAS Number:** 90-11-9
	Molar Mass: 207.07 g/mol
	Density: 1485 kg/m^3
	Melting Temperature: 275-279 K
	Boiling Temperature: 556 K

Note: The melting and boiling temperature values at 1 atm.

Table 2.4. Literature data for 1-bromonaphthalene: thermodynamic properties, studied temperatures, $\Delta_{trans}H^{o}_{m}(T)$ and used methods.

Thermodynamic Parameter	**Studied Temperatures (K)**	$\Delta_{trans}H^{o}_{m}(T)$ **(kJ.mol^{-1})**	***T* (K)**	**Method**	**References**
$\Delta^{l}_{cr}H^{o}_{m}(T)$		15.16	271.4		[2]
$\Delta^{g}_{l}H^{o}_{m}(T)$	(303-336)	63.9 ± 0.4	298	GS	[3]
$\Delta^{g}_{l}H^{o}_{m}(T)$	(357-555)	58.5	372		[4]
$\Delta^{g}_{l}H^{o}_{m}(T)$	(295-359)	56 ± 6	329	ME	[5]
$\Delta^{g}_{l}H^{o}_{m}(T)$	(469-559)	45.8	484	A,EB	[4]

Note: GS – Gas Saturation/Transpiration; ME – Mass Effusion/Knudsen Effusion; A/EB - Ebulliometer.

1-Iodonaphthalene

Table 2.5. Properties of 1-iodonaphthalene: CAS number, molar mass, density, melting and boiling temperatures. [1]

Structure	**Molecular Formula:** $C_{10}H_7I$
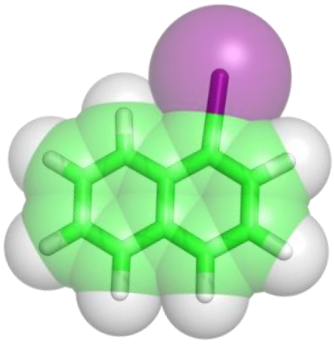	**CAS Number:** 90-14-2
	Molar Mass: 254.07 g/mol
	Density: 1744 kg/m^3
	Melting Temperature: 280 K
	Boiling Temperature: 575.2 K

Note: The melting and boiling temperature values at 1 atm.

Table 2.6. Literature data for 1-iodonaphthalene: thermodynamic properties, studied temperatures, $\Delta_{trans}H^0_m(T)$ and used methods.

Thermodynamic Parameter	**Studied Temperatures (K)**	$\Delta_{trans}H^0_m(T)$ **(kJ.mol^{-1})**	***T* (K)**	**Method**	**References**
$\Delta^l_{cr}H^0_m(T)$		15.91	280		[2]
$\Delta^g_lH^0_m(T)$		72.4 ± 5.9		V	[6]
$\Delta^g_lH^0_m(T)$		66±2	298	V	[7]
$\Delta^g_lH^0_m(T)$	(321-428)	78.9	336		[8]
$\Delta^g_lH^0_m(T)$	(303-347)	69.9 ± 0.3	298	GS	[3]

Note: GS – Gas Saturation/Transpiration; V – Viscosity Gauge.

2.1.2. 2-Halogenated napthalenes

2-Chloronaphthalene

Table 2.7. Properties of 2-chloronaphthalene: CAS number, molar mass, density, melting and boiling temperatures. [1]

Structure	**Molecular Formula:** $C_{10}H_7Cl$
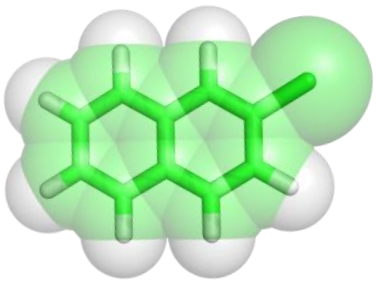	**CAS Number:** 91-58-7
	Molar Mass: 162.62 g/mol
	Density: 1266 kg/m^3
	Melting Temperature: 331-333 K
	Boiling Temperature: 529.2 K

Note: The melting and boiling temperature values at 1 atm.

Table 2.8. Literature data for 2-chloronaphthalene: thermodynamic properties, studied temperatures, $\Delta_{trans}H^0_m(T)$ and used methods.

Thermodynamic Parameter	**Studied Temperatures (K)**	$\Delta_{trans}H^0_m(T)$ **(kJ.mol^{-1})**	***T* (K)**	**Method**	**References**
$\Delta^{l}_{cr}H^0_m(T)$		13.39 ± 0.84	333.2		[9]
$\Delta^{l}_{cr}H^0_m(T)$		14.7	332		[10]
$\Delta^{l}_{cr}H^0_m(T)$		14.7	332		[2]
$\Delta^{l}_{cr}H^0_m(T)$		14.00 ± 0.02	331.2		[11]
$\Delta^{g}_{l}H^0_m(T)$	(400-435)	57.9	417		[8]
$\Delta^{g}_{l}H^0_m(T)$	(323-423)	58.5	373	GS	[12]
$\Delta^{g}_{l}H^0_m(T)$	(332-362)	62.3 ± 1.1	298	GS	[3]
$\Delta^{g}_{cr}H^0_m(T)$		75.7 ± 0.3	298		[3]
$\Delta^{g}_{cr}H^0_m(T)$		82.0 ± 5.9			[13]

Note: GS – Gas Saturation/Transpiration.

2-Bromonaphthalene

Table 2.9. Properties of 2-bromonaphthalene: CAS number, molar mass, density, melting and boiling temperatures. [1]

Structure	**Molecular Formula:** $C_{10}H_7Br$
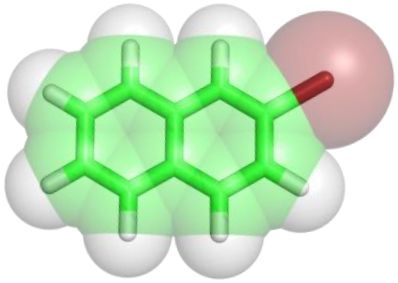	**CAS Number:** 580-13-2
	Molar Mass: 207.7 g/mol
	Density: 1605 kg/m^3
	Melting Temperature: 327-331 K
	Boiling Temperature: 555.9 K

Note: The melting and boiling temperature values at 1 atm.

Table 2.10. Literature data for 2-bromonaphthalene: thermodynamic properties, studied temperatures, $\Delta_{trans}H^0_m(T)$ and used methods.

Thermodynamic Parameter	**Studied Temperatures (K)**	$\Delta_{trans}H^0_m(T)$ **(kJ.mol^{-1})**	***T* (K)**	**Method**	**References**
$\Delta^{l}_{cr}H^0_m(T)$		11.97	332		[10]
$\Delta^{l}_{cr}H^0_m(T)$		14.4	329		[14]
$\Delta^{l}_{cr}H^0_m(T)$		13.2 ± 0.2	328.7		[11]
$\Delta^{g}_{l}H^0_m(T)$	(322-359)	40.4	340	ME, TE	[15]
$\Delta^{g}_{l}H^0_m(T)$	(330-378)	42.5	354		[8]
$\Delta^{g}_{l}H^0_m(T)$	(330-360)	66.08 ± 0.41	298	GS	[3]
$\Delta^{g}_{cr}H^0_m(T)$	(275-378)	64 ± 5	298	ME, TE	[15]
$\Delta^{g}_{cr}H^0_m(T)$		81.2 ± 1.0	298	C	[16]
$\Delta^{g}_{cr}H^0_m(T)$	(319-328)	78.01 ± 0.62	298		[3]
$\Delta^{g}_{cr}H^0_m(T)$	(280-318)	81.60 ± 0.36	298		[3]

Note: GS – Gas Saturation/Transpiration; ME – Mass Effusion/Knudsen Effusion; TE – Torsion Effusion; C – Calorimetric determination.

2-Iodonaphthalene

Table 2.11. Properties of 2-iodonaphthalene: CAS number, molar mass, density, melting and boiling temperatures. [1]

Structure	**Molecular Formula:** $C_{10}H_7I$
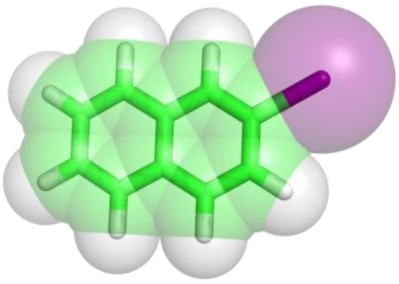	**CAS Number:** 612-55-5
	Molar Mass: 254.07 g/mol
	Density: 1745 kg/m^3
	Melting Temperature: 327.5 K
	Boiling Temperature: 580.5 K

Note: The melting and boiling temperature values at 1 atm.

Table 2.12. Literature data for 2-iodonaphthalene: thermodynamic properties, studied temperatures, $\Delta_{trans}H^0_m(T)$ and used methods.

Thermodynamic Parameter	**Studied Temperatures (K)**	$\Delta_{trans}H^0_m(T)$ **(kJ.mol^{-1})**	***T* (K)**	**Method**	**References**
T_{fus}			327.5 ± 0.5		[10]
$\Delta^l_{cr}H^0_m(T)$		16.04	327.6		[2]
$\Delta^l_{cr}H^0_m(T)$	298	15.58*	327.5		[3]
$\Delta^g_lH^0_m(T)$	280-318	69.8 ± 0.5*	298		[3]
$\Delta^g_{cr}H^0_m(T)$		90.8 ± 6.7			[6]
$\Delta^g_{cr}H^0_m(T)$		85.3 ± 0.5*	298		[3]

Note: *- estimated in reference [3]

2.2. Characterization of compounds

2.2.1. Gas-liquid chromatography

Sample purities were evaluated by gas-liquid chromatography analysis in an Agilent 4890D gas chromatograph equipped with HP-5 column, crosslinked, 5% diphenyl and 95% dimethylpolysiloxane (15m long, 0.530 mm i.d., 1.5 μm film thickness) and a flame ionization detector. The observed final purities are in all the cases higher than 99%.

Figure 2.1. Gas-liquid chromatography apparatus.

The *purity* of each sample was calculated as mass/mass (m/m) fraction, according to equation 2.1:

$$purity(m/m) = A(compound) / \sum A_i \qquad \textbf{(2.1)}$$

where, $A(compound)$ is the area of the GC peak of the compound, and $\sum A_i$ is the sum of the areas of all the peaks presented in the chromatogram.

The sample purities are presented in table 2.13:

Table 2.13. Resume of the supplier information purities and measured purities by GC analysis in (%) of the studied compounds.

Compound	Source	Purity (Lote) / %	Purity (m/m, GC) / %
1-fluoronaphthalene	Sigma-Aldrich	≥ 99%	99.98
1-bromonaphthalene	Sigma-Aldrich	> 97%	99.76
1-iodonaphthalene	TCI-Europe	≥ 98%	99.24
2-chloronaphthalene	TCI-Europe	≥ 98%	99.99*
2-bromonaphthalene	Sigma-Aldrich	≥ 97%	99.50*
2-iodonaphthalene	Sigma-Aldrich	≥ 99%	99.30*

Note: * - GC not made in this three cases. The purity presented is certified by the source.

2.2.2. Fourier Transform Infrared spectroscopy

Introduction

Fourier Transform Infrared Spectroscopy is a spectroscopy technique used to obtain an infrared spectrum of absorption, emission, photoconductivity or Raman scattering of a solid, liquid or gas. [17] A FTIR spectrometer simultaneously collects spectral data in a wide spectral range. This confers a significant advantage over a dispersive spectrometer which measures intensity over a narrow range of wavelengths at a time. FTIR has made dispersive infrared spectrometers obsolete (except for some particular methodologies in the near infrared), opening up new applications of infrared spectroscopy.

The term Fourier transform infrared spectroscopy originates from the fact that a Fourier transform (a mathematical process) is required to convert the raw data into the actual spectrum. The raw data is sometimes called an "interferogram" and Fourier transform spectroscopy is a less intuitive way to obtain the same information. Rather than shining a monochromatic beam of light at the sample, this technique shines a beam containing many frequencies of light at once, and measures how much of that beam is absorbed by the sample. Next, the beam is modified to contain a different combination of frequencies, giving a second data point. This process is repeated

several times. [18] The beam described before is generated by starting with a broadband light source—one containing the full spectrum of wavelengths to be measured. The light shines into a Michelson interferometer—a certain configuration of mirrors, one of which is moved by a motor. As this mirror moves, each wavelength of light in the beam is periodically blocked, transmitted, by the interferometer, due to wave interference. Different wavelengths are modulated at different rates, so that at each moment, the beam coming out of the interferometer has a different spectrum. [18]

Principles of ATR-FTIR

Attenuated Total Reflectance (ATR) is today the most widely used FTIR sampling tool. [19] ATR generally allows qualitative or quantitative analysis of samples with little or no sample preparation, which greatly speeds sample analysis. The main benefit of using ATR comes from the very thin sampling path length and depth of penetration of the IR beam into the sample. This is in contrast to traditional FTIR sampling by transmission where the sample must be diluted with IR transparent salt, pressed into a pellet or pressed to a thin film, prior to analysis to prevent totally absorbing bands in the infrared spectrum. [19]

In transmission spectroscopy, the IR beam passes through the sample and the effective path length is determined by the thickness of the sample and its orientation to the directional plane of the IR beam. With ATR sampling the IR beam is directed into a crystal of relatively high refractive index. The IR beam reflects from the internal surface of the crystal and creates an evanescent wave, which projects orthogonally into the sample in intimate contact with the ATR crystal. Some of the energy of the evanescent wave is absorbed by the sample and the reflected radiation (some is absorbed by the sample) is returned to the detector.

Figure 2.2 and 2.3 presents schematically, the working principle of a single reflection ATR:

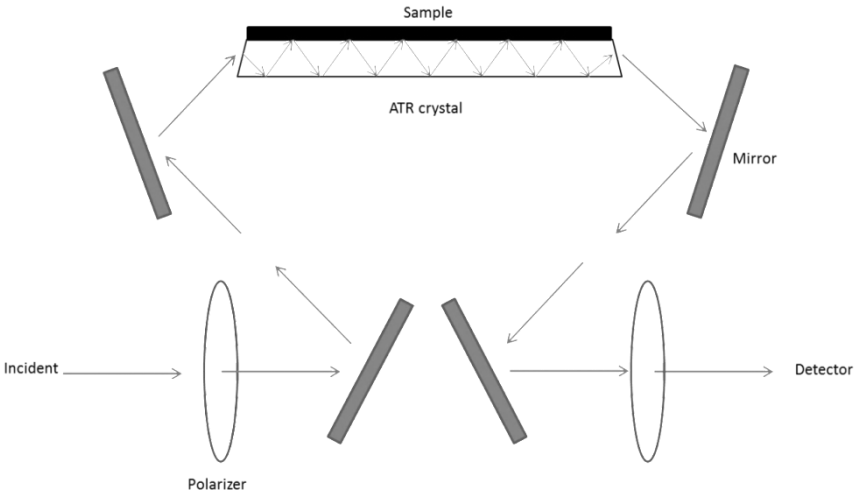

Figure 2.2. Scheme of the ATR-FTIR principle.

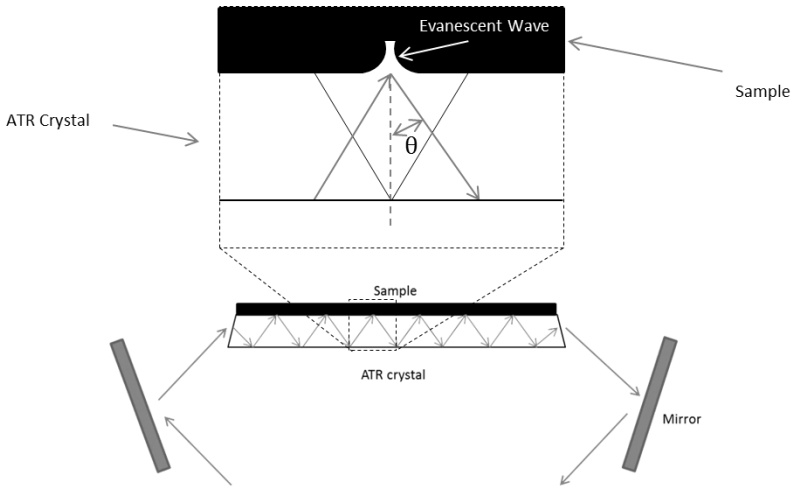

Figure 2.3. Graphical representation of a single reflection ATR.

Some factors have to be taken into account in FTIR/ATR spectroscopy and how it could affect the quality of the final spectrum, such as:

- Refractive indices of the ATR crystal and the sample;
- Angle of incidence of the IR beam;
- Critical angle;
- Depth of penetration;
- Wavelength of the IR beam;
- Number of reflections;
- Quality of the sample etc.

Experimental

The FTIR measurements were performed using a Perkin-Elmer FTIR Spectrum BX II spectrometer, equipped with a GladiATR diamond crystal ATR sampling accessory with temperature control (from 298 K to 470 K).

A total of 30 scans, at each temperature, were taken for the six studied compounds with a spectrum resolution of 4 cm^{-1}. FTIR spectra for 1-fluoronaphthalene, 1-bromonaphthalene and 1-iodonaphthalene were recorded at T = 298.15K. For 2-chloronaphthalene, 2-bromonaphthalene and 2-iodonaphthalene the temperature dependence of the FTIR spectra was evaluated from 298.15 to 343.15 K (at 5 K intervals). The software package Spectrum v5.3.1 from Perkin Elmer was used in the data acquisition and spectral analysis.

Figure 2.4. Spectrum BX-FTIR apparatus used in this work.

Results

The results for 2-bromonaphthalene are presented below. The other spectra of the other compounds are presented in Supplementary Information – Attachment A.

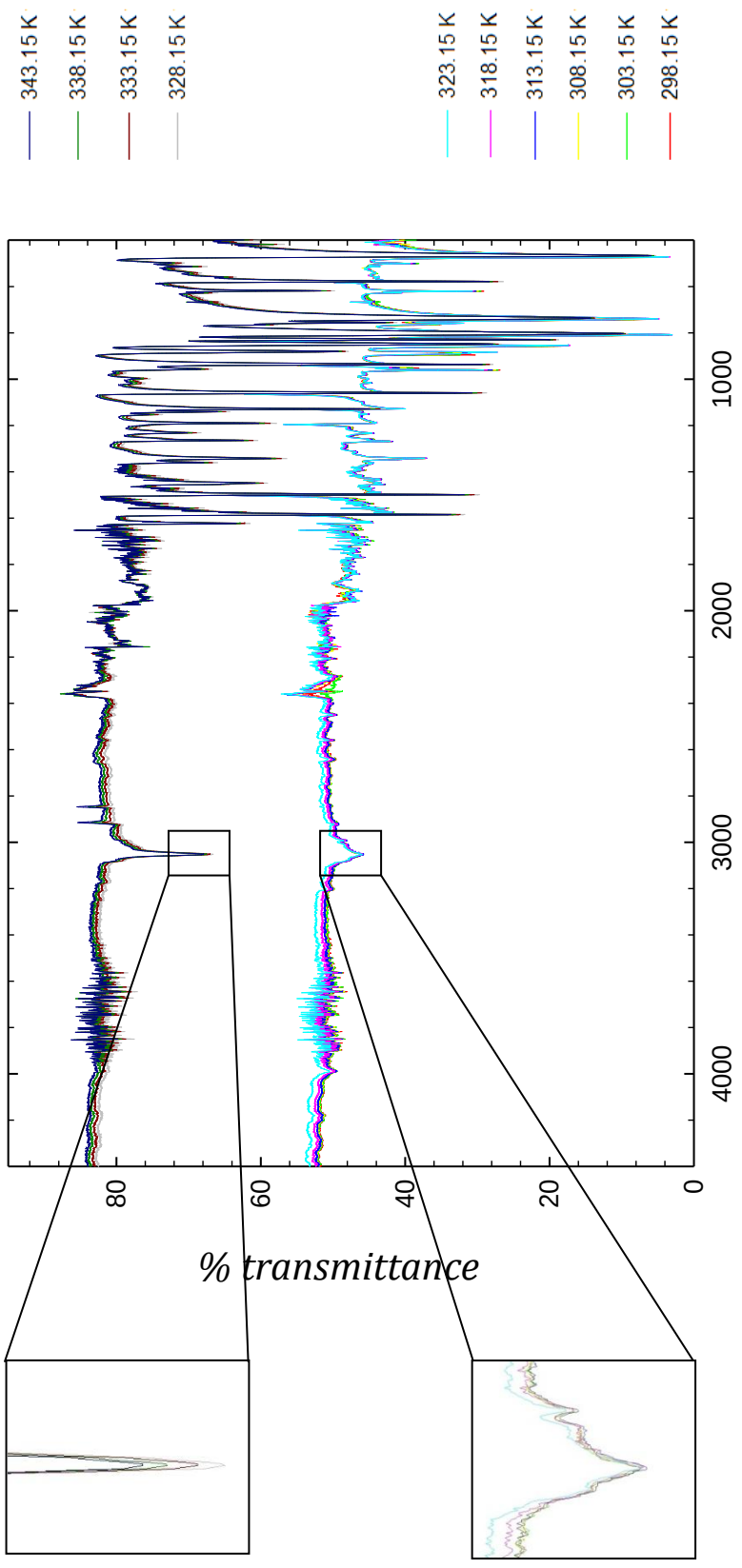

Figure 2.5. FTIR spectra for 2-bromonaphthalene. $298.15 \leq T\,(K) \leq 343.15$

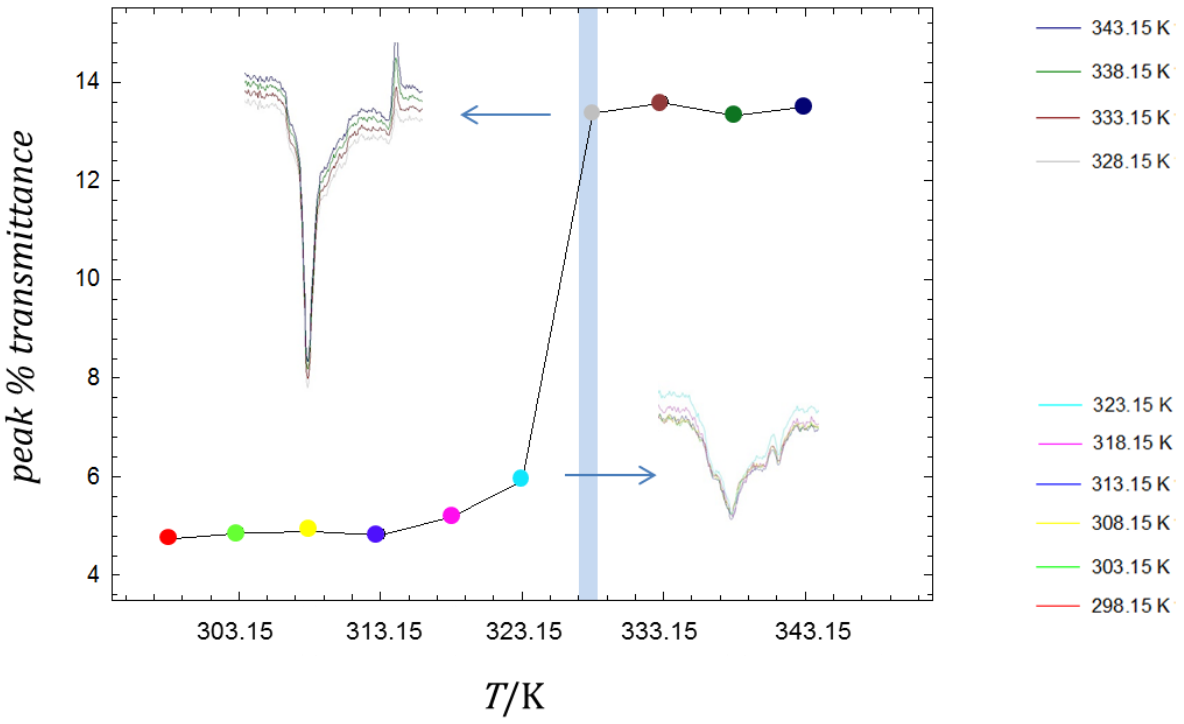

Figure 2.6. Peak high (at v=3056 cm^{-1}, aromatic C-H stretching) as a function of temperature for 2-bromonaphthalene. - Literature fusion temperature of 2-bromonaphthalene. *T*= 327.5 to 329 K [14]

References

[1] http://webbook.nist.gov/

[2] W.E.Acree, Jr., *Thermochim. Acta*, 189 (1991) 37.

[3] Verevkin, S.P., *J.Chem.Thermodyn*., 35 (2003) 1237.

[4] Stephenson, R. M.; Malanowski, S., *Handbook of the Thermodynamics of Organic Compounds*, Elsevier, New York, (1987).

[5] Urbani, M.; Gigli, R.; Picente, V., *J. Chem. Eng. Data*, 25 (1980) 97.

[6] Smith, L., *Acta Chem. Scand.*, (1956) 884-886.

[7] Pelino, M. et al, *Thermochim. Acta*, 41 (1980) 297-304.

[8] Dykyj, J.; Svoboda, J.; Wilhoit, R. C.; Frenkel, M. L.; Hall, K. R., *Vapor Pressure of Chemicals: Part A.*, Berlin, (1999), Springer.

[9] Chanh, N. B. et al, *J. Chim. Phys. Phys. Chim. Biol*., 67 (1970) 1198-1205.

[10] Khetarpal, K. et al., *Indian J. Chem*., 20 (1981) 544.

[11] Calvet, T. et al, *J. Chem. Phys.,* 110 (1999) 4841-4846.

[12] Lei, Y. D.; Wania, F.; Shiu, W. Y., *J. Chem. Eng. Data*, 44 (1999) 577.

[13] Smith, L.; Bjellerup, L.; Krook, S.; Westermark, H., *Acta Chem. Scand*., 7 (1953) 65.

[14] Domalski, E. S.; Hearing, E. D., *J. Phys. Chem. Ref. Data,* 25 (1996) 1.

[15] Ferro, D.; Piacente, V.; Pelino, M., *Ver. Roum. Chim*., 26 (1981) 9.

[16] Ribeiro da Silva, M. A. V.; Ferrao, M. L. C. C. H.; Lopes, A. J. M., *J. Chem. Thermodyn.,* 25 (1993) 229.

[17] Kirshna, G.M. et al*, Int. J. Pharm*., 3 (2013) 396-402.

[18] Saraswathi, M. et al, *Int. J. ChemTech*., 4 (2012) 1343-1349.

[19] Pike Technologies, *ATR-Theory and Applications*, Note-0402 (2004).

Chapter 3

Vapor Pressure Measurements

3.1. Introduction

- 3.1.1. Concepts
- 3.1.2. Vapor pressure equations
  - 3.1.2.1. Clapeyron equation
  - 3.1.2.2. Clausius-Clapeyron equation
  - 3.1.2.3. Clarke-Glew equation
- 3.1.3. Thermodynamic properties calculations at T = 298.15 K
- 3.1.4. The arc method

3.2. The experimental set-up

- 3.2.1. The diaphragm capacitance manometers
- 3.2.2. Tubing
- 3.2.3. Sample cell
- 3.2.4. Vacuum system
- 3.2.5. Temperature control
- 3.2.6. Data acquisition and control

3.3. Experimental procedure

3.4. Experimental results

- 3.4.1. Results of 1-halogenated naphthalenes
  - 3.4.1.1. Results for 1-fluoronaphthalene
  - 3.4.1.2. Results for 1-bromonaphthalene
  - 3.4.1.3. Results for 1-iodonaphthalene
- 3.4.2. Results of 2-halogenated naphthalenes
  - 3.4.2.1. Results for 2-chloronaphthalene
  - 3.4.2.2. Results for 2-bromonaphthalene
  - 3.4.2.3. Results for 2-iodonaphthalene

References

3.1. Introduction

3.1.1. Concepts

Phase equilibria and phase diagrams

A phase is a part of a system, uniform throughout in chemical composition and physical properties. It is separated from other homogeneous parts of the system by boundary surfaces. The phase behaviour exhibited by pure substances is not simple and is quite varied, but thermodynamics help us to understand these phenomena. As can be seen in this chapter, the Clapeyron equation, expresses $\mathrm{d}p/\mathrm{d}T$ for a two-phase system containing one component at equilibrium in terms of other thermodynamic quantities. All the phases of a substance at various temperature and pressures, and the relation between them, can be represented by a phase diagram. A phase diagram summarize the solid-liquid-gas behaviour of a substance (figure 3.1). It indicates under which conditions of pressure and temperature the various phases of a substance may exist in equilibrium.

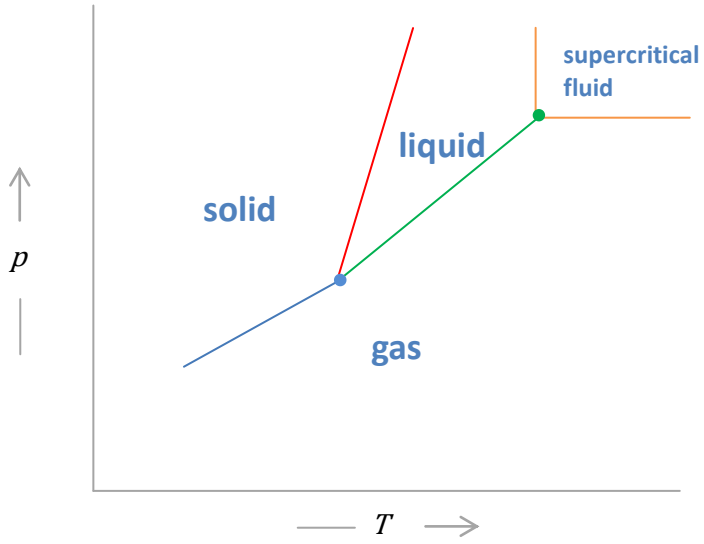

Figure 3.1. Schematic representation of a phase diagram of a pure substance presenting only one crystalline phase. ---- solid-gas equilibrium curve; ---- solid-liquid equilibrium curve; ---- liquid-gas equilibrium curve; ● - triple point; ● - critical point.

The lines that separate two phases indicate the pressures and temperatures at which they coexist at equilibrium (the coexistence curves). At the triple point, there is an equilibrium between three phases (in the figure 3.1., crystalline, liquid and gaseous phases).

When a crystalline solid is heated at constant pressure its chemical potential μ changes accordingly to figure 3.2, being the stable phase, at each temperature, the one presented the lowest value of μ.

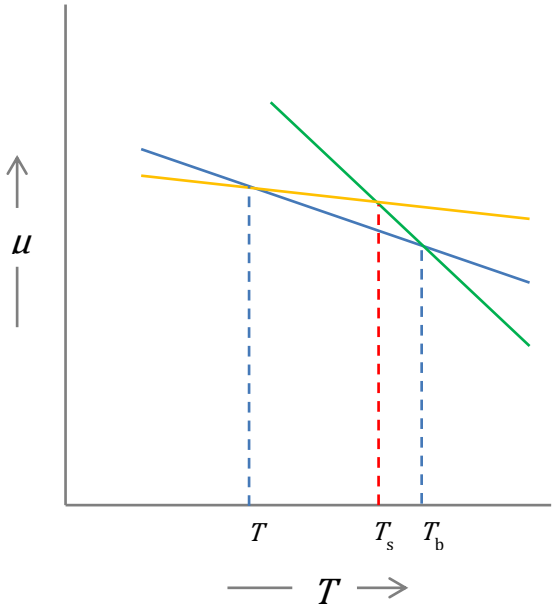

Figure 3.2. Dependence of the chemical potential of crystal, liquid and gas phases on temperature at constant pressure. **Crystal**; **Liquid**; **Gas**; T_m - melting temperature; T_s - hypothetical sublimation temperature; T_b - boiling temperature.

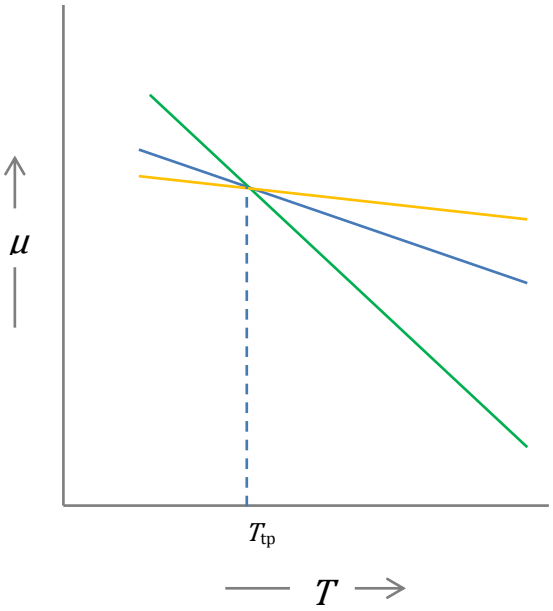

Figure 3.3. Dependence of the chemical potential of crystal, liquid and gas phases on temperature at constant pressure. **Crystal**; **Liquid**; **Gas**; T_{tp} - triple point temperature.

As can be seen in figures 3.2. and 3.3., if two or three phases of a single component have the same chemical potential at a certain temperature and pressure, they will coexist at equilibrium as at the melting point T_m, boiling point T_b, or even triple point. Below the melting point, the crystalline phase has the lowest chemical potential and is therefore the most stable phase. Between T_m and T_b the most stable phase is the liquid and after T_b is the gas phase.

Vapor pressure

Macroscopic point of view

From a macroscopic point of view, vapor pressure is the pressure exerted by a vapor in thermodynamic equilibrium with its condensed phases (solid or liquid) at a given temperature. The vapor pressure is a measure of the tendency of particles to escape from the liquid (or a solid) to the gas phase. A substance with higher vapor pressure at a given temperature is often referred to as the most volatile.

Microscopic point of view

At a microscopic point of view, when a solid or a liquid evaporates to a gas, at the temperature *T* and in a closed container, the molecules cannot escape. Some of the gas molecules will eventually strike the condensed phase and condense back into it. When the rate of condensation of the gas becomes equals the rate of evaporation of the liquid or solid, the amount of gas, liquid and/or solid no longer changes and the gas in the container is in equilibrium with the condensed phase at that temperature.

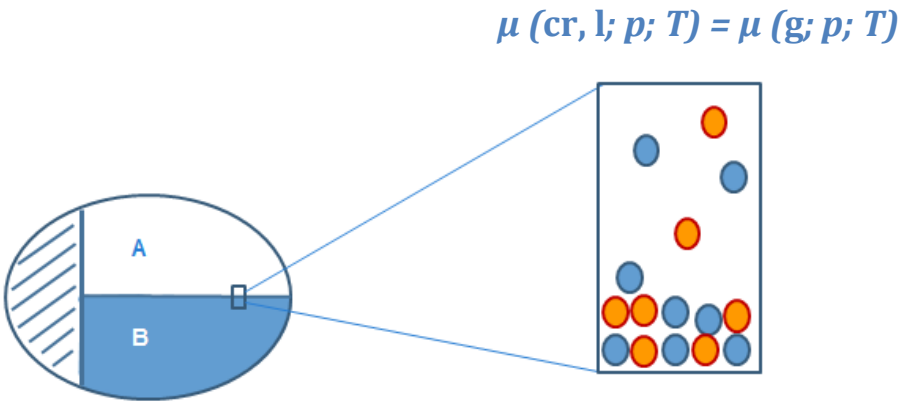

Figure 3.4. Evaporation process - a schematic representation. A- gaseous phase; B- condensed phase (solid or liquid). The two phases are in equilibrium. ● and ● represent the same compound.

Factors that may affect vapor pressure

Type of molecules: at a fixed temperature, the molecules that constitute the condensed phase determine the value of the vapor pressure, so, if the intermolecular forces between molecules are strong enough, the vapor pressure will be relatively low and vice-versa.

Temperature: the vapor pressure of a pure substance increases exponentially with temperature.

3.1.2. Vapor pressure equations

3.1.2.1. Clapeyron equation

Considering a system with one-component and two phases (α and β) at equilibrium, the pressure, the temperature, and chemical potential must be the same in the two phases.

For the chemical potentials,

$$\mu_{\alpha} = \mu_{\beta} \qquad \textbf{(3.1)}$$

When the temperature is changed at constant pressure, or the pressure is changed at constant temperature, one of the phases will vanish. However, if the temperature and pressure are both changed in such a way that the two chemical potentials remain equal to each other, the two phases will continue to coexist. The plot of pressure versus temperature along which the two phases coexist is referred to as the coexistence curve. The necessary relation for $\mathrm{d}p/\mathrm{d}T$ was derived by Clapeyron.

For a change of pressure and temperature along the coexistence curve,

$$d\mu_{\alpha} = d\mu_{\beta} \qquad \textbf{(3.2)}$$

since the chemical potential is equal to the molar Gibbs energy for a one-component system, $d\mu = dG_{\mathrm{m}} = V_{\mathrm{m}}dp - S_{\mathrm{m}}dT$. Thus,

$$V_{\alpha,\mathrm{m}}dp - S_{\alpha,\mathrm{m}}dT = V_{\beta,\mathrm{m}}dp - S_{\beta,\mathrm{m}}dT \qquad \textbf{(3.3)}$$

or

$$\frac{dp}{dT} = \frac{S_{\beta,\mathrm{m}} - S_{\alpha,\mathrm{m}}}{V_{\beta,\mathrm{m}} - V_{\alpha,\mathrm{m}}} = \frac{\Delta S_{\mathrm{m}}}{\Delta V_{\mathrm{m}}} = \frac{\Delta H_{\mathrm{m}}}{T\Delta V_{\mathrm{m}}} \qquad \textbf{(3.4)}$$

This equation is referred as the Clapeyron equation, and it may be applied to vaporization, sublimation, fusion, or the transition between two crystalline phases of a pure substance. The molar enthalpies of sublimation, fusion, and vaporization at a temperature, *T*, are related by:

$$\Delta^{\mathrm{g}}_{\mathrm{cr}}H_{\mathrm{m}}(T) = \Delta^{\mathrm{l}}_{\mathrm{cr}}H_{\mathrm{m}}(T) + \Delta^{\mathrm{g}}_{\mathrm{l}}H_{\mathrm{m}}(T) \qquad \textbf{(3.5)}$$

So, the heat required to sublime a given amount of the solid is the same whether this process is carried out directly or by first melting the solid and then vaporizing the liquid, at the same temperature.

3.1.2.2. Clausius-Clapeyron equation

For vaporization and sublimation, Clausius showed how the Clapeyron equation may be simplified by assuming that the vapor obeys the ideal gas law and by neglecting the molar volume of the liquid $V_{l,m}$ or the solid $V_{cr,m}$ in comparison with the molar volume of the gas $V_{g,m}$. Substituting RT/p for $V_{g,m}$:

$$\frac{dp}{dT} = \frac{\Delta^{g}_{cr,l}H_{m}}{TV_{g,m}} = \frac{p\Delta^{g}_{cr,l}H_{m}}{RT^{2}} \qquad \textbf{(3.6)}$$

On rearrangement of the previous equation:

$$\frac{dp}{p} = d\ln\frac{p}{p^{0}} = \frac{\Delta^{g}_{cr,l}H_{m}}{RT^{2}}dT \qquad \textbf{(3.7)}$$

where p^{0} is the used standard pressure. Integrating on the assumption that $\Delta^{g}_{l}H_{m}$ is independent of pressure and temperature yields:

$$\int d\ln\frac{p}{p^{0}} = \frac{\Delta^{g}_{cr,l}H}{R}\int T^{-2}dT \qquad \textbf{(3.8)}$$

$$\ln\frac{p}{p^{0}} = \frac{\Delta^{g}_{cr,l}H}{RT} + C \qquad \textbf{(3.9)}$$

where C is the integration constant. This suggests that a plot of $\ln(p/p^{0})$ versus $1/T$ should be linear, and this is borne out by data on both vaporization and sublimation processes, in short temperature intervals.

Frequently, it is more convenient to use the equations 3.11 or 3.12 obtained by integrating between limits, T_1 and T_2 and the respective vapor pressures p_1 and p_2, as follows:

$$\int_{p_1}^{p_2} d\ln\frac{p}{p^0} = \frac{\Delta^{\mathrm{g}}_{\mathrm{cr,l}}H}{R}\int_{T_1}^{T_2} T^{-2}dT \qquad \textbf{(3.10)}$$

$$\ln\frac{p_2}{p_1} = -\frac{\Delta^{\mathrm{g}}_{\mathrm{cr,l}}H}{R}\left[\frac{1}{T_2}-\frac{1}{T_1}\right] \qquad \textbf{(3.11)}$$

$$\ln\frac{p_2}{p_1} = \frac{\Delta^{\mathrm{g}}_{\mathrm{cr,l}}H(T_2-T_1)}{RT_1T_2} \qquad \textbf{(3.12)}$$

To represent the vapor pressure as a function of temperature over a wide range, it is necessary to take the temperature dependence of $\Delta^{\mathrm{g}}_{\mathrm{cr,l}}H^0_{\mathrm{m}}$ into account. Another limitation to this simple equation is that the vapor has been assumed as an ideal gas, which for sub-atmospheric pressures it is not an important issue.

Over narrow ranges of temperature, the enthalpy of vaporization can be taken as a linear function of temperature. However, in calculating vapor pressures over a wide range of temperature the enthalpy of vaporization approaches zero as the temperature approaches the critical temperature.

3.1.2.3. Clarke-Glew equation

The Clarke-Glew equation can be deduced considering that the vapor pressure is continuous differentiable, the same happening with the thermodynamic properties $\Delta^{g}_{cr,l}G^{0}_{m}$, $\Delta^{g}_{cr,l}H^{0}_{m}$ and $\Delta^{g}_{cr,l}C^{0}_{p,m}$ [2].

Given the fundamental thermodynamic relationships for a temperature T:

$$R.\ln\left(\frac{p}{p^{0}}\right) = -\frac{\Delta^{g}_{cr,l}G^{0}_{m}(T)}{T} = \Delta^{g}_{cr,l}S^{0}_{m}(T) - \frac{\Delta^{g}_{cr,l}H^{0}_{m}(T)}{T} \quad \textbf{(3.13)}$$

Considering a reference temperature θ, and the standard pressure p^{0}, the standard molar thermodynamic properties at this temperature, $\Delta^{g}_{cr,l}H^{0}_{m}(T)$ can be defined as a disturbance of the value of $\Delta^{g}_{cr,l}H^{0}_{m}(\theta)$:

$$\Delta^{g}_{cr,l}H^{0}_{m}(T) = \Delta^{g}_{cr,l}H^{0}_{m}(\theta) + \int_{\theta}^{T}\Delta^{g}_{cr,l}C^{0}_{p,m}(T)dT \quad \textbf{(3.14)}$$

Similarly, $\Delta^{g}_{cr,l}S^{0}_{m}(T)$ can be defined as:

$$\Delta^{g}_{cr,l}S^{0}_{m}(T) = \Delta^{g}_{cr,l}S^{0}_{m}(\theta) + \int_{\theta}^{T}\frac{\Delta^{g}_{cr,l}C^{0}_{p,m}(T)}{T}dT \quad \textbf{(3.15)}$$

where $\Delta^{g}_{cr,l}C^{0}_{p,m}(T)$ may be represented by the Taylor series expansion [2]:

$$\begin{aligned}\Delta^{g}_{cr,l}C^{0}_{p,m}(T) &= \Delta^{g}_{cr,l}C^{0}_{p,m}(\theta) + (d\Delta^{g}_{cr,l}C^{0}_{p,m}/dT)_{\theta}(T-\theta) \\ &+ \frac{1}{2}(d^{2}\Delta^{g}_{cr,l}C^{0}_{p,m}/dT^{2})_{\theta}(T-\theta)^{2} + \frac{1}{6}(d^{3}\Delta^{g}_{cr,l}C^{0}_{p,m}/dT^{3})_{\theta}(T-\theta)^{3} + \ldots\end{aligned} \quad \textbf{(3.16)}$$

considering that $(d^3\Delta^{g}_{cr,l}C^{0}_{p,m}/dT^3)_\theta$ is constant for any value of T, any higher derivative of greater order are necessarily zero.

$$\Delta^{g}_{cr,l}H^{0}_{m}(T) = \Delta^{g}_{cr,l}H^{0}_{m}(\theta) + \Delta^{g}_{cr,l}C^{0}_{p,m}(\theta)(T-\theta) + \frac{1}{2}(d\Delta^{g}_{cr,l}C^{0}_{p,m}/dT)_\theta(T-\theta)^2 + \frac{1}{6}(d^2\Delta^{g}_{cr,l}C^{0}_{p,m}/dT^2)_\theta(T-\theta)^3 + \frac{1}{24}(d^3\Delta^{g}_{cr,l}C^{0}_{p,m}/dT^3)_\theta(T-\theta)^4 + \ldots \quad \textbf{(3.17)}$$

Given the previous relationships, it is possible to derive the next equation:

$$R\ln(p/p^0) = -\frac{\Delta^{g}_{cr,l}G^{0}_{m}(\theta)}{\theta} + \Delta^{g}_{cr,l}H^{0}_{m}(\theta)\left(\frac{1}{\theta}-\frac{1}{T}\right) + \Delta^{g}_{cr,l}C^{0}_{p,m}(\theta)\left[\left(\frac{\theta}{T}\right)-1+\ln\left(\frac{T}{\theta}\right)\right] + \frac{\theta}{2}(d\Delta^{g}_{cr,l}C^{0}_{p,m}/dT)_\theta\left[\left(\frac{T}{\theta}\right)-\left(\frac{\theta}{T}\right)-2\ln\left(\frac{T}{\theta}\right)\right]+\ldots \quad \textbf{(3.18)}$$

Applying this equation to experimental values of vapor pressures, the terms corresponding to the derivative of $\Delta^{g}_{cr,l}C^{0}_{p,m}$ of greater order, are usually disregarded, if it appears that their values are not significantly different from zero, within the experimental range. In order to maintain the Taylor series expansion valid, when a term corresponding to a particular derivative order is discarded, all the terms related to higher order derivatives must be also discarded. For an experimental range of temperatures below 60 K, there is no advantage in the use of an equation with more than three parameters. [3,4]

$$R\ln(p/p^0) = -\frac{\Delta^{g}_{cr,l}G^{0}_{m}(\theta)}{\theta} + \Delta^{g}_{cr,l}H^{0}_{m}(\theta)\left(\frac{1}{\theta}-\frac{1}{T}\right) + \Delta^{g}_{cr,l}C^{0}_{p,m}(\theta)\left[\left(\frac{\theta}{T}\right)-1+\ln\left(\frac{T}{\theta}\right)\right] \quad \textbf{(3.19)}$$

For experimental range of temperatures lower than 20 K, it is usual to use only two parameters $\Delta^{g}_{cr,l}G^{0}_{m}(\theta)$ and $\Delta^{g}_{cr,l}H^{0}_{m}(\theta)$, which is clearly equivalent to using the Clausius-Clapeyron Equation. The use of the equation with three parameters in

reduced experimental intervals, often leads to the derivation of incorrect values of $\Delta^{g}_{cr,l}C^{0}_{p,m}$, but a known value of $\Delta^{g}_{cr,l}C^{0}_{p,m}$ may be imputed in equation 3.19.

3.1.3. Thermodynamic parameters calculations at *T*=298.15K

Enthalpy of Sublimation

The standard enthalpy of sublimation at temperature T_1, $\Delta^{g}_{cr}H^{0}_{m}(T_1)$, represents the enthalpic variation of the isothermal procedure described as:

crystal (standard state) $\longrightarrow$ gas (standard state)

The standard state of a crystal at the temperature T_1, is the state corresponding to its most stable crystalline form at that temperature and at the standard pressure of 0.1 MPa. For a gas, the standard state at temperature T_1 corresponds to the hypothetical ideal gas at this temperature and at the standard pressure of 0.1 MPa. This state is enthalpically equivalent to the state of the real gas, at the considered temperature and null pressure.

The standard enthalpy of sublimation at temperature T_1, $\Delta^{g}_{cr}H^{0}_{m}(T_1)$, can be related to the measured enthalpy of sublimation at a pressure p_1, at the same temperature, $\Delta^{g}_{cr}H_{m}(T_1)$, by the following scheme:

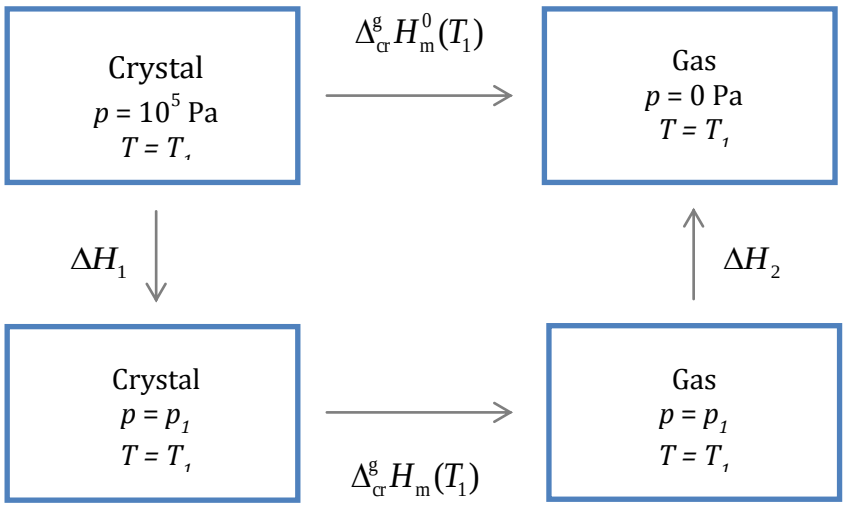

Based on this scheme we can derive the following equation:

$$\Delta_{cr}^{g} H_m^0(T_1) = \Delta H_1 + \Delta_{cr}^{g} H_m(T_1) + \Delta H_2 \qquad \textbf{(3.20)}$$

where the enthalpic variations ΔH_1 e ΔH_2 are defined, respectively by the equations 3.21 and 3.22.

$$\Delta H_1 = \int_{10^5\,Pa}^{p_1} \left[-T_1 \left(\frac{\partial V_{cr,m}}{\partial T} \right)_p + V_{cr,m} \right] dp \qquad \textbf{(3.21)}$$

$$\Delta H_2 = \int_{p_1}^{0} \left[-T_1 \left(\frac{\partial V_{g,m}}{\partial T} \right)_p + V_{g,m} \right] dp \qquad \textbf{(3.22)}$$

Integrating equation 3.21 and considering T_1 = 298.15 K, the molar volume should be around 10^{-1} $dm^3 \cdot mol^{-1}$. [5] ΔH_1 will increase as p_1 approaches to zero, peaking

near 10^4 Pa.dm^3.mol^{-1} which corresponds to ΔH_1=10 J.mol^{-1}. Looking at this low value, ΔH_1 and ΔH_2 can be neglected in equation 3.20with no problems.

In conclusion, it is possible to consider that the equality $\Delta_{cr}^{g} H_m(T_1) = \Delta_{cr}^{g} H_m^0(T_1)$ does not introduce significant errors. A value obtained for the standard molar enthalpy of sublimation with respect to a temperature T_1, $\Delta_{cr}^{g} H_m^0(T_1)$, can be converted into an amount corresponding to a temperature, T_2, $\Delta_{cr}^{g} H_m^0(T_2)$, using the equation 3.23:

$$\Delta_{cr}^{g} H_m^0(T_2) = \Delta_{cr}^{g} H_m^0(T_1) + \int_{T_1}^{T_2} \Delta_{cr}^{g} C_{p,m}^0 dT \qquad \textbf{(3.23)}$$

In the case of the influence of temperature on the term $\Delta_{cr}^{g} C_{p,m}^0$ might be neglected in the temperature range considered, it is possible to use the equation 3.24:

$$\Delta_{cr}^{g} H_m^0(T_2) = \Delta_{cr}^{g} H_m^0(T_1) + (T_2 - T_1)\Delta_{cr}^{g} C_{p,m}^0 \qquad \textbf{(3.24)}$$

where the constant value of $\Delta_{cr}^{g} C_{p,m}^0$ is related to any temperature within the range considered.

Entropy of Sublimation

Considering that the value of $\Delta_{cr}^{g} C_{p,m}^0$ does not change with temperature, the standard molar entropy of sublimation at temperature 298.15 K can be obtained from equation 3.25, where the first term, $\Delta_{cr}^{g} S_m(T_1, p_1)$, represents the molar entropy of sublimation at the temperature T_1 and at a pressure p_1.

$$\Delta_{cr}^{g} S_{m}^{0}(298.15) = \Delta_{cr}^{g} S_{m}(T_1, p_1) + \Delta_{cr}^{g} C_{p,m}^{0} \ln\left(\frac{298.15K}{T_1}\right) - R\ln\left(\frac{p^0}{p_1}\right) \quad \textbf{(3.25)}$$

Gibbs Energy of Sublimation

Based on the two previously discussed standard thermodynamic properties at the temperature 298.15 K, it is possible to calculate the standard Gibbs energy of sublimation at the same temperature, $\Delta_{cr}^{g} G_{m}^{0}$, using equation 3.25:

$$\Delta_{cr}^{g} G_{m}^{0}(298.15K) = \Delta_{cr}^{g} H_{m}^{0}(298.15K) - 298.15\Delta_{cr}^{g} S_{m}^{0}(298.15K) \quad \textbf{(3.26)}$$

For the vaporization process an analogous formalism can be used.

3.1.4. The arc method

In order to analyze the quality of the obtained results the arc method [7] was used. This method was developed by Genderen and Oonk in the Utrecht University, Holland and it uses a simple expression:

$$\ln f = \ln(p / p^0) - \alpha + \beta / T \quad \textbf{(3.27)}$$

The α and β parameters are chosen in such a way that ln *f* is close to 0 for the two extreme pairs of data set (*p,T*). The arc-like appearance is due to the change of $\Delta_{cr,l}^{g} H_{m}^{0}$ with the temperature (which is $\Delta_{cr,l}^{g} C_{p,m}^{0}$).

This method was used when a temperature interval of at least 50 K is presented and when the pressure values are not highly affected by the uncertainty of the apparatus, specially at lower temperatures.

3.2. The experimental set-up

In this work, a static method based on a diaphragm capacitance manometer [8] was used to measure the vapor pressures of six persistent organic pollutants, previously described in Chapter 2.

The vapor pressures of liquid phases of 1-fluoro, 1-bromo and 1-iodonaphthalene in the temperature ranges (274 to 348) K, (281 to 396) K, (304 to 393) K, and the vapor pressures of crystalline and liquid phases of 2-chloro, 2-bromo and 2-iodonaphthalenes were measured in the temperature ranges (280 to 384) K, (291 to 385) K and (302 to 364) K, respectively.

From the experimental results (p,T) measured using this apparatus, the standard molar enthalpies, entropies and Gibbs energies of sublimation and of vaporization, at T = 298.15 K, as well as the triple points (p,T) coordinates, were derived using eq. 3.19. The phase diagrams will be presented in this chapter.

The experimental set-up (figure 3.5) may be divided in five parts: the diaphragm capacitance manometer; the tubing between the cell and the manometer; the cell where the sample is placed; the vacuum system and the temperature control system.

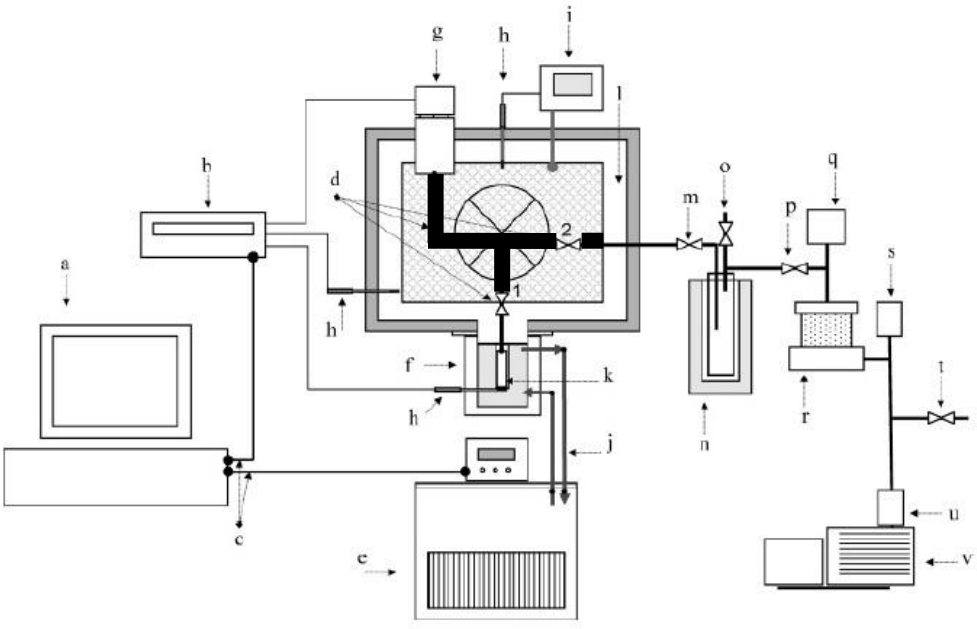

Figure 3.5. Photo and Schematic representation of the measuring system: **a** - computer; **b** - data logger Keithley 2700; **c -** RS 232C; **d** - high-temperature all metal electro pneumatic valves VAT series 57; **e** - temperature-controlled bath JULABO model F33-MW; **f** - heat exchange tube cavity; **g** - pressure transducer, MKS Baratron model 631A01TBEH; **h** - temperature sensor, Pt 100; **I** - PID temperature controller; **j** - bath fluid circulation tubes; **k** - sample cell; **l** - forced air convection oven; **m** - Teflon greaseless valve J. Young SPOR/20; **n** - glass liquid nitrogen trap; **o** - Teflon greaseless gas admittance valve J. Young ALS1; **p** - isolation valve VAT series 010; **q**, wide range vacuum gauge Edwards WRG-S; **r**, turbomolecular vacuum pump system Edwards model EXT70; **s**, Pirani gage Edwards APG-M; **t**, air admittance valve; **u**, foreline trap Edwards FL20K; **v**, rotary pump Edwards RV3. (figure from [8])

3.2.1. The diaphragm capacitance manometers

The pressure is measured using absolute capacitance manometers MKS Baratron 631A, one for measurements below 1.3 x 10^2 Pa (MKS Baratron 631A01TBEH) and other for measurements of less than 1.3 x 10^3 Pa (MKS Baratron 631A11TBFP). Figure 3.6 shows a schematic representation of the MKS Baratron capacitance manometer 631A:

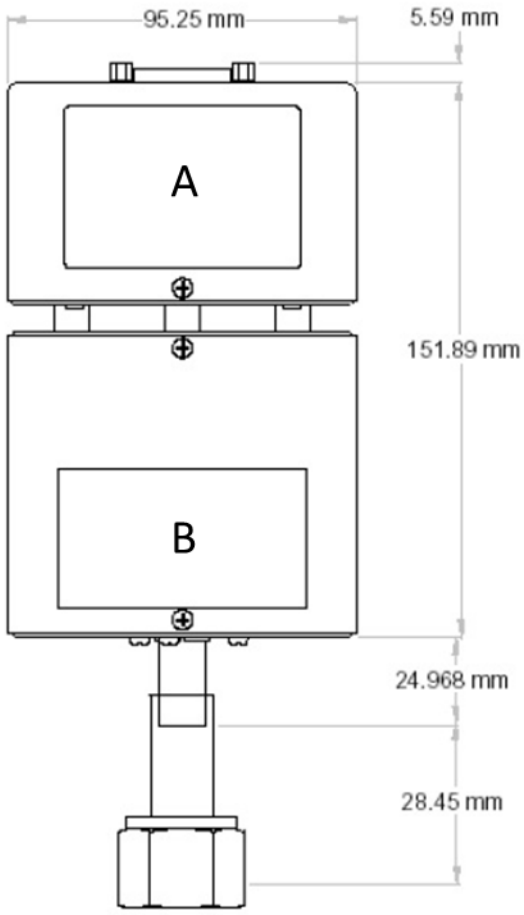

Figure 3.6. Schematic representation of the MKS Baratron capacitance manometer 631A. A – electronic compartment; B – diaphragm and electrode compartment. (figure from [9])

The capacitance manometer 631A has two compartments. The compartment A contains the electronic component and must be kept at a temperature lower than 338 K. The compartment B contains a diaphragm (under tension) (figure 3.7 - F) and a fixed

electrode system (figure 3.7 – E) operating at a self-controlled temperature of 423 K (in case of the MKS Baratron manometer 631A01TBEH) and 473 K in the case of MKS Baratron 631A11TBFP). The manometer is connected to the tubing through a Swagelok / Cajon VCR 8-female linkage, allowing the exchange of manometers.

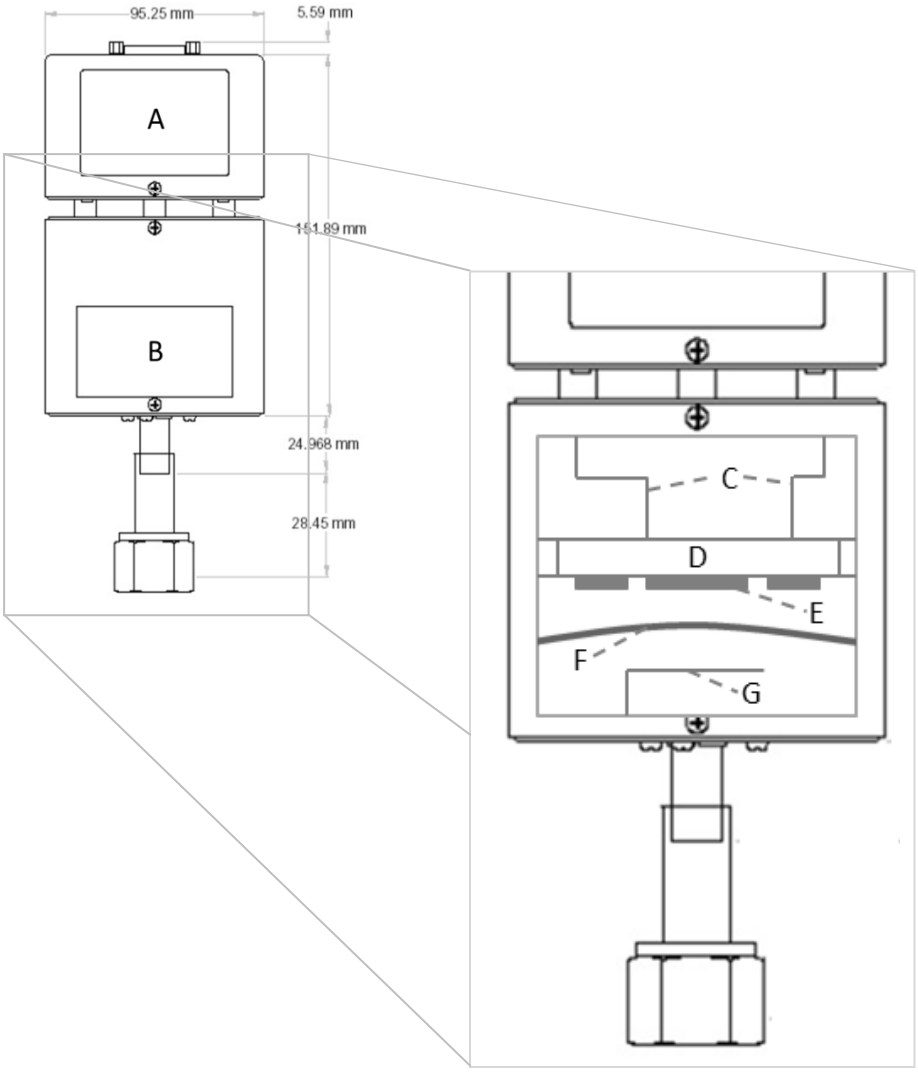

Figure 3.7. Schematic representation of the MKS Baratron capacitance manometer 631A. C – electronic connections; D – ceramic structure that support the electrodes; E – electrodes; F – metallic diaphragm; G – diaphragm protection. (adapted from the source [9])

Note: The space between D and top of compartment B is under ultra-vacuum.

3.2.2. Tubing

The tubing is made of standard stainless steel 304 with an internal diameter of 17 mm, linked by ConFlat DN 16 CF connections (figure 3.8). Such links are metal-metal kind and suitable for ultra-high vacuum (10^{-11} Pa) and are appropriate for broad temperature ranges [73-723] K.

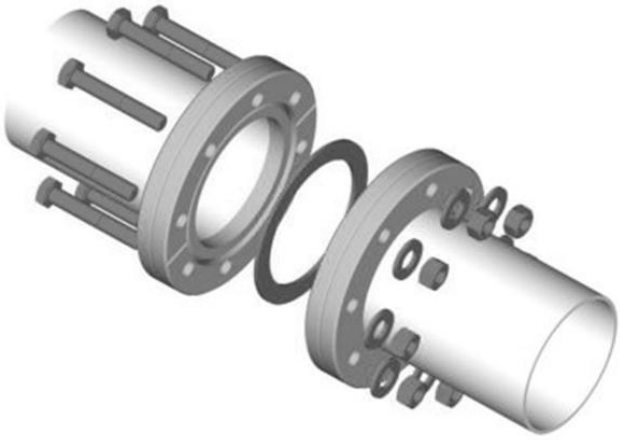

Figure 3.8. Schematic representation of the ConFlat DN16 CF connection. [10]

Two angle valves VAT 57 series all-metal (figure 3.9) are used. These valves are suitable for use in ultra-high vacuum and use VATRING technology, where the closure is carried out by a patented tapered metallic ring.

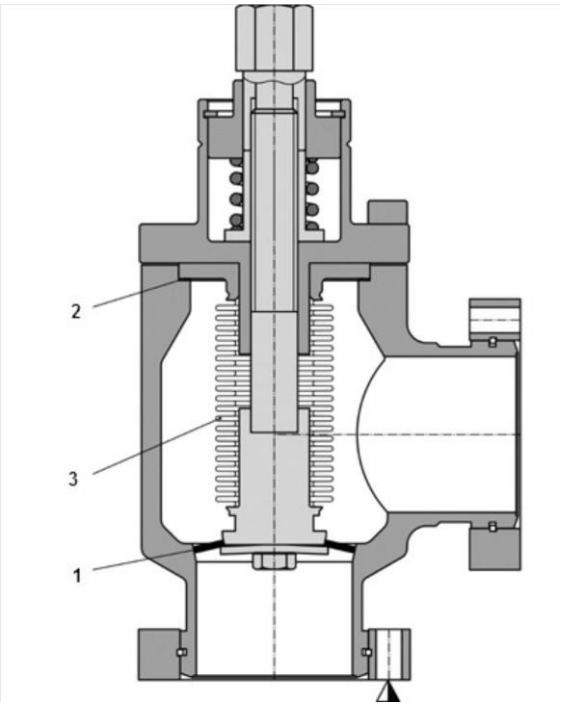

Figure 3.9. Schematic representation of the angle valves VAT 57. 1 – VATRING; 2 – insulator seal; 3 – bellow. [11]

The valves are controlled by an electro-pneumatic system using compressed air at a pressure of 4×10^5 to 5×10^5 Pa, that allows their remote control (figure 3.10). The tubing is inside an oven, at a controlled temperature, slightly higher than the temperature of the sample and lower than the gauge temperature.

Since the upper compartment of the gauge only operates at temperatures lower than 338 K and the electronic components of the valves require temperatures lower than 353 K, these thermal sensitive parts are kept out of the oven. The oven was built by the firm Termolab being constituted of two layers of stainless steel, 2 mm thick, separated by 20 mm of thermal insulating material. The oven temperature is homogenized by forced convection of air, through a fan existing in the rear part and the temperature control is achieved by a Eurotherm PID controller 2116 connected to a platinum resistance thermometer Pt100. The monitoring of the temperature of the tubing is carried out using another platinum resistance thermometer Pt100, being both connected to the data acquisition system.

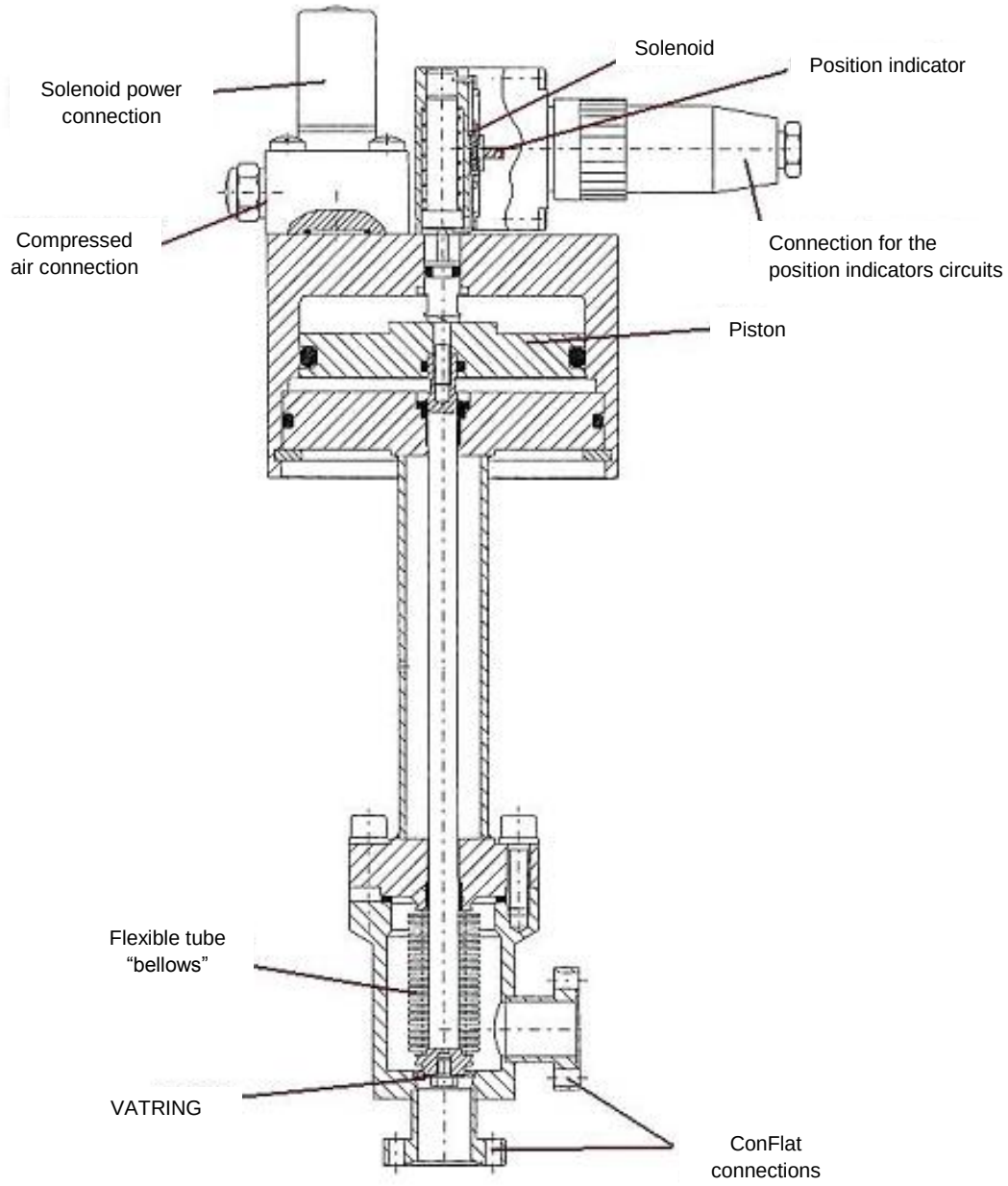

Figure 3.10. Schematic representation of the system that allows the control of all the two valves remotely. [9]

3.2.3. Sample cell

The sample cell is a cylindrical stainless steel tube, closed at the bottom, of 110 mm height and internal diameter φ_i = 12.7 mm. The cell is linked to the tubing through an 8 VCR metal to metal connection where a stainless steel is crushed.

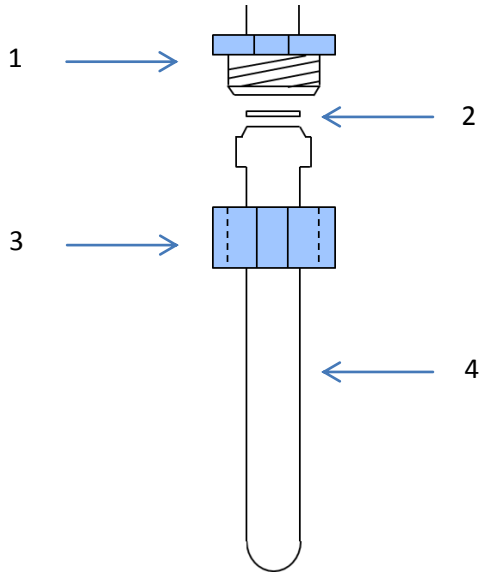

Figure 3.11. Schematic representation of the sample cell. 1 – VCR male connection; 2 – inox steel ring; 3 – VCR female connection; 4 – sample cell.

The sample cell is thermostated using a double wall vessel, schematically represented in figure 3.12. The double-wall vessel has an internal volume of about 400 cm^3, and includes a cavity where the sample cell is enclosed (figure 3.12 – A). A much thinner cavity is able to hold with good thermal contact a platinum resistance thermometer Pt100 (class 1/10) (figure 3.12 – D). The bottom of the sample cell contains a brass block in order to ensure a good thermal contact between the sample cell and the thermometer. In order to promote a good thermal contact between the cell and the vessel walls, a Dow Corning® 340 heat sink substance is applied on the outside walls of the sample cell. This is also applied in the temperature sensor for use in the measuring of the temperature of the sample.

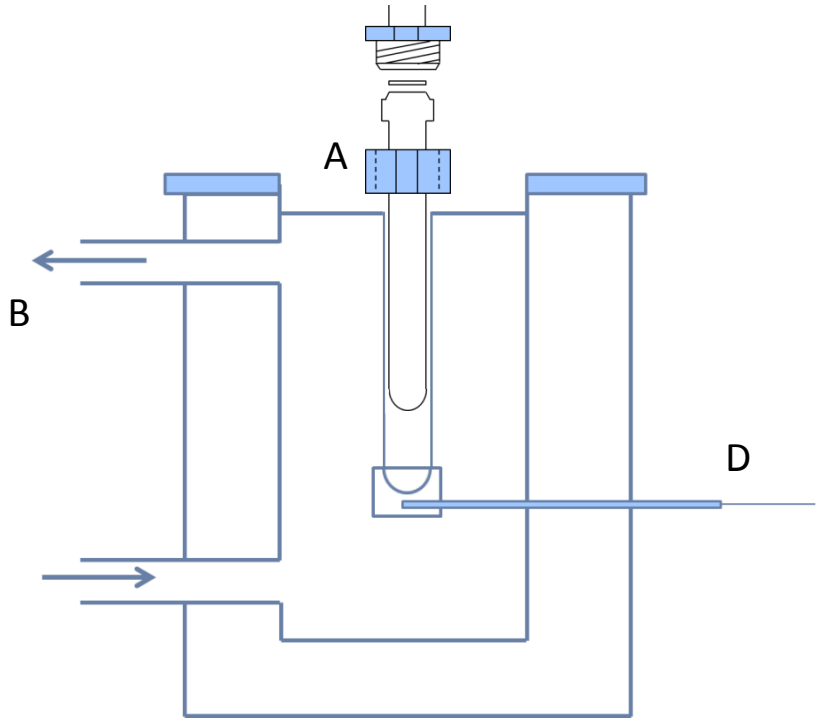

Figure 3.12. Schematic representation of the double walled vessel used to thermostatize the sample cell. A – cavity where the cell is putted; B – output of the thermal fluid; C – input of the thermal fluid; D – cavity for the Pt100.

3.2.4. Vacuum system

The vacuum system consists of a turbomolecular vacuum pump system Edwards model EXT70 and a rotary pump Edwards RV3. The system is equipped with a Pirani gauge Edwards APG-M and a non-return oil trap Edwards FL20K.

The turbomolecular pump links the tubing by a CF DN 63 connection type and is installed on an Edwards EXPB 1.5 base. In this base, there are also installed the Edwards EXC120 controller and the two Edwards AGD pressure indicators.

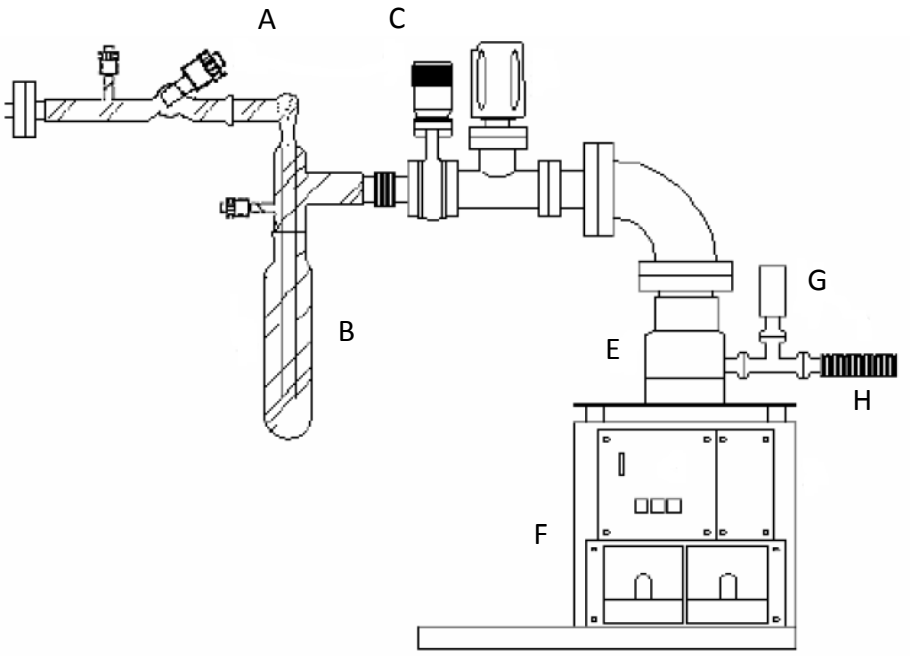

Figure 3.13. Schematic representation of the vaccum system. A – isolation valve; B – trap; C – VAT valve; D – wide range manometer; E – turbomolecular pump; F - Edwards EXPB 1.5 base and EXC120 Edwards controller; G - pressure gauge Edwards APG-Pirani – model M; H – flexible tube connection to the rotative pump. [9]

A VAT valve, number 010 mini UHV, in between the vacuum line and the turbomolecular pump, allows a rapid isolation of the pumping system. In addition to this valve, there is also an Edwards WRG manometer – model S. A glass vacuum line connects the pumping system to the tubing throughout metal-glass connections. The vacuum line includes a glass trap for liquid nitrogen and is equipped with two air intake teflon valves J. Young ASL1 and an isolation teflon valve J. Young SPOR20.

3.2.5. Temperature control

In any experiment leading with phase transitions and thermodynamic parameters study, a good control of the temperature is critic and of great importance. In this case, the temperature of the thermal fluid, which runs into the vessel (figure 3.12), is controlled by a thermostatic bath Julabo F33 - MW equipped with a cooling system. With this thermal fluid (H10S of thermal oil Julabo), the bath is able to control the temperature of the sample between 243 K and 473 K with a stability of ± 0.01 K.

3.2.6. Data acquisition and control

A Keithley 2700 data acquisition program and a HPVEE program were used to monitor and acquire data from the apparatus. Parameters like pressure, temperature of the sample and temperature of the tubing were monitored using these programs.

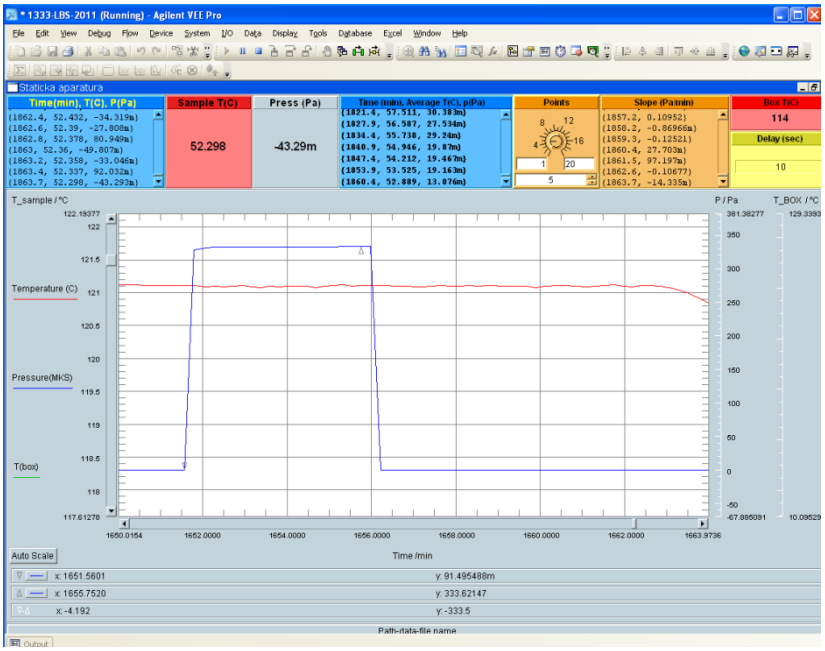

Figure 3.14. Image of the HP-VEE program used in the static apparatus.

The control and programming of the opening and closing of the electro-pneumatic valves is performed using a ADAM-4060 relay module using the program Static Control ON / OFF ADAM [12]. The programming and monitoring of the temperature of the Julabo bath is made using the EasyTemp program [13] supplied by the company Julabo Labortechnik GmbH.

3.3. Experimental procedure

Starting Process

Before any measurement, the tubing must be evacuated until 1×10^{-5} Pa with the sample valve (valve 1 in figure 3.5) closed and the vacuum valve (valve 2 in figure 3.5) open.

With valves 1 and 2 closed, the sample is putted in the cell and pressed to obtain a flat surface in the case of non-liquid samples. Then the cell is connected to the tubing.

After this process it is necessary to outgas the sample. This process is critical in this apparatus, because uncompleted outgassing of the sample will lead to overestimated vapor pressure values. The results can be affected by volatile impurities or gas particles presented in the studied sample.

Outgassing Process

In order to outgas the sample, the cell is maintained at a temperature low enough to assure that the respective vapor pressure is negligible, in order to avoid losses of the compound. Then the valve 2 is opened. For few seconds the valve 1 is also opened. As result, the sample escapes to the tubing provoking an increase of the pressure. After this, the valve 1 must be closed (with valve 2 still open) for a few minutes. At the end of this process an outgassing cycle is completed.

Note 1 - The outgassing process is repeated until consistent values are obtained and there is no significant drift (change in pressure at a given temperature).

Note 2 - The bath and the oven are set to desired temperatures. The oven temperature should be higher than the sample cell temperature and lower than the temperature of the manometer. Generally, the oven temperature is programmed to be 10 K above the sample cell tube temperature.

Measuring Process

With valve 2 closed and valve 1 opened, vapor pressure values are recorded for a few minutes, in order to obtain a baseline. Then, valve 2 is opened and valve 1 is closed generating a sudden increase in pressure. After a few minutes, there is a constant rise and the pressure values can be gathered. After this, valve 2 is closed and valve 1 is opened in order to evacuate the tubing and stabilize the baseline. The process is repeated until consistent values of vapor pressure are obtained.

3.4. Experimental results

3.4.1. Results for 1-halogenated naphthalenes

Using the static apparatus previously described, vapor pressures of the following three 1-halogenated naphthalenes were measured at different temperatures: 1-fluoronaphthalene [274–348] K, 1-bromonaphthalene [281–396] K, and 1-iodonaphthalene [304–393] K.

3.4.1.1. Results for 1-fluoronaphthalene

Table 3.1. Vapor pressure results for 1-fluoronaphthalene.[a]

T / K	p / Pa	$\Delta p/Pa$ [b]	T / K	p / Pa	$\Delta p/Pa$ [b]
		Liquid Phase			
273.55	5.23	-0.04	312.14	99.35	-0.39
276.50	6.82	0.01	314.14	113.83	0.19
278.49	8.11	0.03	316.14	128.65	-0.58
280.47	9.53	-0.02	318.10	146.62	0.31
282.45	11.33	0.08	320.07	165.68	0.20
284.41	13.21	0.01	322.06	187.52	0.45
286.40	15.53	0.04	324.04	211.54	0.56
288.36	18.19	0.11	325.99	237.76	0.62
290.36	21.33	0.20	327.99	267.35	0.46
292.34	24.43	-0.17	329.98	299.89	0.16
294.33	28.69	0.11	332.04	337.27	-0.14
296.32	32.90	-0.25	334.01	377.38	0.10
298.30	38.32	-0.01	335.98	421.59	0.35
300.28	43.93	-0.28	337.97	470.37	0.23
302.25	50.82	-0.04	339.94	523.35	-0.04
304.22	58.04	-0.35	341.92	582.37	0.22
306.22	67.43	0.39	343.91	646.43	-0.51
308.21	76.38	-0.39	345.88	716.61	-0.60
310.19	87.65	-0.03	347.85	792.74	-1.29

[a] Estimated uncertainties are ± 0.01 K for the temperature and [0.1 + 0.0025 (p/Pa)] for the pressures.
[b] $\Delta p = p - p_{calc}$

Note: The used manometer was:
- *MKS Baratron 631A11TBFP* (1333 Pa, 473 K) for temperatures between 273 and 348 K.

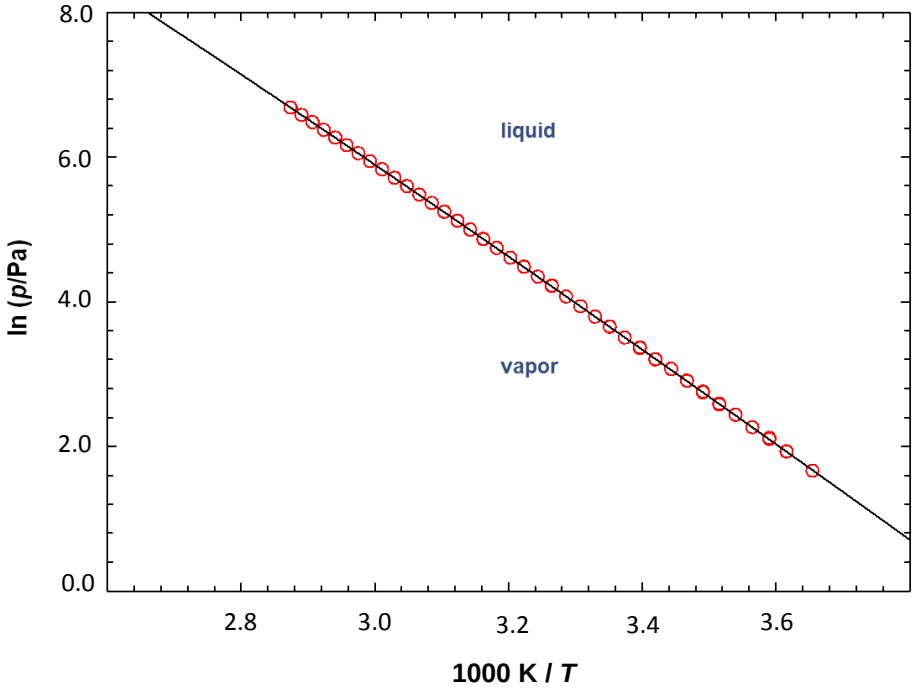

Figure 3.15. Graphic representation of ln(*p*/Pa) = *f* [1000 K/*T*] for 1-fluoronaphthalene.

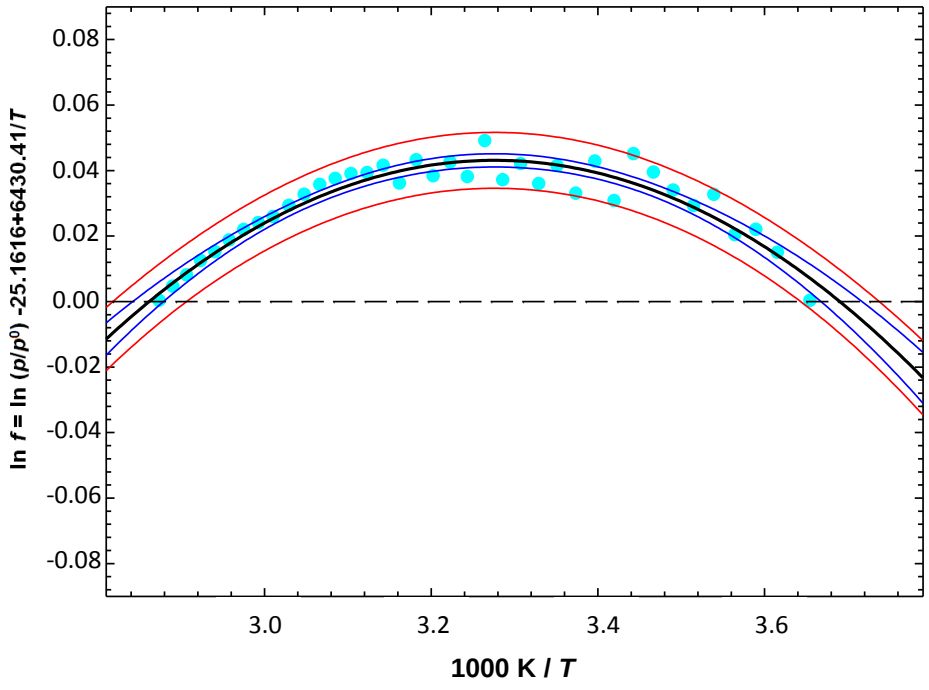

Figure 3.16. Graphic representation of the arc method [7] of the experimental results for 1-fluoronaphthalene.

3.4.1.2. Results for 1-bromonaphthalene

Table 3.2. Vapor pressure results for 1-bromonaphthalene.[a]

T / K	p / Pa	$\Delta p/Pa$ [b]	T / K	p / Pa	$\Delta p/Pa$ [b]
		Liquid Phase			
281.38	0.36	0.01	340.93	43.18	0.20
283.39	0.44	0.01	342.82	48.70	0.22
285.35	0.54	0.01	344.89	55.57	0.35
287.34	0.65	0.01	346.76	62.39	0.36
289.33	0.77	-0.01	348.85	70.72	0.22
291.35	0.93	-0.01	350.71	79.28	0.40
293.32	1.13	0.01	352.82	89.53	0.07
295.34	1.34	-0.01	354.67	99.89	0.15
297.28	1.59	-0.02	356.75	112.71	0.17
299.29	1.92	0.01	358.64	125.27	-0.15
301.24	2.26	-0.01	360.69	140.59	-0.26
303.26	2.68	-0.01	362.64	156.36	-0.69
305.21	3.14	-0.02	364.64	174.93	-0.43
307.23	3.74	0.01	366.60	194.14	-0.93
309.19	4.36	-0.02	369.43	226.87	-0.13
311.21	5.14	-0.01	370.54	239.81	-0.93
313.16	5.99	-0.01	372.53	266.95	-0.21
315.17	6.98	-0.04	374.48	294.96	-0.54
317.10	8.06	-0.07	376.46	326.97	0.04
319.09	9.45	-0.01	378.42	360.17	-0.71
321.14	11.01	0.01	380.43	398.35	-0.51
323.06	12.72	0.05	382.35	438.18	-0.17
325.10	14.61	-0.07	384.36	483.58	0.29
327.03	16.95	0.11	386.31	529.87	-0.81
329.06	19.45	0.02	388.30	583.43	0.29
330.97	22.13	-0.04	390.25	639.31	0.44
333.03	25.57	0.05	392.33	702.11	-1.22
334.94	29.13	0.10	394.19	766.31	0.64
336.98	33.42	0.18	396.18	839.02	1.42
338.89	37.82	0.15			

[a] Estimated uncertainties are ± 0.01 K for the temperature, [0.01 + 0.0025 (*p*/Pa)] for the pressures measured bellow 357 K and [0.1+0.0025(*p*/Pa)] for the pressures measured above 357 K.

[b] $\Delta p = p - p_{calc}$

Note: The used manometers were:
- *MKS Baratron 631A01TBEH* (133 Pa, 423 K) for temperatures between 281 and 357 K.
- *MKS Baratron 631A11TBFP* (1333 Pa, 473 K) for temperatures between 357 and 396 K.

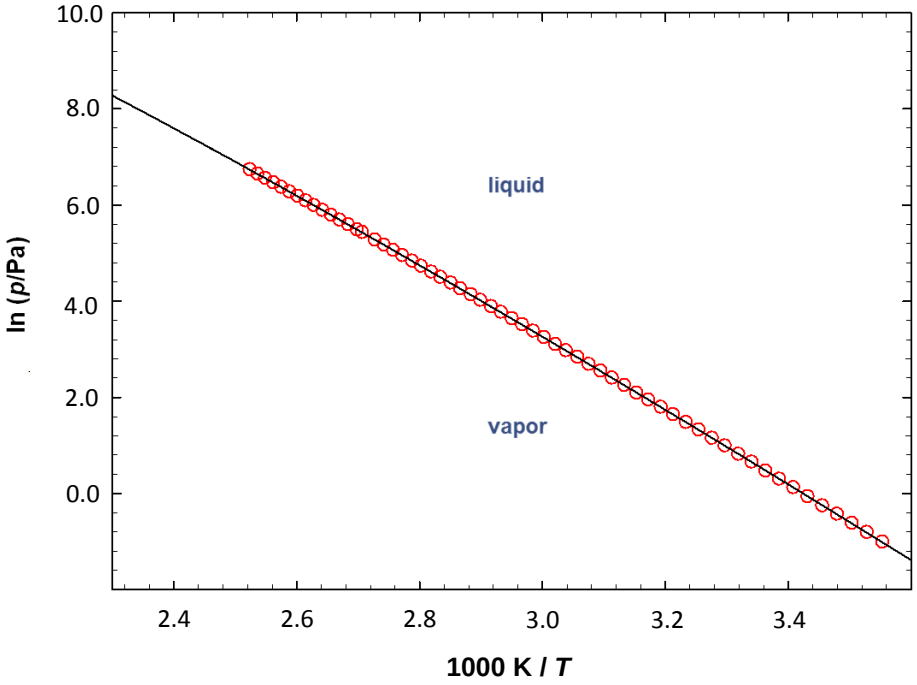

Figure 3.17. Graphic representation of ln(*p*/Pa) = *f* [1000 K/*T*] for 1-bromonaphthalene.

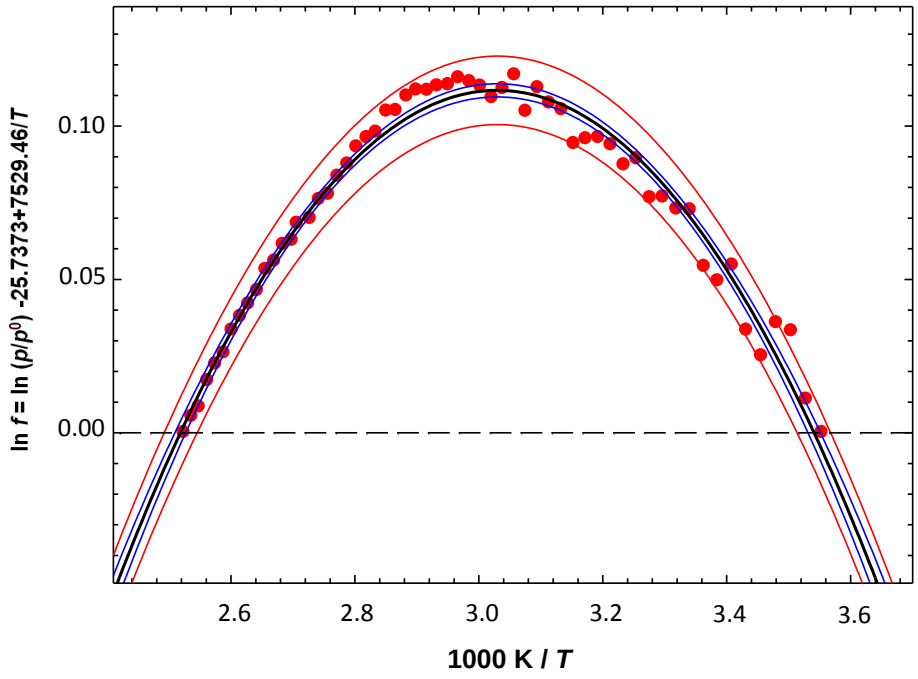

Figure 3.18. Graphic representation of the arc method [7] of the experimental results for 1-bromonaphthalene.

3.4.1.3. Results for 1-iodonaphthalene

Table 3.3. Vapor pressure results for 1-iodonaphthalene.[a]

T / K	p / Pa	$\Delta p/Pa$ [b]	T / K	p / Pa	$\Delta p/Pa$ [b]
		Liquid Phase			
304.23	0.84	-0.01	349.73	26.17	-0.04
306.20	0.99	-0.02	351.72	29.55	-0.18
308.22	1.21	0.01	353.65	33.49	-0.05
310.15	1.42	0.01	355.63	37.45	-0.43
312.17	1.66	-0.02	357.61	42.71	-0.02
314.16	1.96	-0.02	359.59	48.05	-0.06
316.11	2.33	0.01	361.55	53.86	-0.16
318.11	2.76	0.03	363.54	60.59	-0.09
320.09	3.21	0.01	365.64	68.16	-0.31
322.10	3.80	0.05	367.49	75.85	-0.21
324.05	4.40	0.05	369.57	85.43	-0.03
326.04	5.19	0.12	371.54	94.05	-1.24
328.01	5.93	0.06	373.51	106.15	0.04
329.99	6.86	0.06	375.48	118.26	0.27
331.98	7.89	0.03	377.45	130.26	-0.76
333.94	9.10	0.06	379.43	144.77	-0.59
335.93	10.41	0.01	381.39	159.97	-0.93
337.85	11.87	-0.03	383.36	177.58	-0.37
339.87	13.61	-0.07	385.33	196.98	0.42
341.83	15.74	0.12	387.29	217.47	0.73
343.80	17.74	-0.08	389.28	240.86	1.82
345.76	20.15	-0.13	391.23	264.98	2.18
347.76	22.94	-0.16	393.22	292.62	3.49

[a] Estimated uncertainties are ± 0.01 K for the temperature , [0.01 + 0.0025 (*p*/Pa)] for the pressures measured bellow 374 K and [0.1+0.0025(*p*/Pa)] for the pressures measured above 374 K.

[b] $\Delta p = p - p_{calc}$

Note: The used manometers were:
- *MKS Baratron 631A01TBEH* (133 Pa, 423 K) for temperatures between 304 and 374 K.
- *MKS Baratron 631A11TBFP* (1333 Pa, 473 K) for temperatures between 375 and 393 K.

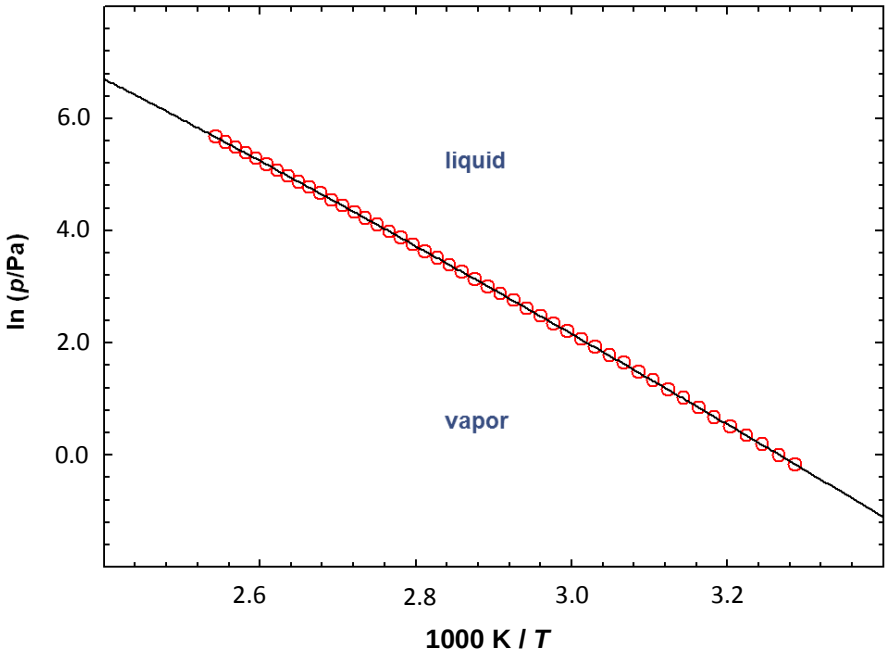

Figure 3.19. Graphic representation of ln(*p*/Pa) = *f* [1000 K/*T*] for 1-iodonaphthalene.

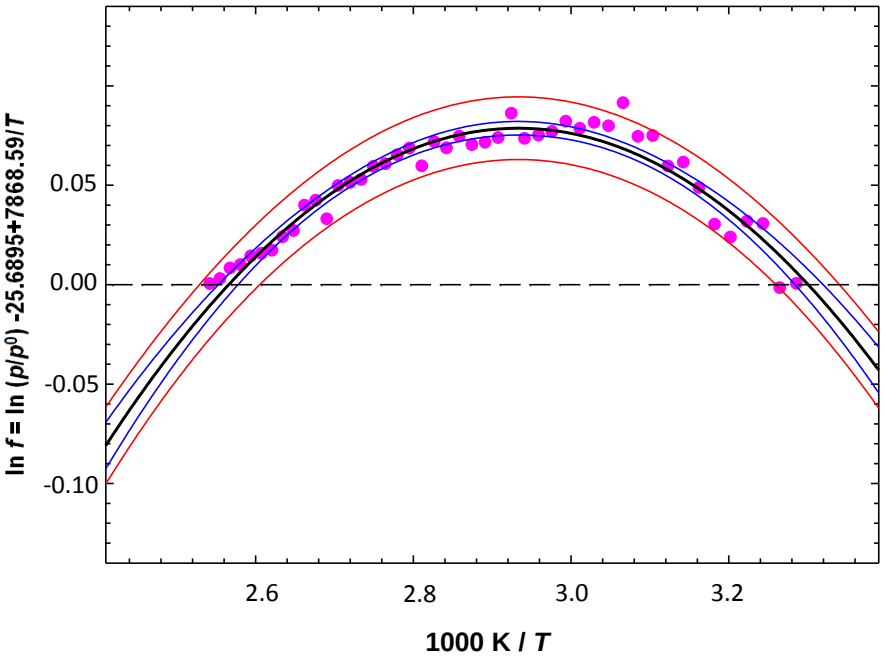

Figure 3.20. Graphic representation of the arc method [7] of the experimental results for 1-iodonaphthalene.

Table 3.4. Standard (p^0 = 0.1 MPa) molar properties of vaporization derived from the fitting of the Clarke and Glew equation (3.18) to the experimental *p,T* results for 1-halogenated naphthalenes.

T	θ	$\Delta_l^g G_m^0(\theta)$	$\Delta_l^g H_m^0(\theta)$	$\Delta_l^g S_m^0(\theta)$	R^2	$-\Delta_l^g C_{p,m}^0$	s[a]
K	K	kJ·mol^{-1}	kJ·mol^{-1}	J·K^{-1}·mol^{-1}		J·K^{-1}·mol^{-1}	
			1-fluoronaphthalene				
274 to 348	298.15	19.53 ± 0.01	53.82 ± 0.04	115.01 ± 0.04	1.0000	44 ± 3[b]	0.004
	310.70[c]	18.10 ± 0.01	53.27 ± 0.02	113.20 ± 0.02			
			1-bromonaphthalene				
281 to 396	298.15	27.18 ± 0.01	64.74 ± 0.04	125.98 ± 0.04	1.0000	63 ± 1[b]	0.004
	338.78[c]	22.23 ± 0.01	62.17 ± 0.02	117.89 ± 0.02			
			1-iodonaphthalene				
304 to 393	298.15	30.32 ± 0.01	68.95 ± 0.19	129.57 ± 0.19	1.0000	80 ± 4[b]	0.008
	348.73[c]	24.10 ± 0.01	64.88 ± 0.05	116.94 ± 0.05			

[a] s is the standard deviation of the fit defined as $s = \left[\frac{\sum_{i=1}^{n}(\ln p - \ln p_{calc})_i^2}{n-m}\right]^{1/2}$ where n is the number of experimental points used in the fit and m is the number of adjustable parameters of Clarke and Glew equation;
[b] Adjustable parameter;
[c] Mean temperature.

Table 3.5. Absolute entropies derived from experimental and computational results for 1-halogenated naphthalenes.

θ	$S_{liq}(\theta)$[a]	$S_g(\theta)$[b]
K	J·K^{-1}·mol^{-1}	J·K^{-1}·mol^{-1}
	1-fluoronaphthalene	
298.15	249.14	364.15
	1-bromonaphthalene	
298.15	261.53	387.51
	1-iodonaphthalene	
298.15	265.83	395.40

[a] derived as $S_{liq}(\theta) = S_g(\theta) - \Delta_l^g S_m^0(\theta)$
[b] Values obtained using Isodesmic Reactions.

3.4.2. Results for 2-halogenated naphthalenes

Using the static apparatus previously described, vapor pressures of following three 2-halogenated naphthalenes were measured at different temperatures: 2-chloronaphthalene [280 – 384] K, 2-bromonaphthalene [291 – 385] K, and 2-iodonaphthalene [302 – 364] K.

3.4.2.1. Results for 2-chloronaphthalene

Table 3.6 Vapor pressure results for 2-chloronaphthalene.[a]

T / K	p / Pa	$\Delta p/Pa$ [b]	T / K	p / Pa	$\Delta p/Pa$ [b]
		Crystalline Phase			
280.37	0.36	-0.01	306.20	5.71	-0.02
282.40	0.46	-0.01	308.20	6.96	0.01
284.30	0.59	0.01	310.20	8.43	0.02
286.30	0.73	0.01	312.10	10.12	0.07
288.47	0.91	-0.01	314.20	12.24	0.04
290.30	1.13	0.01	316.10	14.47	-0.04
292.30	1.38	-0.01	318.10	17.29	-0.08
294.30	1.74	0.02	320.10	20.63	-0.12
296.20	2.12	0.02	322.00	24.46	-0.06
298.30	2.60	-0.01	324.00	28.99	-0.17
300.30	3.21	0.01	326.00	34.56	-0.04
302.20	3.89	0.02	327.00	37.45	-0.20
304.20	4.69	-0.02	328.90	44.74	0.58
		Liquid Phase			
335.00	66.79	-0.01	360.67	300.07	0.19
336.96	76.07	0.42	362.65	333.05	-0.08
338.98	85.45	-0.39	364.55	367.93	-0.27
340.91	96.58	-0.10	366.60	410.02	0.63
342.90	109.00	-0.10	368.45	451.51	1.38
344.86	122.74	0.01	370.55	501.30	0.66
346.85	138.09	0.06	372.45	549.44	-1.12
348.82	154.90	0.02	374.50	609.78	0.62
350.80	173.54	-0.09	376.45	666.94	-2.67
352.78	194.20	-0.11	378.44	736.20	-0.77
354.75	217.09	0.13	380.40	809.73	0.95
356.75	242.09	-0.26	382.37	887.76	0.98
358.71	269.86	0.16	384.36	972.43	-0.29

[a] Estimated uncertainties are ± 0.01 K for the temperature, [0.01 + 0.0025 (*p*/Pa)] for the pressures measured bellow 341 K and [0.1+0.0025(*p*/Pa)] for the pressures measured above 341 K.

[b] $\Delta p = p - p_{calc}$

Note: The used manometers were:
- *MKS Baratron 631A01TBEH* (133 Pa, 423 K) for temperatures between 280 and 341 K.
- *MKS Baratron 631A11TBFP* (1333 Pa, 473 K) for temperatures between 342 and 384 K.

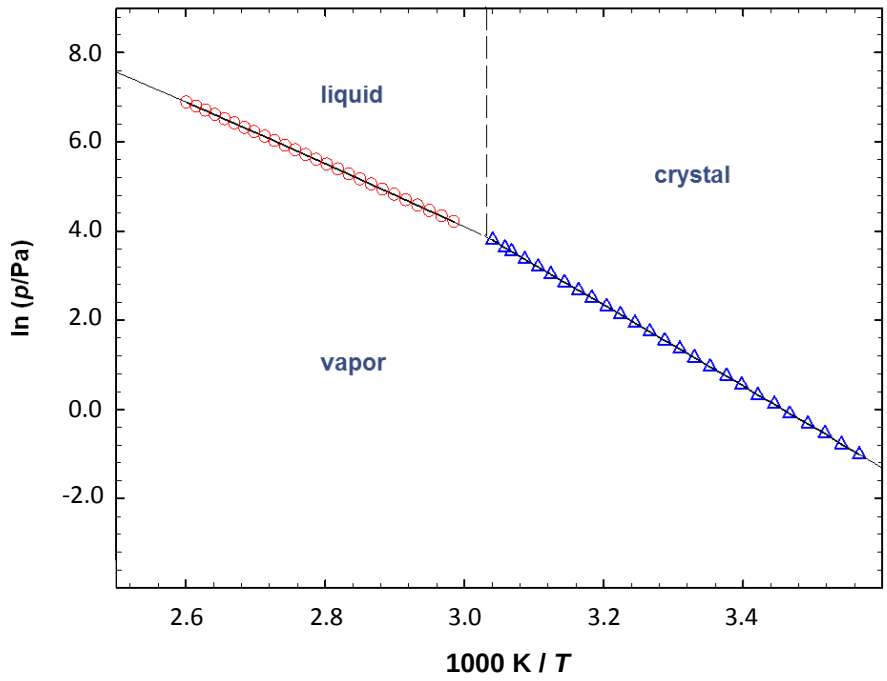

Figure 3.21. Graphic representation of ln(p/Pa) = f [1000 K/T] for 2-chloronaphthalene.

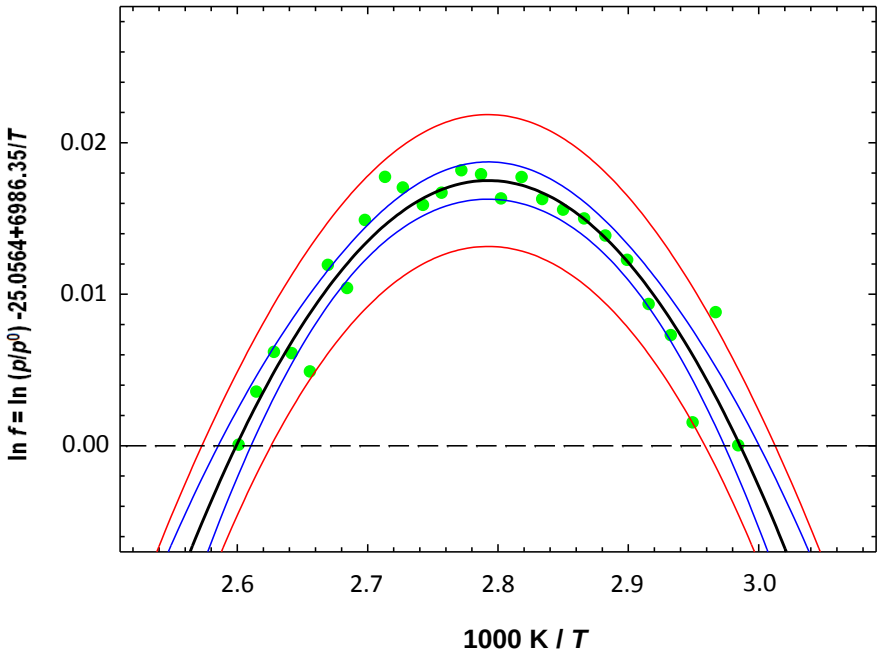

Figure 3.22. Graphic representation of the arc method [7] of the experimental results for 2-chloronaphthalene.

3.4.2.2. Results for 2-bromonaphthalene

Table 3.7. Vapor pressure results for 2-bromonaphthalene.[a]

T / K	p / Pa	$\Delta p/Pa$ [b]	T / K	p / Pa	$\Delta p/Pa$ [b]
Crystalline Phase II			Crystalline Phase I[c]		
291.32	0.44	-0.01	321.11	9.44	0.02
293.32	0.55	-0.01	322.07	10.83	0.57
295.30	0.69	-0.01	323.06	11.21	0.01
297.32	0.86	-0.01	325.05	13.37	0.02
299.27	1.08	0.01	326.09	14.62	-0.01
301.28	1.34	0.01			
303.24	1.65	0.01			
305.24	2.03	0.01			
307.21	2.47	0.01			
309.24	3.04	0.01			
311.16	3.68	0.01			
313.17	4.46	-0.02			
315.14	5.35	-0.07			
Liquid Phase					
329.97	19.94	-0.01	359.70	129.47	-0.63
332.02	22.83	-0.17	361.68	145.29	-0.20
333.92	26.18	-0.02	363.64	161.72	-0.57
335.97	30.07	-0.01	365.64	181.14	-0.03
337.95	34.48	0.17	367.59	200.77	-0.63
339.93	39.05	-0.01	369.58	223.89	-0.18
341.95	44.64	0.12	371.54	247.91	-0.65
343.89	50.51	0.14	373.52	275.61	-0.03
345.89	57.22	0.10	375.48	304.44	-0.51
347.84	64.79	0.32	377.46	337.72	0.43
349.82	73.01	0.23	379.33	371.35	0.80
351.78	81.86	-0.06	381.40	411.27	0.61
353.78	92.42	0.14	383.38	453.39	0.89
355.74	103.34	-0.22	385.35	498.19	0.43
357.73	116.34	0.11			

[a] Estimated uncertainties are ± 0.01 K for the temperature , [0.01 + 0.0025 (*p*/Pa)] for the pressures measured bellow 354 K and [0.1+0.0025(*p*/Pa)] for the pressures measured above 354 K.

[b] $\Delta p = p - p_{calc}$

[c] crystal-crystal transition reported by Verevkin [14]

Note: The used manometers were:
- *MKS Baratron 631A01TBEH* (133 Pa, 423 K) for temperatures between 291 and 354 K.
- *MKS Baratron 631A11TBFP* (1333 Pa, 473 K) for temperatures between 355 and 385 K.

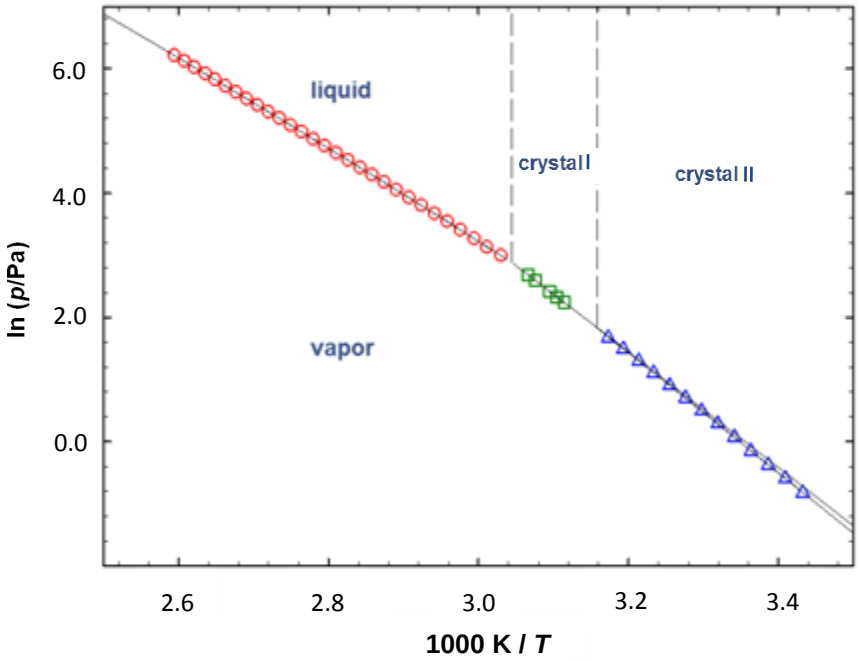

Figure 3.23. Graphic representation of ln(p/Pa) = f [1000 K/T] for 2-bromonaphthalene.

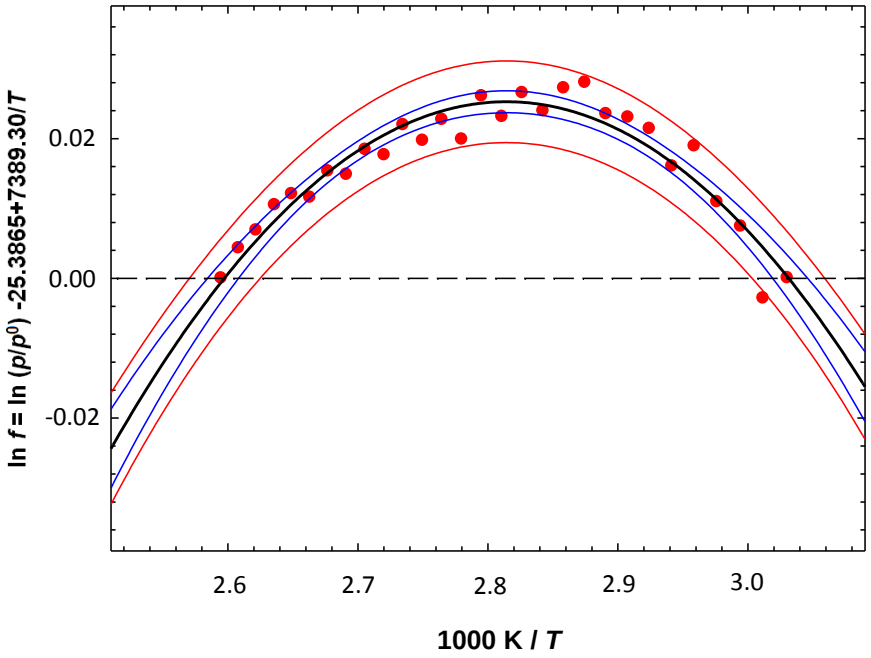

Figure 3.24. Graphic representation of the arc method [7] of the experimental results for 2-bromonaphthalene.

3.4.2.3. Results for 2-iodonaphthalene

Table 3.8. Vapor pressure results for 2-iodonaphthalene.[a]

T / K	p / Pa	$\Delta p/Pa$ [b]	T / K	p / Pa	$\Delta p/Pa$ [b]
		Crystalline Phase			
302.25	0.35	0.01	314.13	1.27	0.01
304.26	0.43	-0.01	316.13	1.56	0.01
306.20	0.54	0.01	318.10	1.90	-0.01
308.20	0.68	0.01	320.09	2.33	-0.01
310.20	0.83	-0.01	322.07	2.86	0.01
312.17	1.02	-0.01	324.04	3.46	-0.01
		Liquid Phase			
310.19	1.21	-0.01	339.95	12.28	-0.06
312.17	1.44	-0.01	341.82	14.09	0.05
314.14	1.72	0.02	343.91	16.33	0.13
317.14	2.20	0.01	345.75	18.41	0.08
319.64	2.67	-0.02	347.86	21.15	0.06
322.05	3.23	-0.03	349.82	23.75	-0.23
324.08	3.81	-0.01	351.82	26.97	-0.29
326.03	4.45	0.01	353.78	30.66	-0.24
329.98	6.03	0.03	355.76	35.04	0.06
332.05	7.05	0.05	357.76	39.64	0.07
333.93	8.01	-0.03	359.73	44.59	-0.03
336.00	9.32	-0.01	361.69	50.36	0.12
337.84	10.72	0.08	363.66	56.75	0.28

[a] Estimated uncertainties are ± 0.01 K for the temperature and [0.01 + 0.0025 (*p*/Pa)] for the pressures.

[b] $\Delta p = p - p_{calc}$

Note: The used manometers were:
- *MKS Baratron 631A01TBEH* (133 Pa, 423 K) for temperatures between 302 and 364 K.

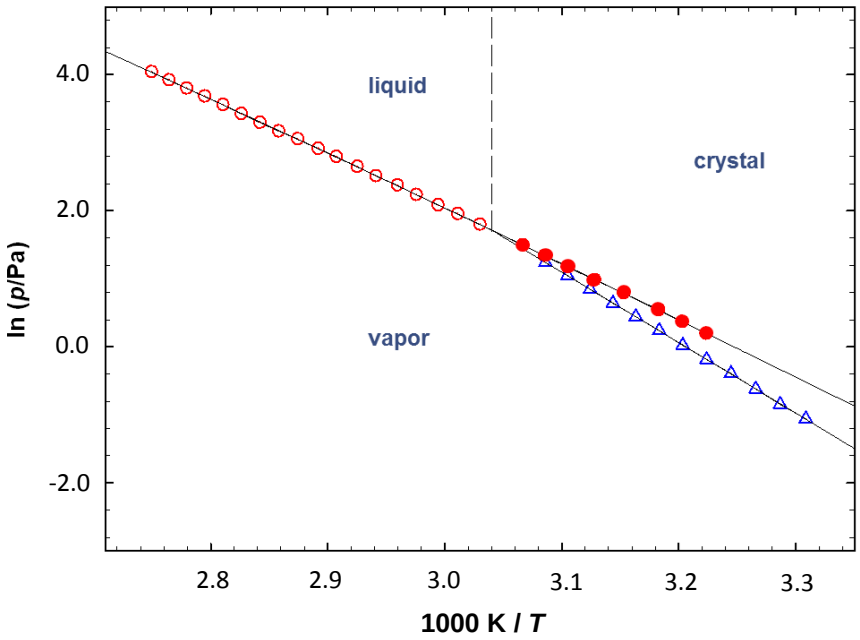

Figure 3.25. Graphic representation of ln(p/Pa) = f [1000 K/T] for 2-iodonaphthalene.

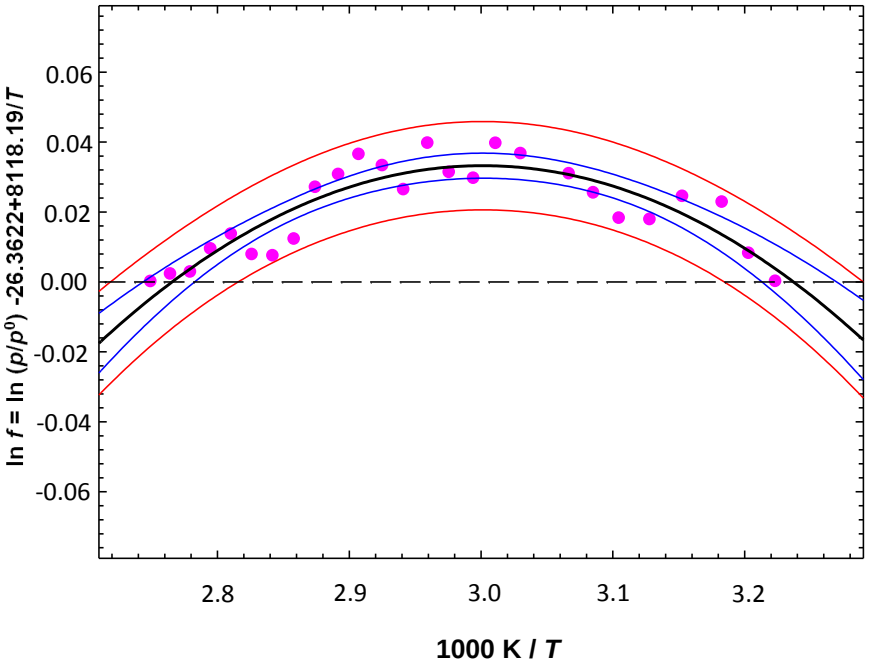

Figure 3.26. Graphic representation of the arc method [7] of the experimental results for 2-iodonaphthalene.

Table 3.9. Standard (p^0 = 0.1 MPa) molar properties of sublimation derived from the fitting of the Clarke and Glew equation to the experimental *p,T* results for 2-halogenated naphthalenes.

T	θ	$\Delta^{g}_{cr}G^{0}_{m}(\theta)$	$\Delta^{g}_{cr}H^{0}_{m}(\theta)$	$\Delta^{g}_{cr}S^{0}_{m}(\theta)$	R^2	$-\Delta^{g}_{cr}C^{0}_{p,m}$	s[a]
K	K	kJ·mol^{-1}	kJ·mol^{-1}	J·K^{-1}·mol^{-1}		J·K^{-1}·mol^{-1}	
			2-chloronaphthalene				
280 to 329	298.15	26.20 ± 0.01	75.82 ± 0.08	166.43 ± 0.08	1.0000	27.3[c]	0.008
	304.64[b]	25.13 ± 0.01	75.64 ± 0.08	165.80 ± 0.08			
	329.85[d]	20.97 ± 0.01	74.95 ± 0.08	163.65 ± 0.08			
			2-bromonaphthalene				
			Crystal II				
291 to 315	298.15	28.67 ± 0.01	80.42 ± 0.20	173.57 ± 0.20	0.9999	27.7[c]	0.007
	303.23[b]	27.79 ± 0.01	80.28 ± 0.20	173.10 ± 0.20			
	328.49[d]	23.45 ± 0.01	79.58 ± 0.20	170.87 ± 0.20			
			Crystal I				
321 to 326	298.15	28.51 ± 0.05	77.68 ± 0.58	164.92 ± 0.58	0.9998		0.003
	323.60[b]	24.35 ± 0.01	76.98 ± 0.58	162.64 ± 0.58			
	328.49[d]	23.55 ± 0.01	76.84 ± 0.58	162.23 ± 0.58			
			2-iodonaphthalene				
302 to 324	298.15	32.35 ± 0.01	86.50 ± 0.18	181.62 ± 0.18	1.0000	27.9[c]	0.005
	313.14[b]	29.63 ± 0.01	86.08 ± 0.18	180.27 ± 0.18			
	328.91[d]	26.80 ± 0.01	85.64 ± 0.18	178.89 ± 0.18			

[a] s is the standard deviation of the fit defined as $s = \left[\frac{\sum_{i=1}^{n} (\ln p - \ln p_{calc})_i^2}{n-m} \right]^{1/2}$ where n is the number of experimental points used in the fit and m is the number of adjustable parameters of Clarke and Glew equation;
[b] Mean temperature;
[c] Estimated value from quantum chemical calculations and using $\Delta^{g}_{cr}C^{0}_{p,m}$ = -(0.9+0.176 $C^{0}_{p,m}(g)$); [15]
[d] Temperature of triple point.

Table 3.10. Standard (p^0 = 0.1 MPa) molar properties of vaporization derived from the fitting of the Clarke and Glew equation to the experimental *p,T* results for 2-halogenated naphthalenes.

T	θ	$\Delta_l^g G_m^0(\theta)$	$\Delta_l^g H_m^0(\theta)$	$\Delta_l^g S_m^0(\theta)$	R^2	$-\Delta_l^g C_{p,m}^0$	s[a]
K	K	kJ·mol^{-1}	kJ·mol^{-1}	J·K^{-1}·mol^{-1}		J·K^{-1}·mol^{-1}	
			2-chloronaphthalene				
335 to 384	298.15	24.80 ± 0.02	61.77 ± 0.27	123.99 ± 0.27	1.0000	61 ± 4[b]	0.002
	359.68[c]	17.53 ± 0.01	58.02 ± 0.03	112.57 ± 0.03			
	329.85[e]	20.97 ± 0.01	59.83 ± 0.03	117.81 ± 0.03			
			2-bromonaphthalene				
330 to 385	298.15	27.33 ± 0.02	65.46 ± 0.27	127.89 ± 0.27	1.0000	70 ± 5[b]	0.003
	357.66[c]	20.01 ± 0.01	61.31 ± 0.03	115.19 ± 0.03			
	328.49[e]	23.55 ± 0.01	63.34 ± 0.03	121.13 ± 0.03			
			2-iodonaphthalene				
310 to 364[d]	298.15	30.78 ± 0.02	70.62 ± 0.35	133.62 ± 0.35	1.0000	88 ± 9[b]	0.006
	336.92[c]	25.81 ± 0.01	67.21 ± 0.07	122.88 ± 0.07			
	328.91[e]	26.80 ± 0.01	67.92 ± 0.07	125.02 ± 0.07			

[a] s is the standard deviation of the fit defined as $s = \left[\frac{\sum_{i=1}^{n} (\ln p - \ln p_{calc})_i^2}{n-m} \right]^{1/2}$ where n is the number of experimental points used in the fit and m is the number of adjustable parameters of Clarke and Glew equation;
[b] Adjustable parameter;
[c] Mean temperature;
[d] Including supercooled liquid;
[e] Temperature of triple point.
Note: triple point pressures - 47.81 Pa; 17.97 Pa; 5.54 Pa for 2-ClNaph, 2-BrNaph and 2-INaph, respectively.

Table 3.11. Standard (p^0 = 0.1 MPa) molar properties of fusion derived from the vaporization and sublimation results for 2-halogenated naphthalenes.

θ	$\Delta^{l}_{cr}G^{0}_{m}(\theta)$[a]	$\Delta^{l}_{cr}H^{0}_{m}(\theta)$[b]	$\Delta^{l}_{cr}S^{0}_{m}(\theta)$[c]
K	kJ·mol^{-1}	kJ·mol^{-1}	J·K^{-1}·mol^{-1}
		2-chloronaphthalene	
298.15	1.40 ± 0.01	14.05 ± 0.27	42.44 ± 0.27
		2-bromonaphthalene	
298.15	1.18 ± 0.02	12.22 ± 0.58	37.03 ± 0.58
		2-iodonaphthalene	
298.15	1.57 ± 0.02	15.88 ± 0.35	48.00 ± 0.35

[a] derived as $\Delta^{l}_{cr}G^{0}_{m}(\theta) = \Delta^{g}_{cr}G^{0}_{m}(\theta) - \Delta^{g}_{l}G^{0}_{m}(\theta)$

[b] derived as $\Delta^{l}_{cr}H^{0}_{m}(\theta) = \Delta^{g}_{cr}H^{0}_{m}(\theta) - \Delta^{g}_{l}H^{0}_{m}(\theta)$

[c] derived as $\Delta^{l}_{cr}S^{0}_{m}(\theta) = \Delta^{g}_{cr}S^{0}_{m}(\theta) - \Delta^{g}_{l}S^{0}_{m}(\theta)$

Table 3.12. Absolute entropies derived from experimental and computational results for 2-halogenated naphthalenes.

θ	$S_{cr}(\theta)$[a]	$S_{liq}(\theta)$[b]	$S_{g}(\theta)$[c]
K	J·K^{-1}·mol^{-1}	J·K^{-1}·mol^{-1}	J·K^{-1}·mol^{-1}
		2-chloronaphthalene	
298.15	209.60	252.04	376.03
		2-bromonaphthalene	
298.15	223.35	260.38	388.27
		2-iodonaphthalene	
298.15	215.17	263.17	396.79

[a] derived as $S_{cr}(\theta) = S_{g}(\theta) - \Delta^{g}_{cr}S^{0}_{m}(\theta)$

[b] derived as $S_{liq}(\theta) = S_{g}(\theta) - \Delta^{g}_{l}S^{0}_{m}(\theta)$

[c] Values obtained using Isodesmic Reactions.

References

[1] Fink, J. K., *Physical Chemistry in Depth*, Chapter 8.

[2] Clarke, E. C. W.; Glew D. N., *Trans. Faraday Soc*., 62 (1966) 539-547.

[3] van der Linde, P. R.; Blok, J. G.; Oonk, H. A. J., *J. Chem. Thermodyn.,* 30 (1998) 909 - 917.

[4] Oonk, H. A. J.; van der Linde, P. R.; Huinink, J.; Blok, J. G., *J. Chem. Thermodyn*., 30 (1998) 897 - 907.

[5] Cox, J. D.; Pilcher, G., *Thermochemistry of Organic and Organometallic Compounds*, Academic Press, London, (1970).

[6] Monte, M. J. S., *Aplicação de Técnicas de Efusão à Determinação de entalpias de sublimação*, dissertação de doutoramento, Faculdade de Ciências da Universidade do Porto, Porto, Portugal (1990).

[7] van Genderen, A. C. G., Oonk, H. A. J., *Colloids and Surface A: Physicochem. Eng. Aspects*, 213 (2003) 107-115.

[8] Monte, M. J. S.; Santos, L. M. N. B. F.; Fulem, M.; Fonseca, J. M. S.; Sousa C. A. D., *J. Chem. Eng. Data*, 51 (2006) 757-766.

[9] Fonseca, J. M. S., *Medição de Pressões de Vapor e Estudo Termodinâmico de Transições de Fase de Ácidos Benzóicos Substituídos: Construção e Teste de um Novo Aparelho para Medição de Pressões de Vapor*, dissertação de mestrado, Faculdade de Ciências da Universidade do Porto, Porto, Portugal (2004).

[10] http://eu.trinos.com/vacuum_s/trinos-cf-conflat-16-400-mm.html

[11] http://www.vatvalve.com/products/catalog/E/570_1_V

[12] Santos, L. M. N. B. F., ADAM Control, versão 1.1, 2006.

[13] EasyTemp, versão 2.2.

[14] Verevkin, S.P., *J. Chem. Thermodyn*., 35 (2003) 1237.

[15] Monte M. J. S.; Almeida A. R. R. P. and Matos M. A. R., *J. Chem. Eng. Data*, 55 (2010) 419–423.

Chapter 4

Statistical Thermodynamics

4.1. Quantum chemical calculations

4.1.1. Methods – particularities, advantages and disadvantages

4.1.2. Basis functions/functionals

4.1.3. Basis sets

4.2. Statistical Thermodynamics

4.2.1. Summary

4.3. Geometry optimization and vibrational frequency calculations

4.4. The isodesmic reactions

4.5. Computational results

4.5.1. Results of 1-halogenated naphthalenes

4.5.1.1. Results for 1-fluoronaphthalene

4.5.1.2. Results for 1-chloronaphthalene

4.5.1.3. Results for 1-bromonaphthalene

4.5.1.4. Results for 1-iodonaphthalene

4.5.2. Results of 2-halogenated naphthalenes

4.5.2.1. Results for 2-fluoronaphthalene

4.5.2.2. Results for 2-chloronaphthalene

4.5.2.3. Results for 2-bromonaphthalene

4.5.2.4. Results for 2-iodonaphthalene

References

4.1. Quantum chemical calculations

Quantum chemical calculations area nowadays is a powerful tool in physical chemistry that can be used for the theoretical prediction and simulation as well as in the interpretation of experimental data. Figure 4.1 presents a schematic diagram showing how scientists (and chemists in particular) typically input their decision to solve some real problem or question.

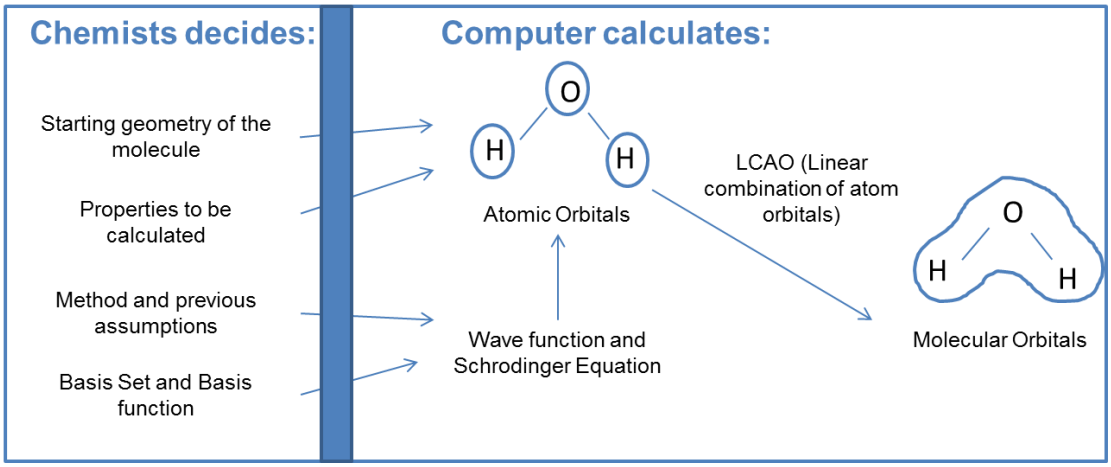

Figure 4.1. Scheme of the quantum chemical calculations typical "procedure".

In this work, decisions and options have been done along the quantum chemical calculations:

- **Starting geometry of the molecules**: designed and optimized in Gaussian programs [1];
- **Properties to be calculated:** gas phase heat capacities and absolute entropies;
- **Method:** Density-Functional Theory;
- **Basis functions/functionals:** B3-LYP; B-LYP and BP86;
- **Basis sets:** 6-311++G(d,p); cc-pVTZ and TZVP.

4.1.1. Methods – particularities, advantages and disadvantages

Ab initio

- It is based on quantum mechanics.
- Does not include empirical parameters.
- Mathematically rigorous.
- It is based on wave functions.

Density Functional Theory (DFT)

- It is based on functional density.
- Uses functional parameters.

Semiempirical and empirical

- Uses experimental and empirical parameters simplifications.
- Includes several approaches across the calculations.
- It is based on wave functions.

Table 4.1. Resume of the advantages and disadvantages of quantum chemical methods.

Method	Advantages	Disadvantages
Ab initio	• Can be used on every types of system. • Do not depend on experimental data. • Allow the calculation of transition and excited states.	• Computationally demanding.
Density Functional Theory (DFT)	• Include the electronic correlation term. • Less computationally demanding when compared to *ab initio*, of the same "quality". • Allow the calculation of transition states.	• Less rigorous than *ab initio* method. • Not possible to calculate excited states. • Not possible to systematically improve the results. • Poorly describes dispersive interactions.
Semiempirical & Empirical	• Less computationally demanding when compared with *ab initio* and DFT methods. • Allows the calculation of transition and excited states.	• Requires experimental data or calculations *ab initio* for the derivation of parameters. • Less rigorous than *ab initio* and DFT.

4.1.2. Basis functions/functionals

The two most popular functionals are known as BLYP (from the name Becke for the exchange part and Lee, Yang and Parr for the correlation part) and B3LYP which are hybrid functionals in which the exchange energy, in this case from Becke's exchange functional, is combined with the exact energy from Hartree–Fock theory. In B3LYP along with the component exchange and correlation functionals, three parameters define the hybrid functional, specifying how much of the exact exchange is "mixed in". Unfortunately, although the results obtained with these functionals are usually sufficiently accurate for most applications, there is no systematic way of improving them. Hence in the current DFT approach it is not possible to estimate the error of the calculations without comparing them to other methods or experiments. [2]

The BP86 functional has the same exchange correction as BLYP, but uses the Perdew86 correlation functional. [2]

4.1.3. Basis sets

A basis set is basically a group of functions which are combined in linear combinations to create molecular orbitals. For convenience these functions are typically atomic orbitals centered on atoms, but can theoretically be any combination of function that are fitted in order to reproduce a good description of a molecular orbital; plane waves are frequently used in bulk materials calculations. The accuracy or reliability of a quantum-chemical calculation depends on the size of the basis set used.

Pople basis sets

The notation for the split-valence basis sets arising from the group of John Pople, typically X-YZg. [3] In this case, X represents the number of primitive Gaussians comprising each core atomic orbital basis function. The Y and Z indicate that the valence orbitals are composed of two basis functions each, the first one composed of a linear combination of Y primitive Gaussian functions, the other composed of a linear

combination of Z primitive Gaussian functions. In this case, the presence of two numbers after the hyphens implies that this basis set is a split-valence double-zeta basis set. Split-valence triple- and quadruple-zeta basis sets are also used, denoted as X-YZWg, X-YZWVg, etc. [4]

Correlation-consistent basis sets

Some of the most widely used basis sets are those developed by Dunning and co-workers, [5] since they are designed to converge systematically to the complete-basis-set (CBS) limit using empirical extrapolation techniques. For first- and second-row atoms, the basis sets are cc-pVNZ where *N=D,T,Q,5,6*,... (D=double, T=triples, etc.).

The 'cc-p', stands for “correlation-consistent polarized” and the “V” indicates they are valence-only basis sets. These basis sets include successively larger shells of polarization (correlating) functions (d, f, g, etc.) and more recently have become widely used and are the current state of the art for correlated or post-Hartree-Fock calculations.

Other used basis sets

TZVP basis set, augmented with polarization functions (p on H, d on first- and second-row atoms [6])

LANL2DZ basis set used in this work for iodine. This basis set uses an effective core for all atoms larger than Ne. [7]

4.2. Statistical Thermodynamics

The key feature in Statistical thermodynamics is the partition function. [8] The partition function allows the calculation of all macroscopic functions. For a single molecule is usually denoted q and defined as a sum of exponential terms involving all possible quantum energy states; Q is the partition function for N identities that could be a molecule or a particule. [8]

$$q = \sum_{i}^{allstates} e^{-\varepsilon_i / k_B T} \quad \textbf{(4.1)}$$

$$Q = q^N \text{ (different particles)} \quad \textbf{(4.2)}$$

$$Q = \frac{q^N}{N!} \text{ (identical particles)} \quad \textbf{(4.3)}$$

The partition function may alternatively be written as a sum over all distinct energy levels, times a degeneracy factor g_i.

$$q = \sum_{i}^{allstates} g_i e^{-\varepsilon_i / k_B T} \quad \textbf{(4.4)}$$

Once the partition function is known, thermodynamic functions such as the internal energy U and Helmoltz free energy A may be calculated according to:

$$U = k_B T^2 \left(\frac{\partial \ln Q}{\partial T} \right)_V \quad \textbf{(4.5)}$$

$$A = -k_B T \ln Q \quad \textbf{(4.6)}$$

Macroscopic observables, such as pressure P or heat capacity at constant volume C_v, may be calculated as derivatives of thermodynamic functions.

$$P = -\left(\frac{\partial A}{\partial V}\right)_T = k_B T\left(\frac{\partial \ln Q}{\partial V}\right)_T \quad \textbf{(4.7)}$$

$$C_V = \left(\frac{\partial U}{\partial T}\right)_V = 2k_B T\left(\frac{\partial \ln Q}{\partial T}\right)_V + k_B T^2\left(\frac{\partial^2 \ln Q}{\partial T^2}\right)_V \quad \textbf{(4.8)}$$

Other thermodynamic functions, such as the enthalpy H, the entropy S and Gibbs free energy G, may be constructed from these previous relations.

$$H = U + PV = k_B T^2\left(\frac{\partial \ln Q}{\partial T}\right)_V + k_B TV\left(\frac{\partial \ln Q}{\partial V}\right)_T \quad \textbf{(4.9)}$$

$$S = \frac{U - A}{T} = k_B T\left(\frac{\partial \ln Q}{\partial T}\right)_V + k_B \ln Q \quad \textbf{(4.10)}$$

$$G = H - TS = k_B TV\left(\frac{\partial \ln Q}{\partial V}\right)_T - k_B T \ln Q \quad \textbf{(4.11)}$$

In order to calculate q(Q) all possible quantum states are needed. It is usually assumed that the energy of a molecule can be approximated as a sum of terms involving translational, rotational, vibrational and electronic states. This is a good approximation, but for linear molecules, for example, the separation of the rotational and vibrational components may be problematic. [8]

The assumption that the energy can be written as a sum of terms implies that the partition function can be written as a product of terms. As the enthalpy and entropy contributions involve taking the logarithm of q, the product thus transforms into sums of enthalpy and entropy contributions.

$$\varepsilon_{tot} = \varepsilon_{trans} + \varepsilon_{rot} + \varepsilon_{vib} + \varepsilon_{elec} \quad \textbf{(4.12)}$$

$$q_{tot} = q_{trans} q_{rot} q_{vib} q_{elec} \quad \textbf{(4.13)}$$

$$H_{tot} = H_{trans} + H_{rot} + H_{vib} + H_{elec} \quad \textbf{(4.14)}$$

$$S_{tot} = S_{trans} + S_{rot} + S_{vib} + S_{elec} \quad \textbf{(4.15)}$$

For each of the partition functions the sum over allowed quantum states runs to infinity; however, since the energies become larger, the partition functions are finite.

- **Contributions from translation motion**

Partition function - translational

The allowed quantum states for the translational energy are determined by placing the molecule in a "box". [8] The solutions to the Schrödinger equation for such a "particle in a box" are standing waves, cosine and sine functions, and the energy levels are very close together. The summation in the partition function can therefore be replaced by an integral (an integral is just a sum in the limit of infinitely small contributions).

The translational partition function becomes:

$$q_{trans} = \left(\frac{2\pi M k_B T}{h^2} \right)^{3/2} V \qquad \textbf{(4.16)}$$

The only molecular parameter in this case, is the total molecular mass M. The volume depends on the number of particles. It is usually to work on a molar scale, in which case V is the volume of one mole of (ideal) gas.

Enthalpy – translational

The enthalpy may be calculated by carrying out the required differentiations in 4.9:

$$H_{trans} = \frac{5}{2} RT \qquad \textbf{(4.17)}$$

Entropy - translational

The entropy may be calculated by carrying out the required differentiations in 4.10:

$$S_{trans} = \frac{5}{2} R + R \ln \left(\frac{V}{N_A} \left(\frac{2\pi M k_B T}{h^2} \right)^{3/2} \right) \qquad \textbf{(4.18)}$$

- **Contributions from electronic motion**

Partition function – electronic

The electronic partition function involves a sum over electronic quantum states. These are the solutions to the electronic Schrödinger equation. [8] The energy difference between the ground and excited states is usually much larger than $k_B T$, which means that only the first term in the partition function summation (equation 4.4) is important. Defining the zero point for the energy as the electronic energy of the reactant, the electronic partition functions for the reactant and transition state (TS) become:

$$q_{elec}^{react} = g \qquad \textbf{(4.19)}$$

$$q_{elec}^{TS} = g e^{-\frac{\Delta E^{\neq}}{k_B T}} \qquad \textbf{(4.20)}$$

The $\Delta E^{\neq}$ term is the difference in electronic energy between the reactant and TS, and g is the electronic degeneracy of the wave function. [8] The degeneracy may be either in the spin part (g= 1 for a singlet, 2 for a doublet, 3 for a triplet etc.) or in the spatial part for an E, π or Δ representation, 3 for a T representation etc.). The large majority of stable molecules have non-degenerate ground-state wave functions, and consequently g=1.

Enthalpy – electronic

The enthalpy may be calculated by carrying out the required differentiations in 4.9:

$$H_{elec}^{react} = 0$$
$$H_{elec}^{TS} = \Delta E^{\neq} \qquad \textbf{(4.21)}$$

Entropy – electronic

The entropy may be calculated by carrying out the required differentiations in 4.10:

$$S_{elec}^{react} = S_{elec}^{TS} = R\ln(g) \qquad \textbf{(4.22)}$$

- **Contributions from rotational motion**

Partition function - rotational

In the lowest approximation the rotation of a molecule is assumed to occur with a geometry that is independent of the rotational quantum number. A more refined treatment allows the geometry to “stretch” with rotational energy; this may be described by adding a “centrifugal” correction. Such corrections are typically of the order of a small fraction of the rotational energy. The energy levels calculated from the Schrödinger equation for a diatomic “rigid rotor” are given by:

$$\varepsilon_{rot} = J(J+1)\frac{h^2}{8\pi^2 I} \qquad \textbf{(4.23)}$$

Where, J is a quantum number running from zero to infinity and I is the moment of inertia given by:

$$I = m_1 r_1^2 + m_2 r_2^2 \qquad \textbf{(4.24)}$$

With, r_i being a coordinate relative to the centre of mass. For all molecules, except very light species such as H_2 and LiH, the moment of inertia is so large that the spacing between the rotational energy levels is much smaller than $k_B T$ at ambient temperatures. As for q_{trans}, this means the summation in eq.4.1 can be replaced by an integral, yielding:

$$q_{rot} = \frac{8\pi^2 I k_B T}{h^2 \sigma} \qquad \textbf{(4.25)}$$

The symmetry index σ is 2 for homonuclear and 1 for a heteronuclear diatomic molecule.

For a polyatomic molecule the equivalent of equation 6.24 is a 3x3 matrix.

$$I = \begin{pmatrix} \sum_i m_i (y_i^2 + z_i^2) & -\sum_i m_i x_i y_i & -\sum_i m_i x z_i \\ -\sum_i m_i x_i y_i & \sum_i m_i (x_i^2 + z_i^2) & -\sum_i m_i y_i z_i \\ -\sum_i m_i x_i z_i & -\sum_i m_i y_i z_i & \sum_i m_i (x_i^2 + y_i^2) \end{pmatrix} \qquad \textbf{(4.26)}$$

Where, the coordinates again are relative to the centre of mass. For a general polyatomic molecule the rotational energy levels cannot be written in a simple form. A good approximation, however, can be obtained from classical mechanics, resulting in the following partition function:

$$q_{rot} = \frac{\sqrt{\pi}}{\sigma}\left(\frac{8\pi^2 k_B T}{h^2}\right)^{3/2}\sqrt{I_1 I_2 I_3} \qquad \textbf{(4.27)}$$

Here, I_i are the three moments of inertia. The symmetry index σ is the order of the rotational subgroup in the molecular point group. The rotational partition function requires only information about the atomic masses and positions, i.e. the molecular geometry. [8]

Enthalpy - rotational

The enthalpy may be calculated by carrying out the required differentiations in 4.9:

$$H_{rot}(\text{non linear}) = \frac{3}{2}RT$$
$$H_{rot}(\text{linear}) = RT \qquad \textbf{(4.28)}$$

Entropy - rotational

The entropy may be calculated by carrying out the required differentiations in 4.10:

$$S_{rot}(\text{non linear}) = \frac{1}{2}R\left[3 + \ln\left(\frac{\sqrt{\pi}}{\sigma}\left(\frac{8\pi^2 k_B T}{h^2}\right)^{3/2}\sqrt{I_1 I_2 I_3}\right)\right] \qquad \textbf{(4.29)}$$

$$S_{rot}(\text{linear}) = R\left[1 + \ln\left(\left(\frac{8\pi^2 I k_B T}{\sigma h^2}\right)\right)\right] \qquad \textbf{(4.30)}$$

- **Contributions from vibrational motion**

Partition function – vibrational

In the lowest approximation the molecular vibrations may be described as those of a harmonic oscillator. These can be derived by expanding the energy as a function of the nuclear coordinates in a Taylor series around the equilibrium geometry. For a diatomic molecule this is the internuclear distance R. [8]

$$E(R) = E(R_0) + \frac{dE}{dR}(R - R_0) + \frac{1}{2}\frac{d^2E}{dR^2}(R - R_0)^2 + \frac{1}{6}\frac{d^3E}{dR^3}(R - R_0)^3 + \ldots \quad \textbf{(4.31)}$$

The first term may be taken as zero, this is just the zero point for the energy. The second term (the gradient) vanishes since the expansion is around the equilibrium geometry. Keeping only the lowest non-zero term, results in the harmonic approximation, with k being the force constant.

$$E(\Delta R) \cong \frac{1}{2}\frac{d^2E}{dR^2}\Delta R^2 = \frac{1}{2}k\Delta R^2 \quad \textbf{(4.32)}$$

Including higher-order terms leads to anharmonic corrections to the vibration, such effects are typically of the order of a few %. The energy levels obtained from the Schrödinger equation for a one-dimensional harmonic oscillator (diatomic system) are given by:

$$\varepsilon_{vib} = \left(n + \frac{1}{2}\right)h\nu$$
$$\nu = \frac{1}{2\pi}\sqrt{\frac{k}{\mu}} \quad \textbf{(4.33)}$$

Where, n is a quantum number running from zero to infinity and υ is the vibrational frequency given in terms of the force constant $k(\partial^2 E/\partial R^2)$ and the reduced mass $\mu = m_1 m_2/(m_1+m_2)$. Contrary to the translational and rotational energies, the difference between vibrational energy levels is not small compared to $k_B T$, it is typically of the same order of magnitude for temperatures around 300 K. The summation for q_{vib} can therefore not be replaced by an integral. Owing to the regular spacing of the energy level, however, the infinite summation can be written in a closed form.

$$q_{vib} = \sum_{n=0}^{\infty} e^{-\left(n+\frac{1}{2}\right)\frac{h\nu}{k_B T}} = e^{-\frac{h\nu}{2k_B T}} \sum_{n=0}^{\infty} e^{-\frac{nh\nu}{k_B T}} \qquad \textbf{(4.34)}$$

$$q_{vib} = e^{-\frac{h\nu}{2k_B T}} \left(1 + e^{-\frac{h\nu}{k_B T}} + e^{-\frac{2h\nu}{k_B T}} + e^{-\frac{3h\nu}{k_B T}} + \ldots\right)$$

$$\left(1 + e^{-\frac{h\nu}{k_B T}} + e^{-\frac{2h\nu}{k_B T}} + e^{-\frac{3h\nu}{k_B T}} + \ldots\right) = \frac{1}{1 - e^{-\frac{h\nu}{k_B T}}} \qquad \textbf{(4.35)}$$

$$q_{vib} = \frac{e^{-\frac{h\nu}{2k_B T}}}{1 - e^{-\frac{h\nu}{k_B T}}}$$

In the infinite sum each successive term is smaller than the previous by a constant factor ($e^{-h\nu/kT}$, which is □1), and can therefore be expressed in a closed form. Only the vibrational frequency is needed for calculating the vibrational partition function for a harmonic oscillator, i.e. only the force constant and the atomic masses are required.

For a polynuclear molecule the force constant *k* is replaced by a 3N x 3N matrix (N being the number of atoms in the molecule) containing all the second derivatives of the energy with respect to the coordinates. By a mass-weighting and transformation to a new coordinate system called the vibrational normal coordinates, this may be brought

to a diagonal form. In the vibrational normal coordinates, the 3N-dimensional Schrödinger equation can be separated into 3N one-dimensional equations, each having the form of a harmonic oscillator. Of these three describe the overall translation and three (two for a linear molecule) describe the overall rotation, surface, the eigenvalues of the force constant matrix are all positive. [8]

For a polyatomic molecule the total vibrational energy may be written as a sum of energies for each vibration, and the partition function as a product of partition functions.

$$q_{vib} = \prod_{i=1}^{3N-6} \frac{e^{-\frac{h\nu_i}{2k_BT}}}{1-e^{\frac{-h\nu_i}{k_BT}}} \qquad \textbf{(4.36)}$$

Only the vibrational frequencies are needed, which can be calculated from the force constant matrix and atomic masses.

Enthalpy – vibrational

The enthalpy may be calculated by carrying out the required differentiations in 4.9:

$$H_{vib} = R\sum_{i=1}^{3N-6}\left(\frac{h\nu_i}{2k_B} + \frac{h\nu_i}{k_B}\frac{1}{e^{h\nu_i/k_BT}-1}\right) \qquad \textbf{(4.37)}$$

Entropy – vibrational

The entropy may be calculated by carrying out the required differentiations in 4.10:

$$S_{vib} = R\sum_{i=1}^{3N-6}\left(\frac{h\nu_i}{k_BT}\frac{1}{e^{h\nu_i/k_BT}-1} - \ln(1-e^{-h\nu_i/k_BT})\right) \qquad \textbf{(4.38)}$$

4.2.1. Summary

Table 4.2. Resume of the different contributions (translational; electronic; rotational and vibrational).

	Translational	Electronic	Rotational (non linear)	Vibrational
q_i	$\frac{\frac{k_B T}{101325}}{\left(\frac{\sqrt{h^2}}{2\pi M k_B T}\right)^3}$	1	$\frac{\pi T^{3/2}}{\sigma\sqrt{I_1 I_2 I_3}}$	$\prod_{i=1}^{3N-6} \frac{e^{-\frac{h\nu_i}{2k_B T}}}{1-e^{\frac{-h\nu_i}{k_B T}}}$
H	$\frac{5}{2}RT$	0	$\frac{3}{2}RT$	$R\sum_{i=1}^{3N-6}\left(\frac{h\nu_i}{2k_B}+\frac{h\nu_i}{k_B}\frac{1}{e^{h\nu_i/k_B T}-1}\right)$
S	$R.\ln(q_{trans}+\frac{5}{2})$	0	$R.\ln(q_{rot}+\frac{3}{2})$	$R\sum_{i=1}^{3N-6}\left(\frac{h\nu_i}{k_B T}\frac{1}{e^{h\nu_i/k_B T}-1}-\ln(1-e^{-h\nu_i/k_B T})\right)$
C_v	$\frac{3}{2}R$	0	$\frac{3}{2}R$	$R\sum_{i=1}^{3N-6}\left(e^{\frac{h\nu_i}{k_B T}}\left(\frac{\frac{h\nu_i}{k_B T}}{e^{\frac{h\nu_i}{k_B T}}-1}\right)^2\right)$

4.3. Geometry optimization and vibrational frequency calculations

After the geometry optimization, the vibrational frequencies were calculated using the levels of theory previously described. These values were then corrected using the scaling factors calculated by Radom et al. [9-10] The used scaling factors are in fact, practically the same of the ones estimated by a simple correlation between experimental and computational vibrational frequencies obtained in this thesis, which confirms that the scaling factors presented by Radom et al could be used when the molecules in study have also and at least an aromatic ring.

The obtained results are presented in Supplementary informations and are discussed in the chapter 5 – Discussion and final remarks.

Table 4.3. Applied anharmonicity scaling factors for the correction of the vibrational frequencies for the different quantum chemical models.

Model/basis set	Anharmonicity scaling factors	ref
B3LYP/6-311++G(d,p)	0.9688	9
B3LYP/TZVP		
B3LYP/cc-pVTZ	0.9661	10
BLYP/6-311++G(d,p)	1.0001	9
BLYP/TZVP		
BLYP/cc-pVTZ	0.9970	10
BP86/6-311++G(d,p)	0.9978	9
BP86/TZVP		
BP86/cc-pVTZ	0.9978	9

4.4. The isodesmic reactions

In this work, the theoretical gaseous phase heat capacity and the absolute entropy for the eight mono-halogenated naphthalenes were calculated, exploring a method that combines computational calculations with isodesmic reactions, joining theoretical with experimental data, in order to overcome the experimental and theoretical drawbacks. These drawbacks cause erroneous estimates of the thermodynamic properties of these mono-halogenated naphthalenes. This methodology was previously described by Santos et al. [11]

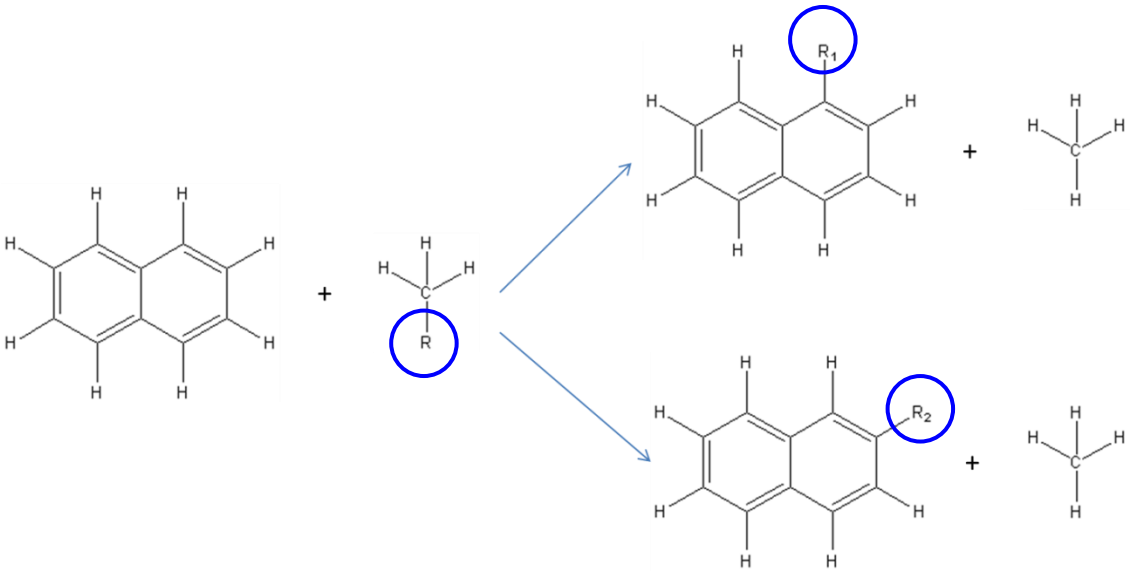

Figure 4.2. Reaction scheme used in the isodesmic estimation procedure of the gaseous phase molar heat capacity and absolute entropy for mono-halogenated naphthalenes. R – halogen atoms; R_1 – fluorine, bromine and iodine atoms; R_2 – chlorine, bromine and iodine atoms.

The obtained results for the isodesmic reactions are presented later in this chapter and can be compared with the obtained results using only quantum chemical calculations. Some conclusions are presented in the chapter 5 – Discussion and final remarks.

Results for molecules used in isodesmic reactions

Table 4.4. Results of $C^{0}_{p,\mathrm{m}}$ (J.K^{-1}.mol^{-1}) using several models/basis sets for the molecules used in isodesmic reactions at *T* = 298.15 K.

Model/Basis set	*Naphthalene*	*Methane*	*FMet*	*ClMet*	*BrMet*	*IMet*
B3LYP/6-311++G(d,p)	134.00	35.74	38.03	41.32	43.11	44.68
B3LYP/TZVP	130.02	35.36	37.38	40.74	42.47	43.85
B3LYP/cc-pVTZ	133.71	35.75	37.86	41.43	43.14	44.63
BLYP/6-311++G(d,p)	134.14	35.64	38.21	41.48	43.32	44.83
BLYP/TZVP	134.78	35.60	38.07	41.57	43.33	44.68
BLYP/cc-pVTZ	133.78	35.65	37.99	41.59	43.35	44.77
BP86/6-311++G(d,p)	134.84	35.80	38.11	41.30	43.12	44.68
BP86/TZVP	135.53	35.73	37.94	41.31	43.11	44.48
BP86/cc-pVTZ	134.02	35.80	37.89	41.36	43.10	44.58
Mean Values	**134.08* 133.02[12]**	**35.73* 35.69[13]**	**38.02* 37.49[14]**	**41.41* 40.75[14]**	**43.19* 42.43[14]**	**44.58* 44.10[14]**

Note: * - the values from TZVP basis set weren't used in the calculation of the mean values, because the scaling factor used in these two cases was 1.
Values at J·K^{-1}·mol^{-1}.
The used scaling factors are presented in table 4.3.

Table 4.5. Results of S_m^0 (J.K^{-1}.mol^{-1}) using several models/basis sets for the molecules used in isodesmic reactions at *T* = 298.15 K.

Model/Basis set	*Naphthalene*	*Methane*	*FMet*	*ClMet*	*BrMet*	*IMet*
B3LYP/6-311++G(d,p)	335.09	186.26	223.01	234.67	246.34	254.74
B3LYP/TZVP	332.49	186.15	222.80	234.49	246.08	254.23
B3LYP/cc-pVTZ	334.80	186.20	222.84	234.65	246.27	254.46
BLYP/6-311++G(d,p)	335.35	186.39	223.35	235.02	246.78	255.15
BLYP/TZVP	335.81	186.35	223.26	235.10	246.81	255.00
BLYP/cc-pVTZ	334.97	186.33	223.15	235.01	246.71	254.87
BP86/6-311++G(d,p)	335.96	186.46	223.21	234.74	246.40	254.81
BP86/TZVP	336.53	186.41	223.12	234.78	246.42	254.63
BP86/cc-pVTZ	335.35	186.40	223.03	234.69	246.30	254.50
Mean Values	**335.25* 336.52[15]**	**186.34* 188.66[16]**	**223.10* 222.91[14]**	**234.80* 234.58[14]**	**246.47* 246.38[14]**	**254.76* 254.12[14]**

Note: * - the values from TZVP basis set weren't used in the calculation of the mean values, because the scaling factor used in these two cases was 1.
Values at J·K^{-1}·mol^{-1}.
The used scaling factors are presented in table 4.3.

4.5. Results

4.5.1. Results for 1-halogenated naphthalenes

4.5.1.1. Results for 1-fluoronaphthalene

Table 4.6. Results of 1-fluoronaphthalene for $C_{v,\mathrm{m}}^{0}$, $C_{p,\mathrm{m}}^{0}$, S_{m}^{0} and $\Delta\Delta H$ at T = 298.15K.

Model/Basis set	$C_{v,\mathrm{m}}^{0}$ J.K^{-1}.mol^{-1}	$C_{p,\mathrm{m}}^{0}$ J.K^{-1}.mol^{-1}	S_{m}^{0} J.K^{-1}.mol^{-1}	$\Delta\Delta H$ kJ.mol^{-1}
B3LYP/6-311++G(d,p)	138.14	146.45 (144.98)	365.22 (364.15)	23.26
B3LYP/TZVP	135.04	143.35 (146.13)	362.94 (364.57)	22.87
B3LYP/cc-pVTZ	137.44	145.75 (144.75)	364.51 (363.84)	23.15
BLYP/6-311++G(d,p)	138.69	147.00 (145.11)	365.86 (364.32)	23.34
BLYP/TZVP	140.18	148.49 (146.06)	366.98 (365.03)	23.56
BLYP/cc-pVTZ	137.79	146.10 (144.80)	364.95 (363.93)	23.19
BP86/6-311++G(d,p)	139.12	147.43 (145.10)	366.29 (364.35)	23.42
BP86/TZVP	140.78	149.09 (146.17)	367.68 (365.21)	23.69
BP86/cc-pVTZ	137.81	146.12 (144.83)	365.13 (363.92)	23.23
Mean Values	**138.17***	**146.48* (144.93*)**	**365.33* (364,21*)**	**23.27**

Note: * - the values from TZVP basis set weren't used in the calculation of the mean values, because the scaling factor used in these two cases was 1. Values between parenthesis are the obtained values from the isodesmic reactions. The used scaling factors are presented in table 4.3.

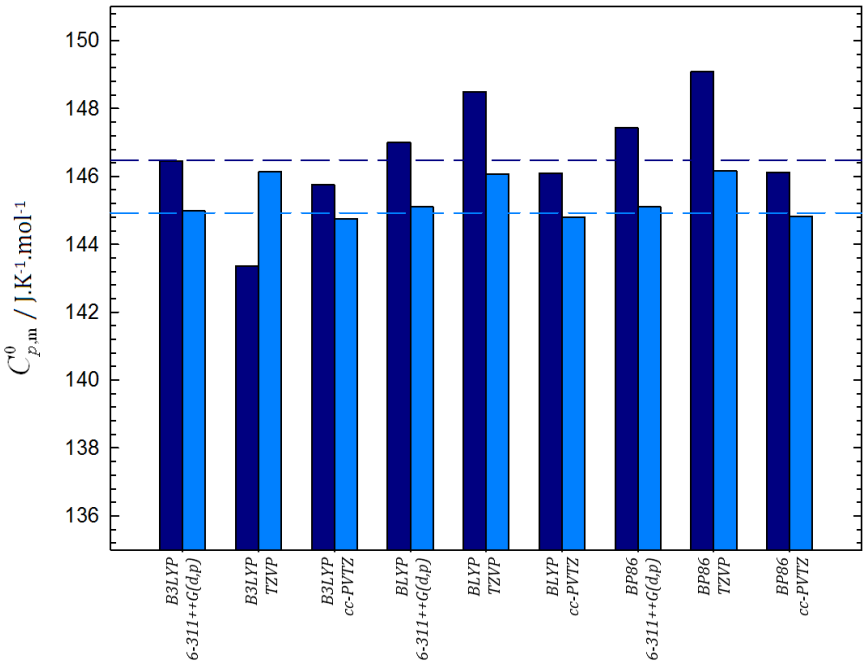

Figure 4.3. Gaseous phase heat capacities results of 1- fluoronaphthalene using several basis sets. ■ – results obtained from quantum chemical calculations; ■ - results obtained using the isodesmic reactions. - - mean value of the results obtained from quantum chemical calculations; - - mean value of the results obtained using the isodesmic reactions.

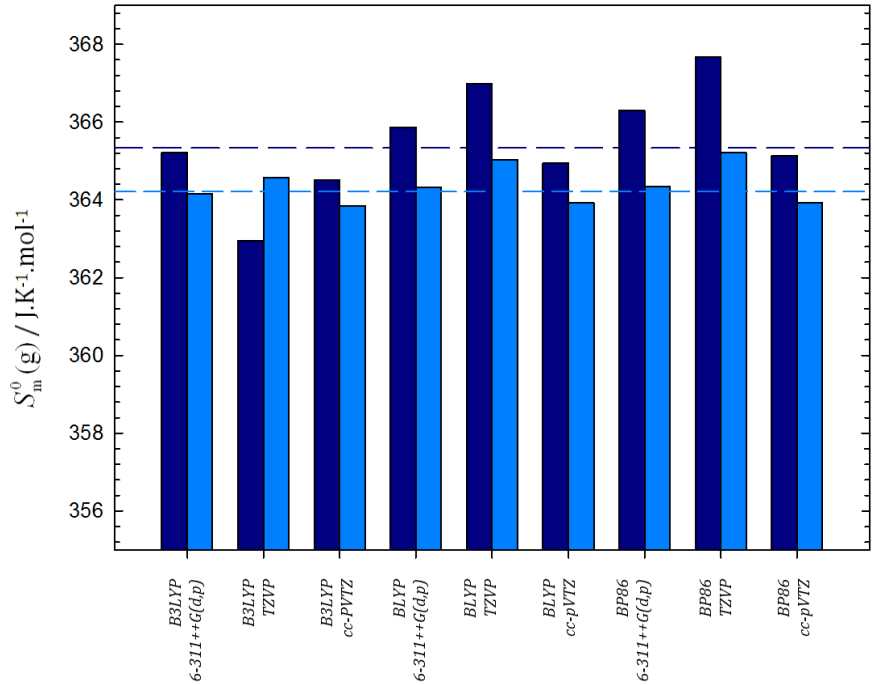

Figure 4.4. Gaseous phase absolute entropies results of 1- fluoronaphthalene using several basis sets. ■ – results obtained from quantum chemical calculations; ■ - results obtained using the isodesmic reactions. - - mean value of the results obtained from quantum chemical calculations; - - mean value of the results obtained using the isodesmic reactions.

4.5.1.2. Results for 1-chloronaphthalene

Table 4.7. Results of 1-chloronaphthalene for $C_{v,\mathrm{m}}^{0}$, $C_{p,\mathrm{m}}^{0}$, S_{m}^{0} and $\Delta\Delta H$ at T = 298.15K.

Model/Basis set	$C_{v,\mathrm{m}}^{0}$ J.K^{-1}.mol^{-1}	$C_{p,\mathrm{m}}^{0}$ J.K^{-1}.mol^{-1}	S_{m}^{0} J.K^{-1}.mol^{-1}	$\Delta\Delta H$ kJ.mol^{-1}
B3LYP/6-311++G(d,p)	141.63	149.94 (148.39)	376.39 (375.33)	24.22
B3LYP/TZVP	137.92	146.23 (148.86)	373.55 (375.16)	23.73
B3LYP/cc-pVTZ	141.27	149.58 (148.22)	376.01 (375.20)	24.17
BLYP/6-311++G(d,p)	142.10	150.41 (148.46)	377.11 (375.57)	24.29
BLYP/TZVP	142.71	151.22 (148.50)	377.77 (375.65)	24.43
BLYP/cc-pVTZ	141.64	149.95 (148.26)	376.59 (375.38)	24.23
BP86/6-311++G(d,p)	142.55	150.86 (148.55)	377.40 (375.60)	24.36
BP86/TZVP	143.49	151.80 (148.72)	378.21 (375.75)	24.52
BP86/cc-pVTZ	141.63	149.94 (148.39)	376.57 (375.37)	24.24
Mean Values	**141.80***	**150.12* (148.48)**	**376.68* (375.41*)**	**24.25***

Note: * - the values from TZVP basis set weren't used in the calculation of the mean values, because the scaling factor used in these two cases was 1. Values between parenthesis are the obtained values from the isodesmic reactions. The used scaling factors are presented in table 4.3.

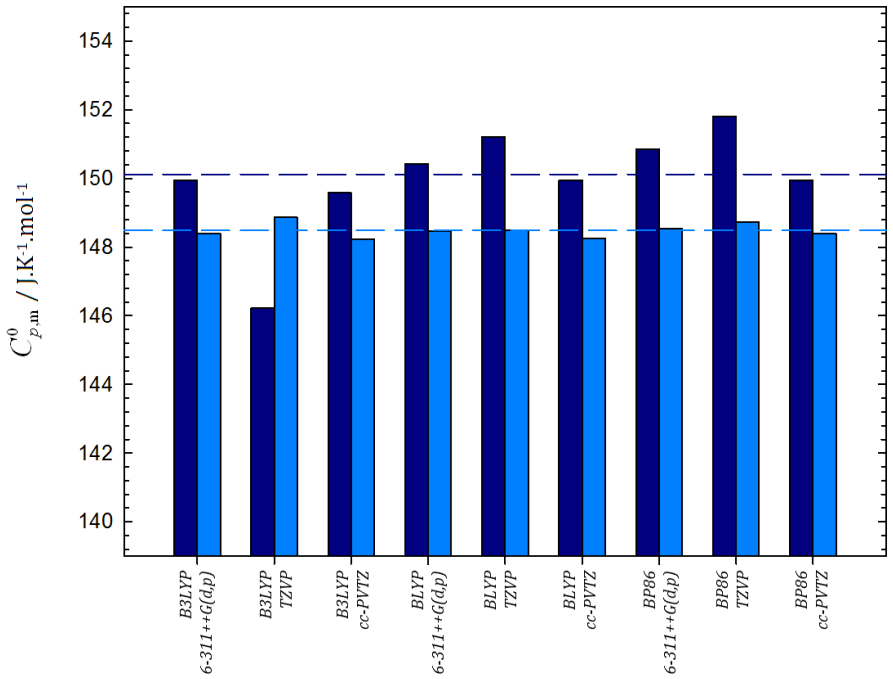

Figure 4.5. Gaseous phase heat capacities results of 1- chloronaphthalene using several basis sets. ■ – results obtained from quantum chemical calculations; ■ - results obtained using the isodesmic reactions. **- -** mean value of the results obtained from quantum chemical calculations; **- -** mean value of the results obtained using the isodesmic reactions.

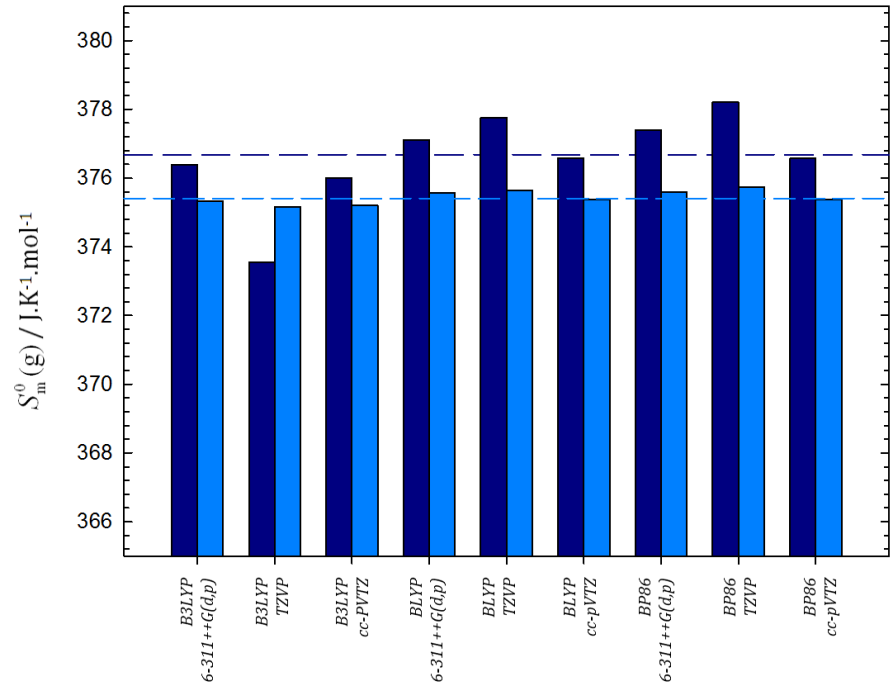

Figure 4.6. Gaseous phase absolute entropies results of 1- chloronaphthalene using several basis sets. ■ – results obtained from quantum chemical calculations; ■ - results obtained using the isodesmic reactions. **- -** mean value from the results obtained from quantum chemical calculations; **- -** mean value from the results obtained using the isodesmic reactions.

4.5.1.3. Results for 1-bromonaphthalene

Table 4.8. Results of 1-bromonaphthalene for $C_{v,\mathrm{m}}^{0}$, $C_{p,\mathrm{m}}^{0}$, S_{m}^{0} and $\Delta\Delta H$ at T = 298.15K.

Model/Basis set	$C_{v,\mathrm{m}}^{0}$ J.K^{-1}.mol^{-1}	$C_{p,\mathrm{m}}^{0}$ J.K^{-1}.mol^{-1}	S_{m}^{0} J.K^{-1}.mol^{-1}	$\Delta\Delta H$ kJ.mol^{-1}
B3LYP/6-311++G(d,p)	143.58	151.89 (150.31)	388.44 (387.51)	24.93
B3LYP/TZVP	139.60	147.91 (150.57)	385.13 (386.95)	24.38
B3LYP/cc-pVTZ	143.05	151.36 (150.05)	387.78 (387.15)	24.84
BLYP/6-311++G(d,p)	144.10	152.41 (150.38)	389.36 (387.86)	25.03
BLYP/TZVP	144.54	152.85 (150.13)	389.57 (387.54)	25.09
BLYP/cc-pVTZ	143.47	151.78 (150.09)	388.55 (387.44)	24.92
BP86/6-311++G(d,p)	144.51	152.82 (150.45)	389.41 (387.75)	25.07
BP86/TZVP	145.09	153.40 (150.28)	389.75 (387.45)	25.16
BP86/cc-pVTZ	143.40	151.71 (150.18)	388.26 (387.25)	24.90
Mean Values	**143.69***	**151.99* (150.24)**	**388.63* (387.50*)**	**24.95***

Note: * - the values from TZVP basis set weren't used in the calculation of the mean values, because the scaling factor used in these two cases was 1. Values between parenthesis are the obtained values from the isodesmic reactions. The used scaling factors are presented in table 4.3.

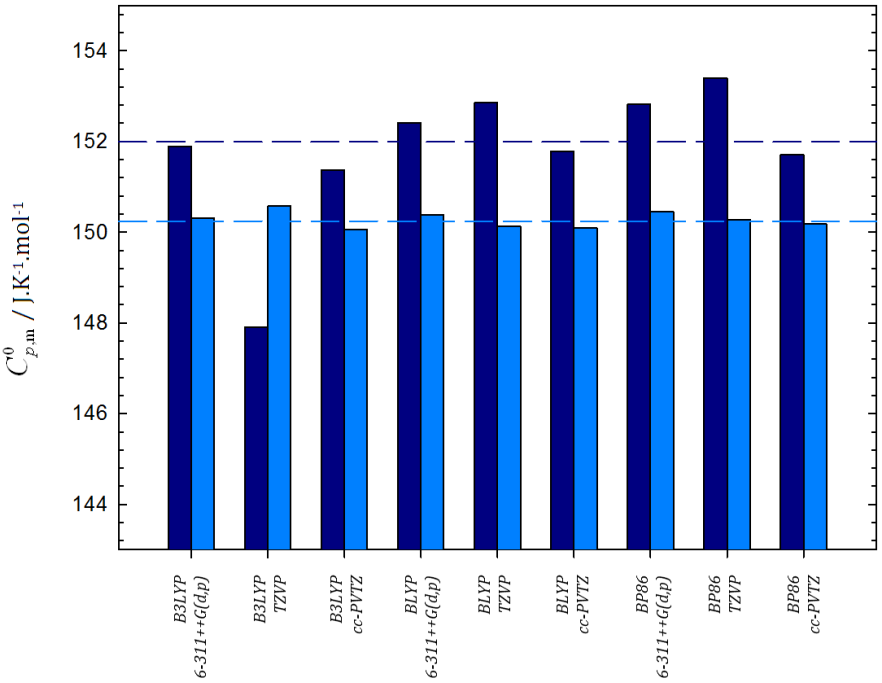

Figure 4.7. Gaseous phase heat capacities results of 1- bromonaphthalene using several basis sets. ■ – results obtained from quantum chemical calculations; ■ - results obtained using the isodesmic reactions. - - mean value of the results obtained from quantum chemical calculations; - - mean value of the results obtained using the isodesmic reactions.

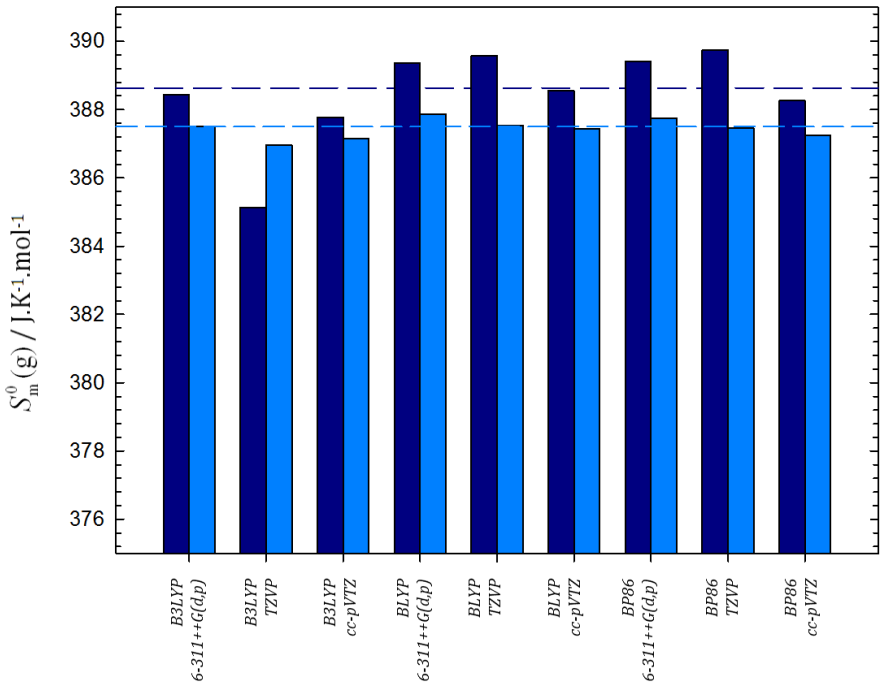

Figure 4.8. Gaseous phase absolute entropies results of 1-bromonaphthalene using several basis sets. ■ – results obtained from quantum chemical calculations; ■ - results obtained using the isodesmic reactions. - - mean value of the results obtained from quantum chemical calculations; - - mean value of the results obtained using the isodesmic reactions.

4.5.1.4. Results for 1-iodonaphthalene

Table 4.9. Results of 1-iodonaphthalene for $C^0_{v,\mathrm{m}}$, $C^0_{p,\mathrm{m}}$, S^0_{m} and $\Delta\Delta H$ at T = 298.15K.

Model/Basis set	$C^0_{v,\mathrm{m}}$ J.K^{-1}.mol^{-1}	$C^0_{p,\mathrm{m}}$ J.K^{-1}.mol^{-1}	S^0_{m} J.K^{-1}.mol^{-1}	$\Delta\Delta H$ kJ.mol^{-1}
B3LYP/6-311++G(d,p)	144.48	152.79 (151.26)	396.99 (395,40)	25.33
BLYP/6-311++G(d,p)	145.01	153.32 (151.40)	397.87 (395.74)	25.43
BP86/6-311++G(d,p)	145.48	153.79 (151.48)	397.97 (395.64)	25.48
Mean Values	**144.99**	**153.30 (151.38)**	**397.61 (395.60)**	**25.41**

Note: * - values between parenthesis are the obtained values from the isodesmic reactions.
The used scaling factors are presented in table 4.3.

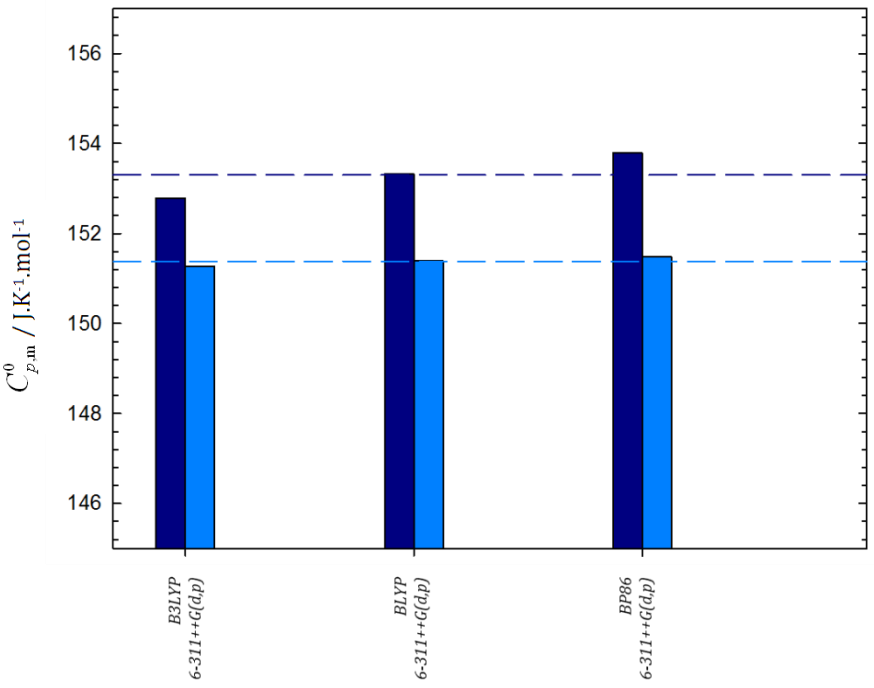

Figure 4.9. Gaseous phase heat capacities results of 1- iodonaphthalene using several basis sets. ■ – results obtained from quantum chemical calculations; ■ - results obtained using the isodesmic reactions. **- -** mean value of the results obtained from quantum chemical calculations; **- -** mean value of the results obtained using the isodesmic reactions.

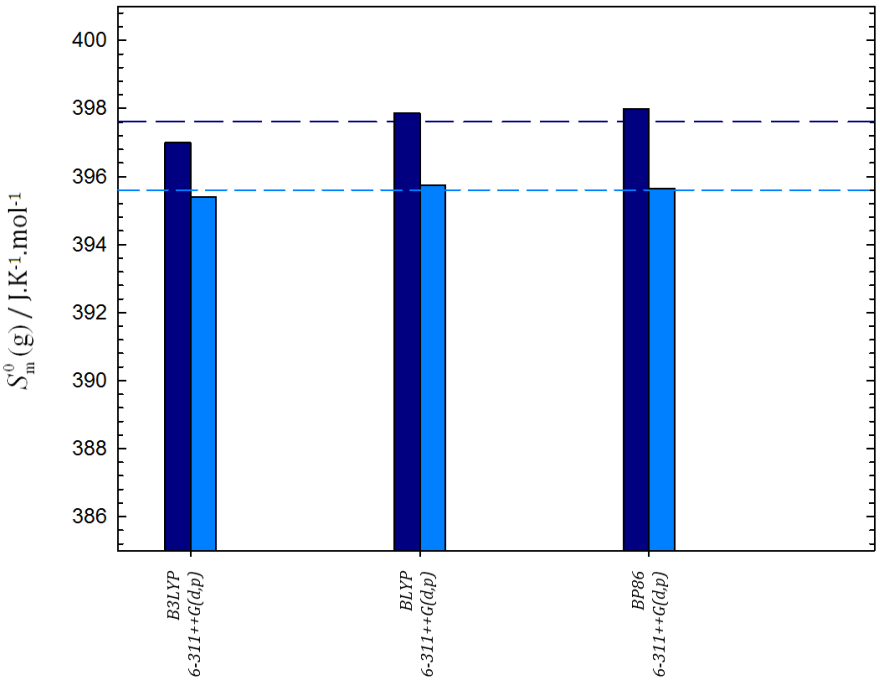

Figure 4.10. Gaseous phase absolute entropies results of 1- iodonaphthalene using several basis sets. ■ – results obtained from quantum chemical calculations; ■ - results obtained using the isodesmic reactions. **- -** mean value of the results obtained from quantum chemical calculations; **- -** mean value of the results obtained using the isodesmic reactions.

4.5.2. Results of 2-halogenated naphthalenes

4.5.2.1. Results for 2-fluoronaphthalene

Table 4.10. Results of 2-fluoronaphthalene for $C_{v,\mathrm{m}}^{0}$, $C_{p,\mathrm{m}}^{0}$, S_{m}^{0} and $\Delta\Delta H$ at T = 298.15K.

Model/Basis set	$C_{v,\mathrm{m}}^{0}$ J.K^{-1}.mol^{-1}	$C_{p,\mathrm{m}}^{0}$ J.K^{-1}.mol^{-1}	S_{m}^{0} J.K^{-1}.mol^{-1}	$\Delta\Delta H$ kJ.mol^{-1}
B3LYP/6-311++G(d,p)	138.71	147.02 (145.55)	365.97 (364.90)	23.32
B3LYP/TZVP	136.39	144.70 (147.48)	364.34 (365.97)	23.06
B3LYP/cc-pVTZ	137.89	146.20 (145.20)	365.16 (364.49)	23.19
BLYP/6-311++G(d,p)	139.20	147.51 (145.62)	366.57 (365.03)	23.39
BLYP/TZVP	141.44	149.75 (147.32)	368.37 (366.42)	23.74
BLYP/cc-pVTZ	138.25	146.56 (145.26)	365.62 (364.60)	23.24
BP86/6-311++G(d,p)	139.78	148.09 (145.76)	367.12 (365.18)	23.49
BP86/TZVP	142.33	150.64 (147.72)	369.46 (366.99)	23.94
BP86/cc-pVTZ	138.38	146.69 (145.40)	365.90 (364.69)	23.29
Mean Values	**138.70***	**147.01* (145.47)***	**366.06* (365.06*)**	**23.32***

Note: * - the values from TZVP basis set weren't used in the calculation of the mean values, because the scaling factor used in these two cases was 1. Values between parenthesis are the obtained values from the isodesmic reactions. The used scaling factors are presented in table 4.3.

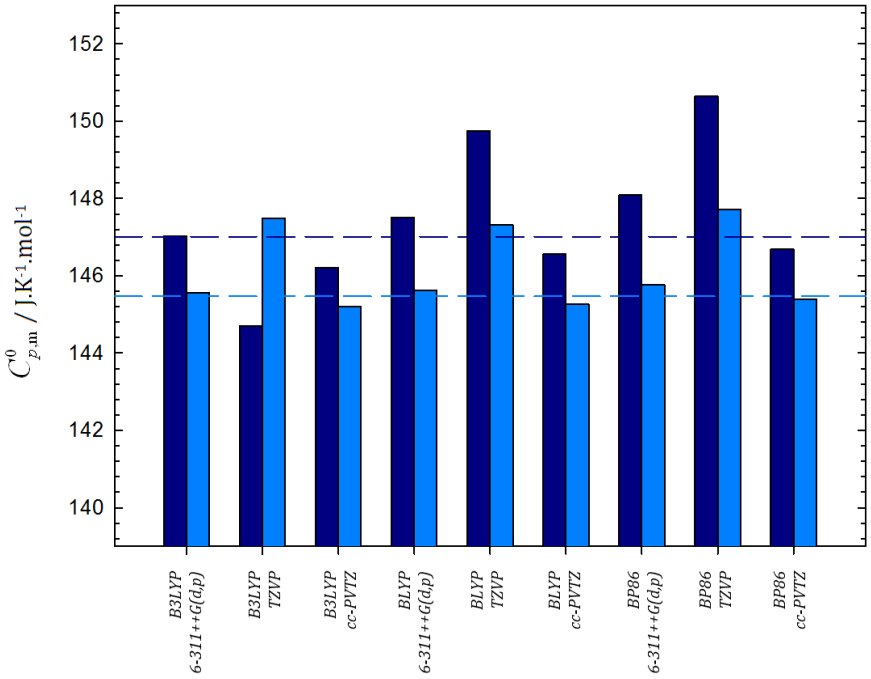

Figure 4.11. Gaseous phase heat capacities results of 2- fluoronaphthalene using several basis sets. ■ – results obtained from quantum chemical calculations; ■ - results obtained using the isodesmic reactions. **- -** mean value of the results obtained from quantum chemical calculations; **- -** mean value of the results obtained using the isodesmic reactions.

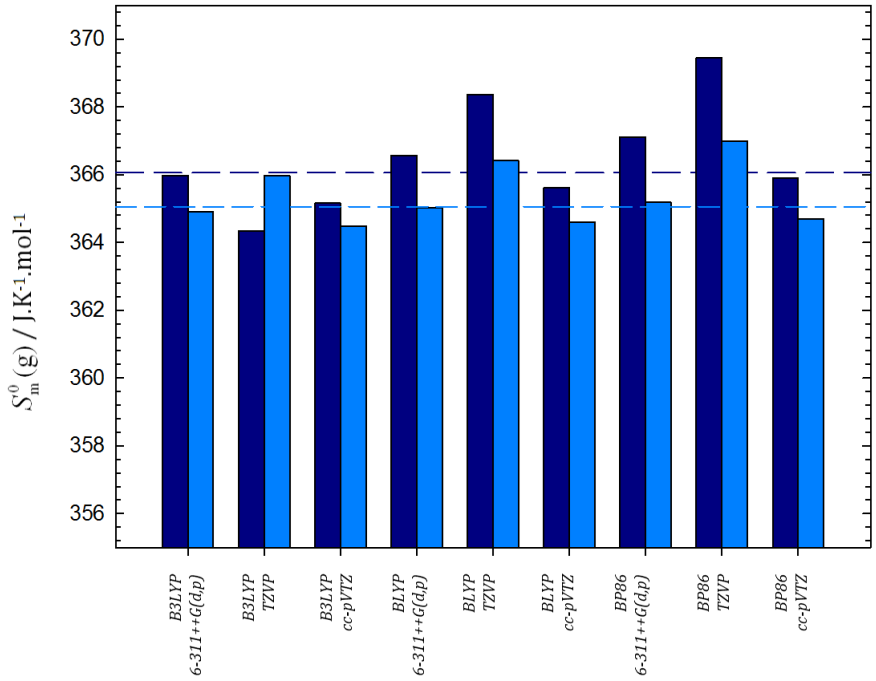

Figure 4.12. Gaseous phase absolute entropies results of 2- fluoronaphthalene using several basis sets. ■ – results obtained from quantum chemical calculations; ■ - results obtained using the isodesmic reactions. **- -** mean value o fthe results obtained from quantum chemical calculations; **- -** mean value of the results obtained using the isodesmic reactions.

4.5.2.2. Results for 2-chloronaphthalene

Table 4.11. Results of 2-chloronaphthalene for $C^0_{v,\mathrm{m}}$, $C^0_{p,\mathrm{m}}$, S^0_{m} and $\Delta\Delta H$ at T = 298.15K.

Model/Basis set	$C^0_{v,\mathrm{m}}$ J.K^{-1}.mol^{-1}	$C^0_{p,\mathrm{m}}$ J.K^{-1}.mol^{-1}	S^0_{m} J.K^{-1}.mol^{-1}	$\Delta\Delta H$ kJ.mol^{-1}
B3LYP/6-311++G(d,p)	141.81	150.12 (148.57)	377.09 (376.03)	24.25
B3LYP/TZVP	138.76	147.07 (149.70)	374.69 (376.30)	23.86
B3LYP/cc-pVTZ	141.42	149.73 (148.37)	376.74 (375.93)	24.20
BLYP/6-311++G(d,p)	142.24	150.55 (148.60)	377.67 (376.13)	24.32
BLYP/TZVP	143.69	152.00 (149.28)	378.77 (376.65)	24.54
BLYP/cc-pVTZ	141.73	150.04 (148.35)	377.17 (375.96)	24.25
BP86/6-311++G(d,p)	142.68	150.99 (148.68)	377.92 (376.12)	24.38
BP86/TZVP	144.40	152.71 (149.63)	379.33 (376.87)	24.66
BP86/cc-pVTZ	141.74	150.05 (148.50)	377.18 (375.98)	24.26
Mean Values	**141.94***	**150.25* (148.51)***	**377.30* (376.03*)**	**24.28***

Note: * - the values from TZVP basis set weren't used in the calculation of the mean values, because the scaling factor used in these two cases was 1. Values between parenthesis are the obtained values from the isodesmic reactions. The used scaling factors are presented in table 4.3.

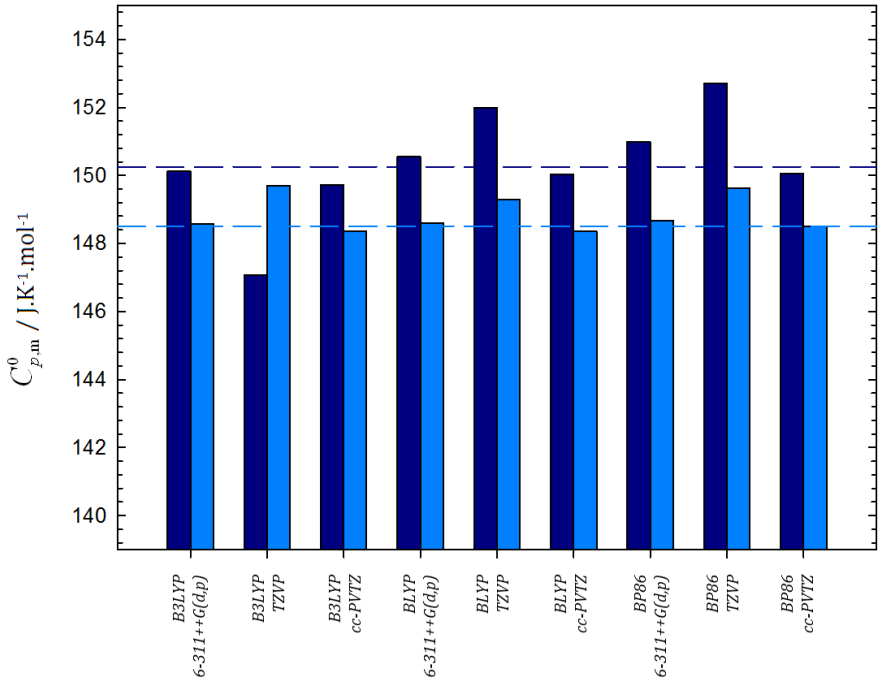

Figure 4.13. Gaseous phase heat capacities results of 2-chloronaphthalene using several basis sets. ■ – results obtained from quantum chemical calculations; ■ - results obtained using the isodesmic reactions. - - mean value of the results obtained from quantum chemical calculations; - - mean value of the results obtained using the isodesmic reactions.

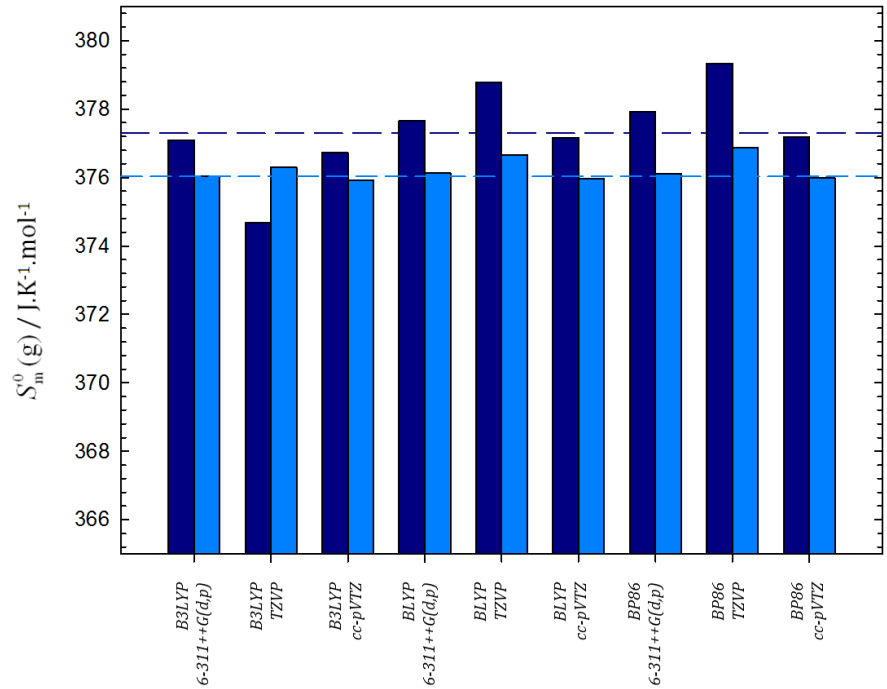

Figure 4.14. Gaseous phase absolute entropies results of 2- chloronaphthalene using several basis sets. ■ – results obtained from quantum chemical calculations; ■ - results obtained using the isodesmic reactions. - - mean value of the results obtained from quantum chemical calculations; - - mean value of the results obtained using the isodesmic reactions.

4.5.2.3. Results for 2-bromonaphthalene

Table 4.12. Results of 2-bromonaphthalene for $C_{v,\mathrm{m}}^{0}$, $C_{p,\mathrm{m}}^{0}$, S_{m}^{0} and $\Delta\Delta H$ at T = 298.15K.

Model/Basis set	$C_{v,\mathrm{m}}^{0}$ J.K^{-1}.mol^{-1}	$C_{p,\mathrm{m}}^{0}$ J.K^{-1}.mol^{-1}	S_{m}^{0} J.K^{-1}.mol^{-1}	$\Delta\Delta H$ kJ.mol^{-1}
B3LYP/6-311++G(d,p)	143.71	152.02 (150.44)	389.20 (388.27)	24.95
B3LYP/TZVP	140.24	148.55 (151.21)	386.28 (388.10)	24.48
B3LYP/cc-pVTZ	143.13	151.44 (150.13)	388.61 (387.98)	24.87
BLYP/6-311++G(d,p)	144.19	152.50 (150.47)	389.92 (388.42)	25.03
BLYP/TZVP	145.12	153.43 (150.71)	390.53 (388.50)	25.17
BLYP/cc-pVTZ	143.48	151.79 (150.10)	389.17 (388.06)	24.92
BP86/6-311++G(d,p)	144.65	152.96 (150.59)	390.07 (388.41)	25.09
BP86/TZVP	145.85	154.16 (151.04)	390.96 (388.66)	25.28
BP86/cc-pVTZ	143.50	151.81 (150.28)	389.06 (388.05)	24.93
Mean Values	**143.78***	**152.09* (150.34)***	**389.34* (388.20*)**	**24.97***

Note: * - the values from TZVP basis set weren't used in the calculation of the mean values, because the scaling factor used in these two cases was 1. Values between parenthesis are the obtained values from the isodesmic reactions. The used scaling factors are presented in table 4.3.

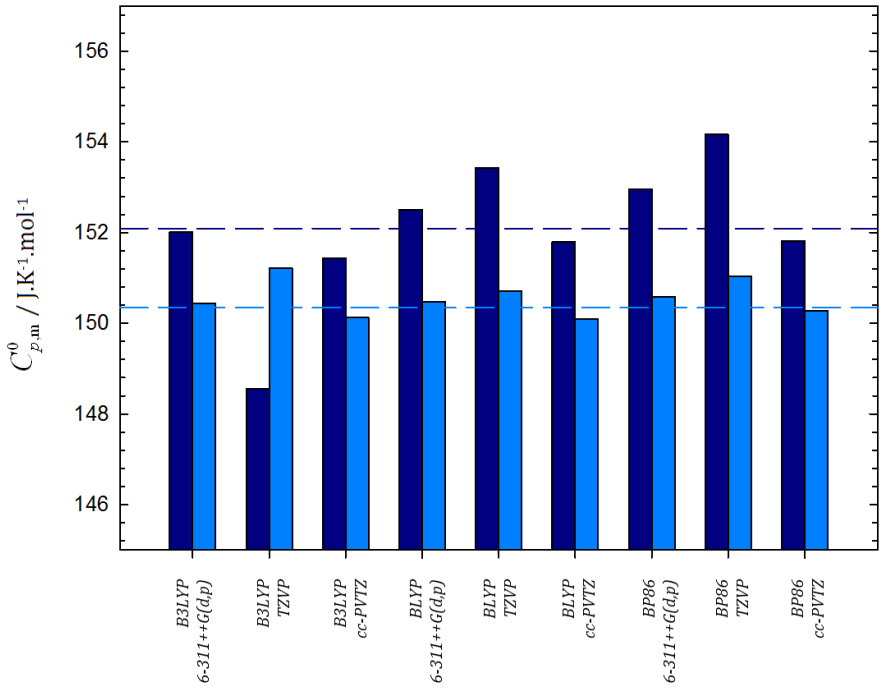

Figure 4.15. Gaseous phase heat capacities results of 2- bromonaphthalene using several basis sets. ■ – results obtained from quantum chemical calculations; ■ - results obtained using the isodesmic reactions. - - mean value of the results obtained from quantum chemical calculations; - - mean value of the results obtained using the isodesmic reactions.

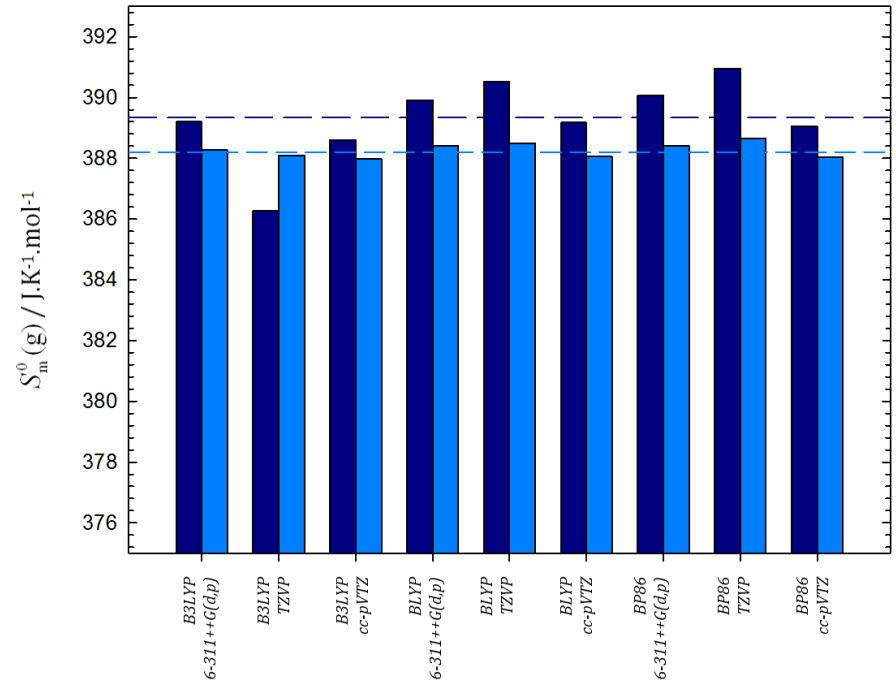

Figure 4.16. Gaseous phase absolute entropies results of 2- bromonaphthalene using several basis sets. ■ – results obtained from quantum chemical calculations; ■ - results obtained using the isodesmic reactions. - - mean value of the results obtained from quantum chemical calculations; - - mean value of the results obtained using the isodesmic reactions.

4.5.2.4. Results for 2-iodonaphthalene

Table 4.13. Results of 2-iodonaphthalene for $C_{v,\mathrm{m}}^{0}$, $C_{p,\mathrm{m}}^{0}$, S_{m}^{0} and $\Delta\Delta H$ at T = 298.15K.

Model/Basis set	$C_{v,\mathrm{m}}^{0}$ J.K^{-1}.mol^{-1}	$C_{p,\mathrm{m}}^{0}$ J.K^{-1}.mol^{-1}	S_{m}^{0} J.K^{-1}.mol^{-1}	$\Delta\Delta H$ kJ.mol^{-1}
B3LYP/6-311++G(d,p)	144.90	153.21 (151.68)	398.38 (396.79)	25.43
B3LYP/cc-pVTZ	143.63	151.94 (150.76)	396.91 (395.83)	25.22
BLYP/6-311++G(d,p)	145.38	153.69 (151.77)	399.05 (396.92)	25.50
BLYP/cc-pVTZ	143.95	152.26 (150.77)	397.41 (395.88)	25.26
BP86/6-311++G(d,p)	145.88	154.19 (151.88)	399.40 (397.07)	25.58
BP86/cc-pVTZ	144.14	152.45 (151.06)	397.62 (396.15)	25.31
Mean Values	**144.65**	**152.96 (151.32)**	**398.13 (396.93)**	**25.38**

Note: * - values between parenthesis are the obtained values from the isodesmic reactions.
The used scaling factors are presented in table 4.3.

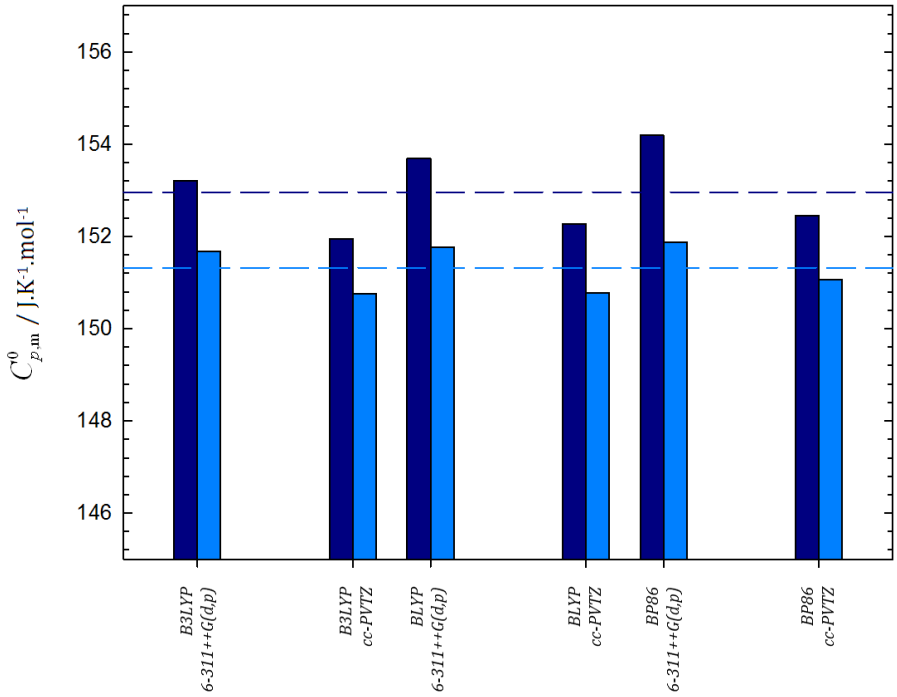

Figure 4.17. Gaseous phase heat capacities results of 2-iodonaphthalene using several basis sets. ■ – results obtained from quantum chemical calculations; ■ - results obtained using the isodesmic reactions. - - mean value of the results obtained from quantum chemical calculations; - - mean value of the results obtained using the isodesmic reactions.

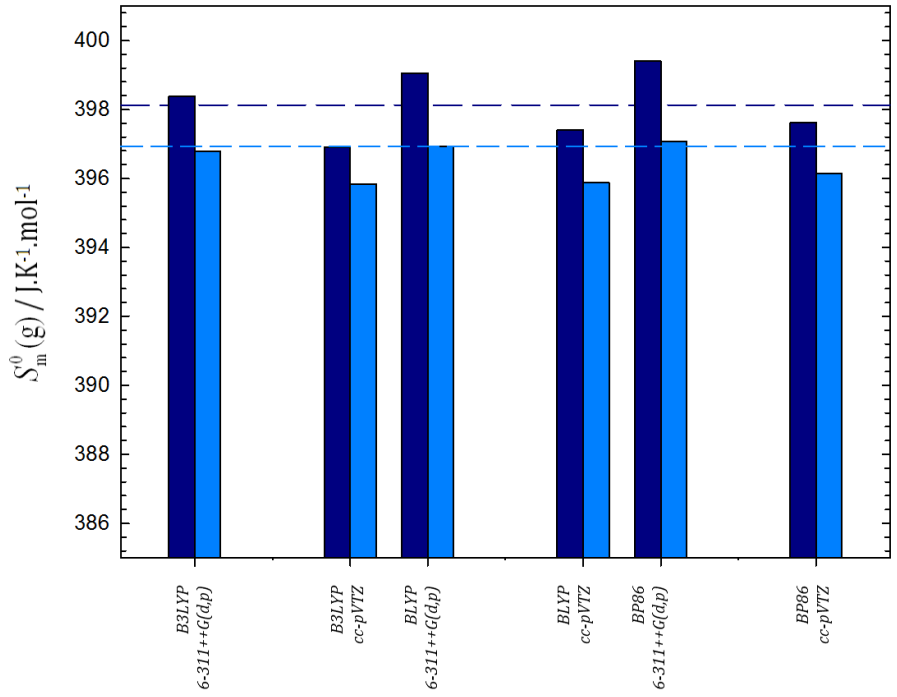

Figure 4.18. Gaseous phase absolute entropies results of 2- iodonaphthalene using several basis sets. ■ – results obtained from quantum chemical calculations; ■ - results obtained using the isodesmic reactions. - - mean value of the results obtained from quantum chemical calculations; - - mean value of the results obtained using the isodesmic reactions.

References

[1] http://www.gaussian.com/

[2] http://www.gaussian.com/g_tech/g_ur/k_dft.htm

[3] Ditchfield, R.; Hehre, W.J.; Pople, J. A., *J. Chem. Phys*., 54 (1971) 724–728.

[4] Leszczynski, J., *Handbook of Computational Chemistry* (2012).

[5] Dunning, T.H., *J. Chem. Phys*., 90 (1989) 1007–1023.

[6] http://www.cfs.dl.ac.uk/docs/html/part3/node14.html

[7] http://www.wavefun.com/support/sp_compfaq/Basis_Set_FAQ.html

[8] Frank Jensen, *Introduction to Computational Chemistry* (1999).

[9] Merrick, J. P.; Moran, D.; Radom, *J. Phys. Chem. A,* 111 (2007) 11683–11700.

[10] Precomputed vibrational scaling factors. Computational Chemistry Comparison and Benchmark Database (CCCBDB), released by National Institute of Standards and Technology (http://www.nist.gov).

[11] Santos, L.M.N.B.F.; Rocha, M.A.A.; Gomes, L.R.; Schröder, B.; Coutinho, J.A.P., *J. Chem. Eng. Data,* 55 (2010) 2799–2808.

[12] Dorofeeva O.V., *Thermochim. Acta,* 102 (1986) 59-66.

[13] Gurvich, L.V.; Veyts, I.V.; Alcock, C.B., *Thermodynamic Properties of Individual Substances*, 4th ed.; Vols. 1 and 2, Hemisphere, New York, (1989).

[14] Wagman, D.D. et al., *J. Phys. Chem. Ref. Data*, Vol.II, Suppl.2, (1982).

[15] Pitzer K.S., *J. Am. Chem. Soc*., 78 (1956) 2707-2711.

[16] Morrison J.A., *J.Chem.Phys*., 39 (1963) 635-653.

Chapter 5

Discussion and Final Remarks

5.1. Experimental results

5.1.1. The influence of the size of the halogen atom

5.1.2. Estimative of the thermodynamic properties of 1-chloronaphthalene

5.2 Statistical thermodynamics results

5.2.1. Calculation methodologies

5.2.2. Influence of Temperature

References

5.1. Experimental results

5.1.1. The influence of the size of the halogen atom

Correlations between the volume of the halogen atom and thermodynamic properties were previously derived for *p*-halobenzoic acids [1], methyl-*p*-halobenzoate [2] and *p*-halophenols [3]. In this chapter the correlation between the volume of the substituted halogen atom and thermodynamic properties of the studied halonaphthalenes, is presented and discussed. Table 5.1 lists the bondi radius and the derived atomic volumes.

Table 5.1 Bondi radius [4] and volume of the halogen atoms.

Halogen Atom	Bondi radius / nm	$10^3 (V/\text{nm}^3)$
Fluorine	0.147	13.30
Chlorine	0.175	22.45
Bromine	0.185	26.45
Iodine	0.198	32.52

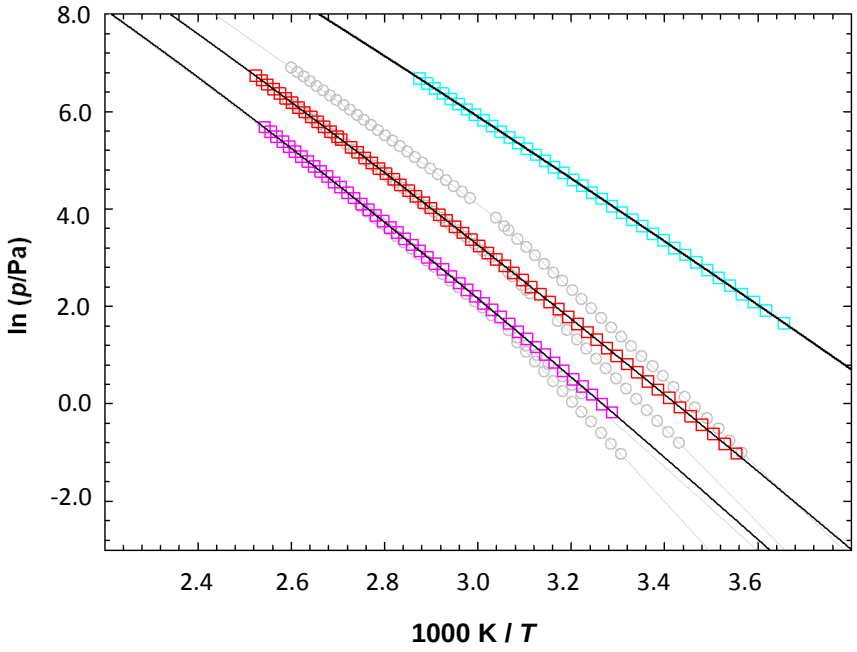

Figure 5.1. Graphic representation of ln(*p*/Pa) = *f* [1000 K/*T*] for liquid 1- halogenated naphthalenes. **purple** – 1-iodonaphthalene; **red** – 1-bromonaphthalene; **blue** – 1-fluoronaphthalene. Grey lines and marker symbols: 2-iodonaphthalene; 2-bromonaphthalene; 2-chlororonaphthalene.

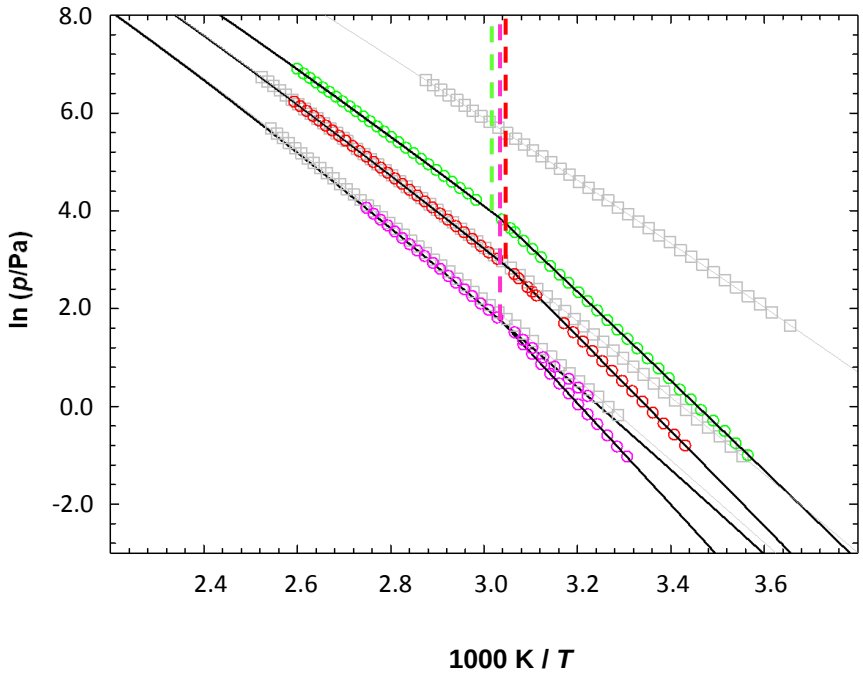

Figure 5.2. Phase diagram of ln(*p*/Pa) = *f* [1000 K/*T*] for the liquid and solid 2- halogenated naphthalenes. **purple** – 2-iodonaphthalene; **red** – 2-bromonaphthalene; **green**– 2-chlororonaphthalene. Grey lines and marker symbols: 1-iodonaphthalene (l); 1-bromonaphthalene (l); 1-fluoronaphthalene (l). ; – – – – · – triple point temperatures of 2-halogenated naphthalenes.

The vapor pressure results for 1- halogenated and 2-halogenated naphthalenes are presented in figures 5.1 and 5.2, respectively. Grey lines and marker symbols are presented for comparative purposes.

The volatility of the liquid phase is very similar for the 1 and 2 isomers with the same halogen substituent, as it is shown in the figures 5.1 and 5.2. The same conclusion could be taken from the standard Gibbs energies of vaporization at 298.15 K diagram depicted in figure 5.3. The identical volatility of the 1 and 2 isomers is a consequence of entropic and enthalpic compensations. However a significant differentiation was found between the entropies and enthalpies of the two isomerization positions 1 and 2. Position 2 presents higher entropies and enthalpies of vaporization.

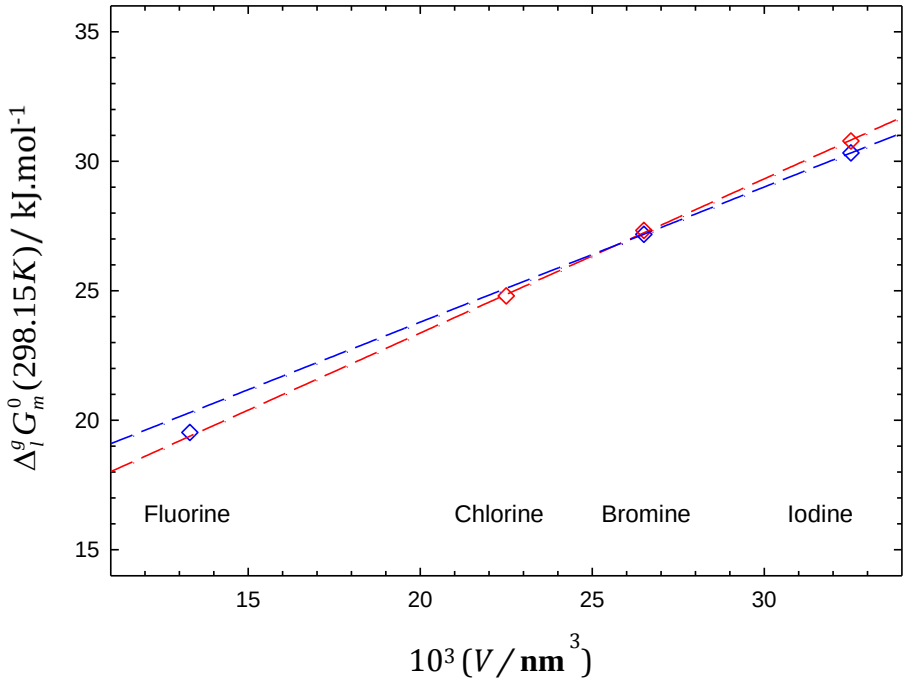

Figure 5.3. Correlation between $\Delta_l^g G_m^0(298.15\mathrm{K})$ and volume of the halogen atom for 1 and 2-halogenated naphthalenes. **blue** - 1-halogenated naphthalenes; **red** – 2-halogenated naphthalenes.

A good correlation between the entropies, enthalpies and Gibbs energy of vaporization and the atomic volume of the halogen was found (see figures 5.3, 5.4, 5.5). The increase of all the thermodynamic properties with the atomic volume is in agreement with the expected increase of the dispersive interactions. The fluorine atom shows an outlier behaviour (1-fluoronaphthalene) in that correlation, following the typical irregular behaviour of the fluorinated compounds that arises from the compactness of the electronic density of fluorine which leads to a low dispersive interaction, as well as, the high sigma-delocalization that significantly changes the electron density in the aromatic moieties.

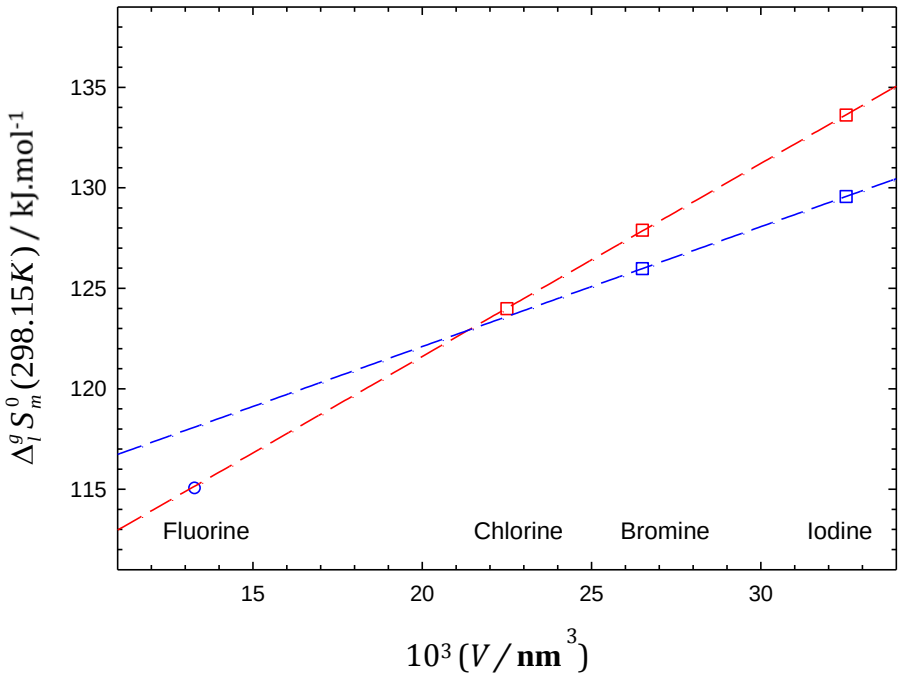

Figure 5.4. Correlation between $\Delta_l^g S_m^0(298.15\mathrm{K})$ and volume of the halogen atom for 1 and 2-halogenated naphthalenes. **blue** - 1-halogenated naphthalenes; **red** – 2-halogenated naphthalenes.

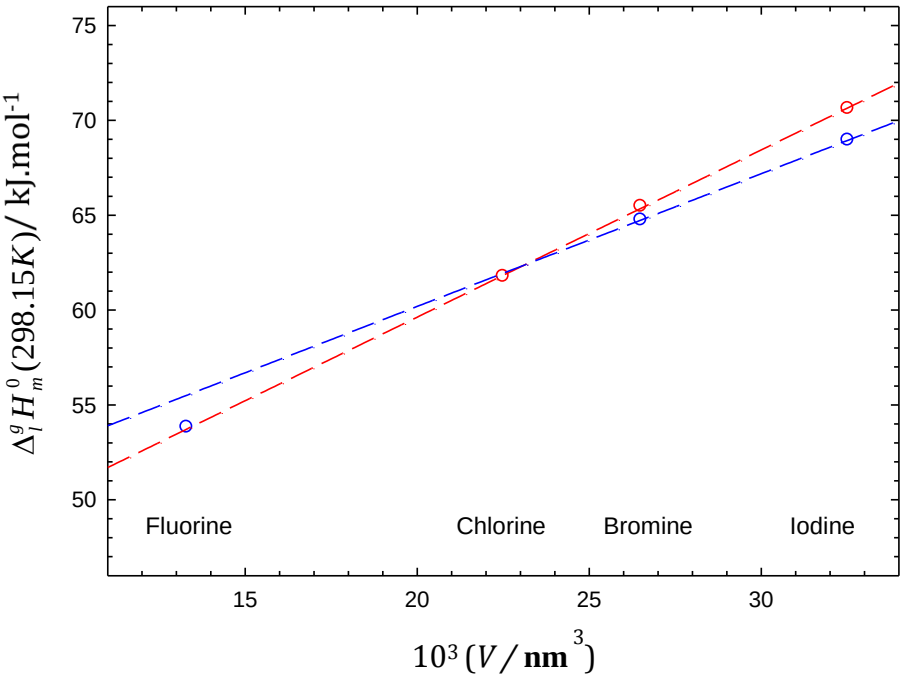

Figure 5.5. Correlation between $\Delta_l^g H_m^0(298.15K)$ and volume of the halogen atom for 1 and 2-halogenated naphthalenes. **blue** - 1-halogenated naphthalenes; **red** – 2-halogenated naphthalenes.

The volatilities, as well as, the thermodynamic properties follow the order of the halogen series,

Volatility:

F-Naph > Cl-Naph > Br-Naph > I-Naph

Entropies of vaporization:

F-Naph < Cl-Naph < Br-Naph < I-Naph

Enthalpies of vaporization:

F-Naph < Cl-Naph < Br-Naph < I-Naph

Figure 5.6 plots the overall (*p,T*) data for the studied compounds together with the semi-quantitative prediction of the (*p,T*) lines for the other isomers.

The construction of the *p,T* phase diagram was done assuming that there is no differentiation on the volatility of the liquid phase between position 1 and 2. The triple point temperatures of 1-halonaphthelenes were taken as the melting temperature of the isomers.

Significant and interesting findings from figure 5.6:

- The triple point temperature of the naphthalene is significantly higher than the mono-halogenated naphthalenes;

- A change in the order of the melting temperatures between the two isomer positions was found. Position 2 presents a significantly higher melting temperature that position 1, in agreement with a smaller influence in the ring to ring "T" shape C-H···Pi interaction of the halogen atom;

- In contrast with the findings for the volatility of the liquids (small volatility differentiation), the crystalline phases presents a significant differentiation between the 1 and 2 isomers, being the 1-isomers much more volatile that the 2-halogenated naphthalenes;

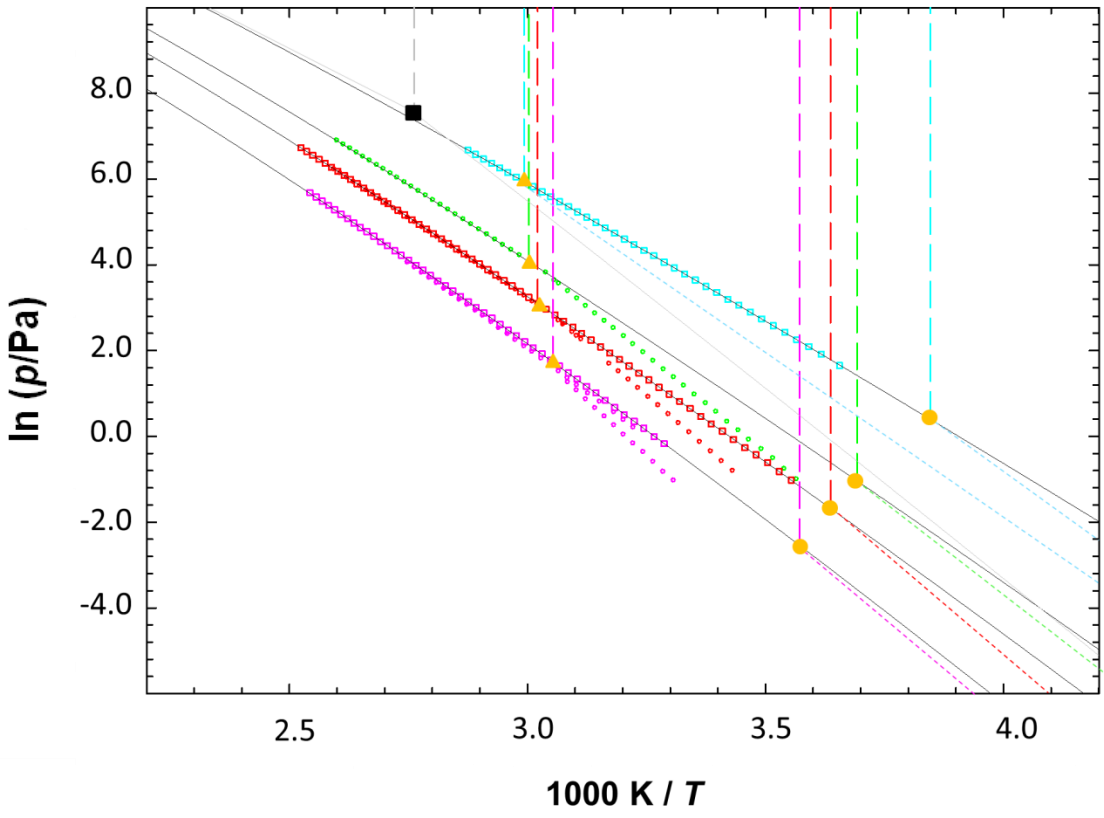

Figure 5.6. Phase diagram of ln(*p*/Pa) = *f* [1000 K/*T*] of the obtained results with static apparatus, for 1 and 2-halogenated naphthalenes. **purple** – 1 and 2-iodonaphthalenes; **red** – 1 and 2-bromonaphthalenes; **green**– 2-chlororonaphthalene; **blue** – 1-fluoronaphthalene; **grey** – naphthalene [2]; □– 1-halogenated naphthalenes; ○ - 2-halogenated naphthalenes; ●– melting temperatures of 1-halogenated naphthalenes; ▲ – melting temperatures of 2-halogenated naphthalenes; ■ – melting temperature of naphthalene; - - - - – hypothetical solid-vapor equilibrium curves for 1-halogenated naphthalenes and 2-fluoronaphthalene.

5.1.2. Estimative of thermodynamic properties of 1-chloronaphthalene

Taking into account the excellent correlation between the atomic volume and the thermodynamic properties of vaporization found for the 2-halogenated naphthalenes (figures 5.3, 5.4, and 5.5), the estimative of the thermodynamic properties of vaporization of the 1-choronaphthalene was done by linear extrapolation of the experimental data of the 1-bromonaphthalene and 1-iodonaphthalene, table 5.2. The predict enthalpy of vaporization is in quite good agreement with the value found in the literature of 62.03 ± 0.39 kJ.mol^{-1}. [3]

$$\Delta_l^g G_m^0(298.15\text{K})\,/\,\text{kJ.mol}^{-1} = 13.50 + 0.52\,V\,(10^{3}/\,\text{nm}^3) \qquad \textbf{(5.1)}$$

$$\Delta_l^g H_m^0(298.15\text{K})\,/\,\text{kJ.mol}^{-1} = 46.39 + 0.69\,V\,(10^{3}/\,\text{nm}^3) \qquad \textbf{(5.2)}$$

$$\Delta_l^g S_m^0(298.15\text{K})\,/\text{J.K}^{-1}\text{.mol}^{-1} = 110.34 + 0.59\,V\,(10^{3}/\,\text{nm}^3) \qquad \textbf{(5.3)}$$

Table 5.2. Thermodynamic properties of vaporization of the 1-halogenated naphthalene at *T*=298.15 K.

Compound	$\Delta_l^g G_m^0$ / kJ.mol^{-1}	$\Delta_l^g H_m^0$ / kJ.mol^{-1}	$\Delta_l^g S_m^0$ / J.K^{-1}.mol^{-1}
1FNaph	19.53 ± 0.01	53.82 ± 0.04	115.01 ± 0.04
1ClNaph	**25.11** (a)	**61.97** (b)	**123.61**(c)
1BrNaph	27.18 ± 0.01	64.74 ± 0.04	125.98 ± 0.04
1INaph	30.32 ± 0.01	68.95 ± 0.19	129.57 ± 0.19

(a), estimated from equation 5.1; (b), estimated from equation 5.2; (c), estimated from equation 5.3.

5.2. Statistical thermodynamic results

5.2.1. Calculation methodologies

The heat capacity, $C^0_{p,\mathrm{m}}$, and the absolute entropy, S^0_{m}, on the gaseous phase, were estimated by statistical thermodynamics using the vibrational frequencies derived from quantum chemical (QC) calculations. A comparative analysis of the different QC functionals, basis sets and computational methodologies was carried out. The homodesmic methodology applied to the statistical thermodynamics calculation, was found to be more efficient in the error cancelation than the use of corrective scaling factors for the vibrational frequencies. The oscillation of the obtained molar heat capacity results using the different methodologies is presented for elucidation in figure 5.7. A standard deviation of ± 0.5 $J.K^{-1}.mol^{-1}$ was obtained for the homodesmic procedure in contrast with ± 1.7 $J.K^{-1}.mol^{-1}$ obtained in the classic approach (scaling the vibrational frequencies).

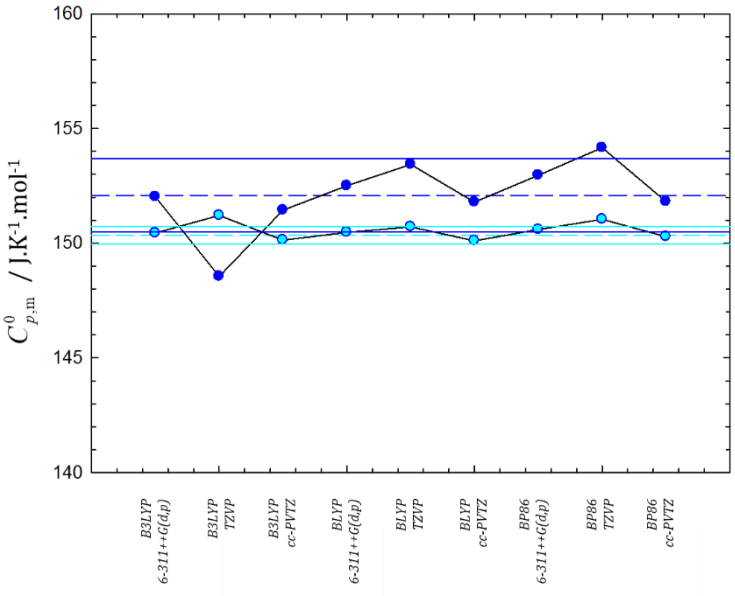

Figure 5.7. Gaseous phase heat capacities results of 2-bromonaphthalene using several basis sets. Difference of using only scaling factors (**dark blue**) and using isodesmic reactions (**light blue**). - - - - mean value of the results obtained from quantum chemical calculations and using only scaling factors; - - - - mean value of the results obtained using isodesmic reactions; —— - standard deviation of the results obtained from quantum chemical calculations and using only scaling factors; —— - standard deviation of the results obtained using isodesmic reactions.

5.2.2. Influence of Temperature

The obtained ideal gas statistical thermodynamic properties results for $C_{p,\mathrm{m}}^{0}$ and S_{m}^{0} of the mono-halogenated naphthalenes between *T* = 100 K and *T* = 1000K, with 100 K steps, are presented in tables 6.12 and 6.13 and graphically represented in figures 5.8 and 5.9, respectively.

The obtained results are very similar for the 1 and 2 isomers. This is in agreement with the conclusions taken from the FTIR spectra experimental results as well as the quantum chemical vibrational frequencies. A very small differentiation was found in the vibrational spectral data.

The derived ideal gas thermodynamic properties at 298.15 K, follows the order of the halogen series,

Heat capacity:

F-Naph < Cl-Naph < Br-Naph < I-Naph

Ideal gas absolute entropy:

F-Naph < Cl-Naph < Br-Naph < I-Naph

In agreement with the observed lower frequency of the vibrational modes associated with the larger halogen atoms.

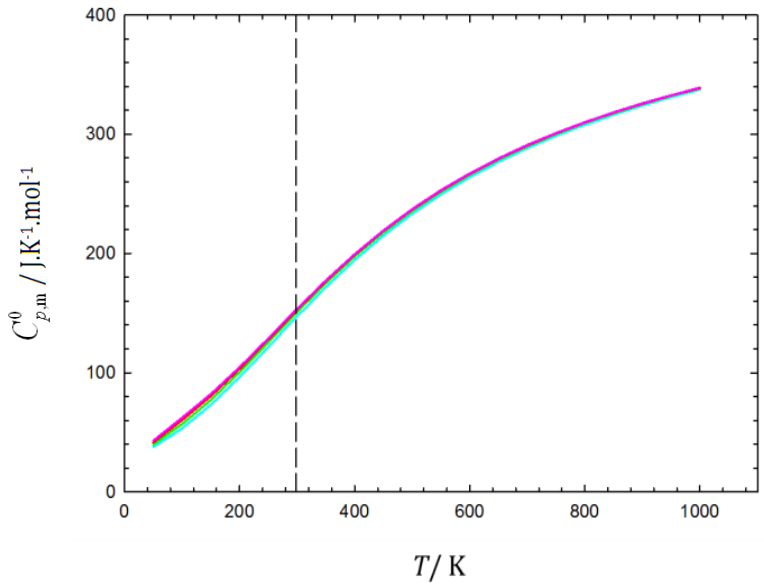

Figure 5.8. Temperature dependence of the ideal gas isobaric (p^o=0.1 MPa) heat capacity. (B3LYP/6-311++G(d,p), scaling factor 0.9688).
Note: In this graphical representation, the results are between T = 50K and T = 1000 K, with 50 K steps.

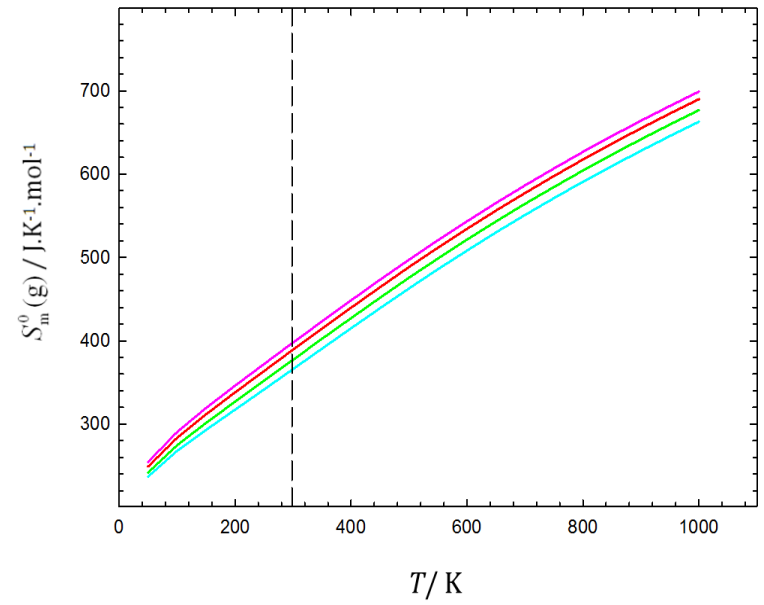

Figure 5.9. Temperature dependence of the ideal gas standard (p^o=0.1 MPa) molar absolute entropies. (B3LYP/6-311++G(d,p), scaling factor 0.9688).
Note: In this graphical representation, the results are between T = 50K and T = 1000 K, with 50 K steps.

References

[1] Ribeiro da Silva, M.A.V.; Fonseca, J.M.S.; Carvalho, R.P.B.M.; Monte, M.J.S. *J. Chem. Thermodynamics*, 37 (2005) 271–279.

[2] Almeida, A.R.R.P.; Monte M.J.S., *J. Chem. Thermodynamics,* 57 (2013) 160–168.

[3] Almeida, A.R.R.P.; Monte M.J.S., *J. Chem. Thermodynamics,* 65 (2013) 150–158.

[4] Rowland, R.S.; Taylor, R., *J. Phys. Chem.,* 100 (1996) 7384–7391.

[5] Monte M. J. S.; Santos L. M. N. B. F.; Fulem M.; Fonseca, J.M.S.; Sousa, C.A.D., *Journal of Chemical Engineering Data,* 51 (2006) 757-766.

[6] Verevkin, S.P., *J.Chem.Thermodyn*., 35 (2003) 1237.

Supplementary Information

Attachment A - FTIR results

- 1-Halogenated naphthalenes
- 2-Halogenated naphthalenes

Attachment B – Ethermo.xls, Worksheet file

Attachment C - Computational results

- 1-Halogenated naphthalenes
  - Results for 1-fluoronaphthalene
  - Results for 1-chloronaphthalene
  - Results for 1-bromonaphthalene
  - Results for 1-iodonaphthalene
- 2-Halogenated naphthalenes
  - Results for 2-fluoronaphthalene
  - Results for 2-chloronaphthalene
  - Results for 2-bromonaphthalene
  - Results for 2-iodonaphthalene

Attachment A - FTIR results

1-Fluoronaphthalene

Table 6.1. Experimental IR spectral data and fundamental vibrational mode assignment, at *T* = 298.15 K, for 1-fluoronaphthalene.

mode description (assignment)	Exp	B3LYP/6-311++G(d,p)		
	ω_{exp} /cm^{-1}	ω_{calc} /cm^{-1}	intensity	ω_{scaled} /cm^{-1}
Aromatic C-H bending	708	719	9.8	697
Aromatic C-H bending	761	781	53.9	757
Aromatic C-H bending	789	806	73.7	781
Aromatic C-H bending	874	884	10.5	856
C-F stretching	1012	1036	15.8	1004
C-F stretching	1034	1054	17.7	1021
C-F stretching	1074	1092	28.4	1058
C-C stretching	1228	1251	41.7	1212
C-C stretching	1260	1283	25.4	1243
C=C-C Aromatic ring stretching	1389	1422	58.4	1378
C=C-C Aromatic ring stretching	1441	1472	9.2	1426
C=C-C Aromatic ring stretching	1463	1494	14.8	1447
C=C-C Aromatic ring stretching	1509	1544	18.2	1496
C=C-C Aromatic ring stretching	1574	1612	19.2	1562
C=C-C Aromatic ring stretching	1599	1641	19.1	1590
C=C stretching	1641	1675	7.7	1623
Aromatic C-H stretching	3058	3187	17.1	3088

Note: - the results were obtained using a Spectrum BX apparatus equipped with a GladiATR.
The used scaling factor for this model/basis set was 0.9688.

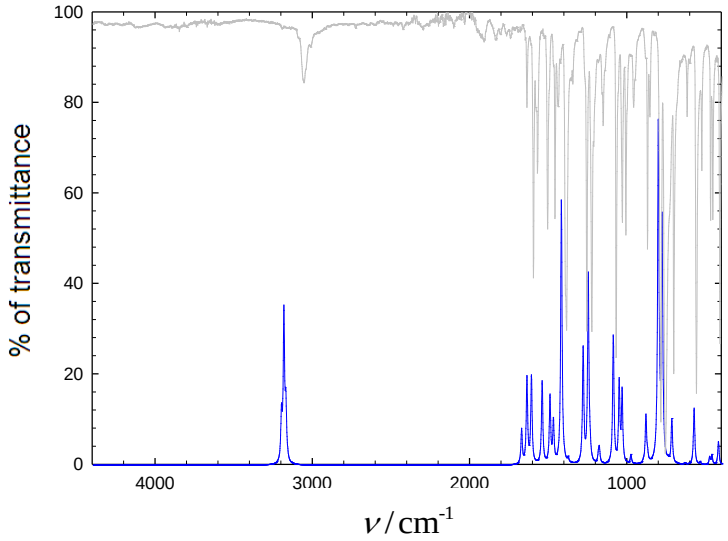

Figure 6.1. Experimental and Theoretical IR spectral data, at *T* = 298.15 K, for 1-fluoronaphthalene.

Note: - the used model/basis set was B3LYP/6-311++G(d,p) using a scaling factor of 0.9688.

1-Bromonaphthalene

Table 6.2. Experimental IR spectral data and fundamental vibrational mode assignment, at *T* = 298.15 K, for 1-bromonaphthalene.

mode description (assignment)	Exp	B3LYP/6-311++G(d,p)		
	ω_{exp} /cm^{-1}	ω_{calc} /cm^{-1}	intensity	ω_{scaled} /cm^{-1}
C-Br stretching	650	664	17.6	643
Aromatic C-H bending	760	783	44.1	759
Aromatic C-H bending	785	807	69.1	782
Aromatic C-H bending	805	817	11.4	792
Aromatic C-H bending	946	962	34.1	932
Aromatic C-H in-plane bending	1021	1045	6.3	1012
Aromatic C-H in-plane bending	1056	1081	4.2	1047
Aromatic C-H in-plane bending	1133	1156	6.4	1120
Aromatic C-H bending	1199	1220	11.8	1182
C-C stretching	1251	1279	11.6	1239
C=C-C Aromatic ring stretching	1376	1407	28.3	1363
C=C-C Aromatic ring stretching	1500	1536	15.1	1488
C=C-C Aromatic ring stretching	1560	1597	16.1	1547
C=C-C Aromatic ring stretching	1590	1633	5.5	1582
Aromatic C-H stretching	3053	3188	18.4	3089

Note: - the results were obtained using a Spectrum BX apparatus equipped with a GladiATR.

The used scaling factor for this model/basis set was 0.9688.

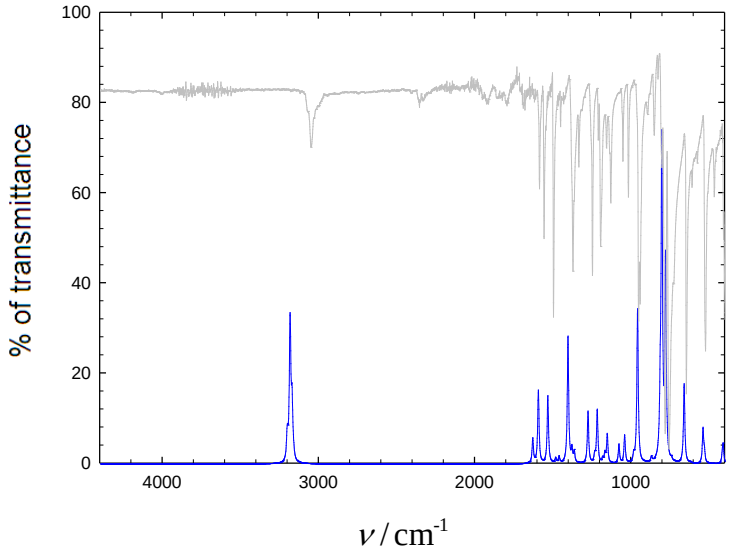

Figure 6.2. Experimental and Theoretical IR spectral data, at *T* = 298.15 K, for 1-bromonaphthalene.

Note: - the used model/basis set was B3LYP/6-311++G(d,p) using a scaling factor of 0.9688.

.

1-Iodonaphthalene

Table 6.3. Experimental IR spectral data and fundamental vibrational mode assignment, at *T* = 298.15 K, for 1-iodonaphthalene.

mode description (assignment)	Exp	B3LYP/6-311++G(d,p)		
	ω_{exp} /cm^{-1}	ω_{calc} /cm^{-1}	intensity	ω_{scaled} /cm^{-1}
C-I stretching	641	654	19.6	634
C-I stretching	760	786	48.0	761
Aromatic C-H bending	783	806	63.9	781
Aromatic C-H bending	942	952	36.6	922
Aromatic C-H in-plane bending	1129	1153	7.6	1117
Aromatic C-H in-plane bending	1199	1224	12.1	1186
Aromatic C-H in-plane bending	1249	1281	14.4	1241
C=C-C Aromatic ring stretching	1380	1408	26.6	1364
C=C-C Aromatic ring stretching	1497	1535	17.2	1487
C=C-C Aromatic ring stretching	1554	1594	21.2	1544
Aromatic C-H stretching	3049	3187	19.1	3088

Note: - the results were obtained using a Spectrum BX apparatus equipped with a GladiATR.

The used scaling factor for this model/basis set was 0.9688.

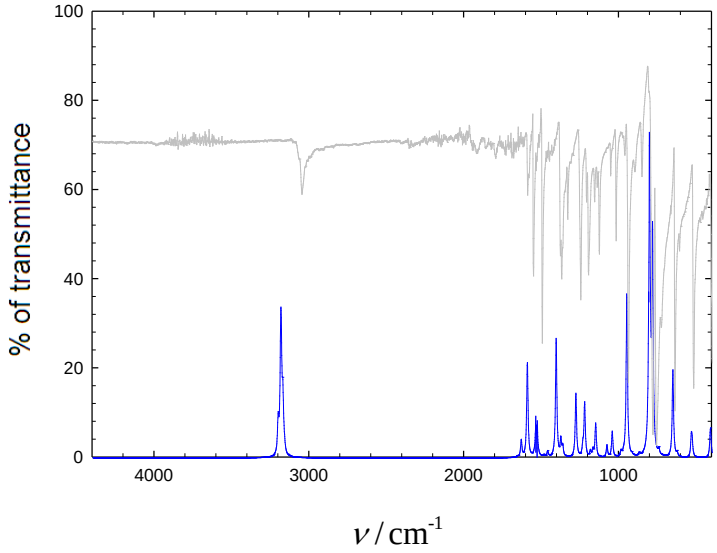

Figure 6.3. Experimental and Theoretical IR spectral data, at T = 298.15 K, for 1-iodonaphthalene.

Note: - the used model/basis set was B3LYP/6-311++G(d,p) using a scaling factor of 0.9688.

2-Chloronaphthalene

Table 6.4. Experimental IR spectral data and fundamental vibrational mode assignment, at *T* = 298.15 K, for 2-chloronaphthalene.

mode description (assignment)	Exp	B3LYP/6-311++G(d,p)		
	ω_{exp} /cm^{-1}	ω_{calc} /cm^{-1}	intensity	ω_{scaled} /cm^{-1}
C-Cl stretching	475	484	20.7	469
C-Cl stretching	603	611	15.9	592
C-Cl stretching	743	758	28.8	734
C-Cl stretching	812	824	40.8	798
Aromatic C-H bending	849	859	33.0	832
Aromatic C-H bending	857	869	24.9	842
Aromatic C-H bending	885	899	10.7	871
Aromatic C-H bending	941	955	21.2	925
Aromatic C-H in-plane bending	1074	1089	34.5	1055
Aromatic C-H in-plane bending	1129	1155	12.1	1119
Aromatic C-H in-plane bending	1192	1221	7.5	1183
Aromatic C-C stretching	1344	1389	7.7	1346
C=C-C Aromatic ring stretching	1452	1487	15.6	1441
C=C-C Aromatic ring stretching	1499	1538	22.4	1490
C=C-C Aromatic ring stretching	1576	1629	33.5	1578
C=C-C Aromatic ring stretching	1623	1663	13.4	1611
Aromatic C-H stretching	3055	3177	23.4	3078

Note: - the results were obtained using a Spectrum BX apparatus equipped with a GladiATR.
The used scaling factor for this model/basis set was 0.9688.

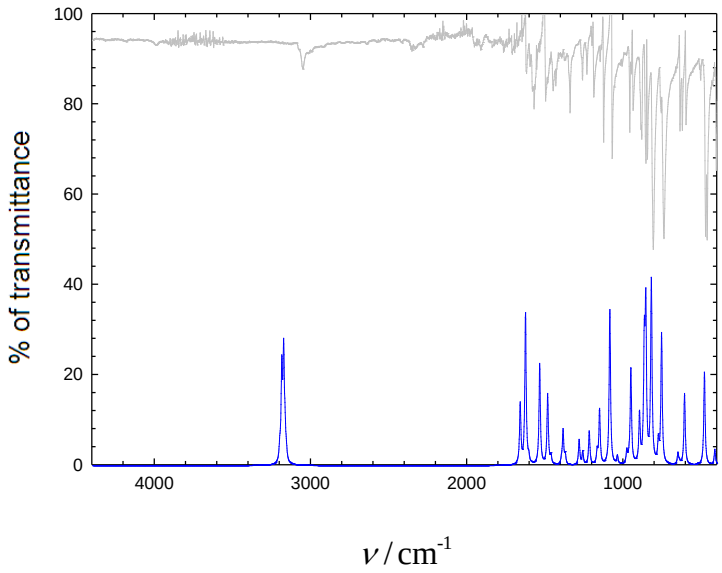

Figure 6.4. Experimental and Theoretical IR spectral data, at *T* = 298.15 K, for 2-chloronaphthalene.

Note: - the used model/basis set was B3LYP/6-311++G(d,p) using a scaling factor of 0.9688.

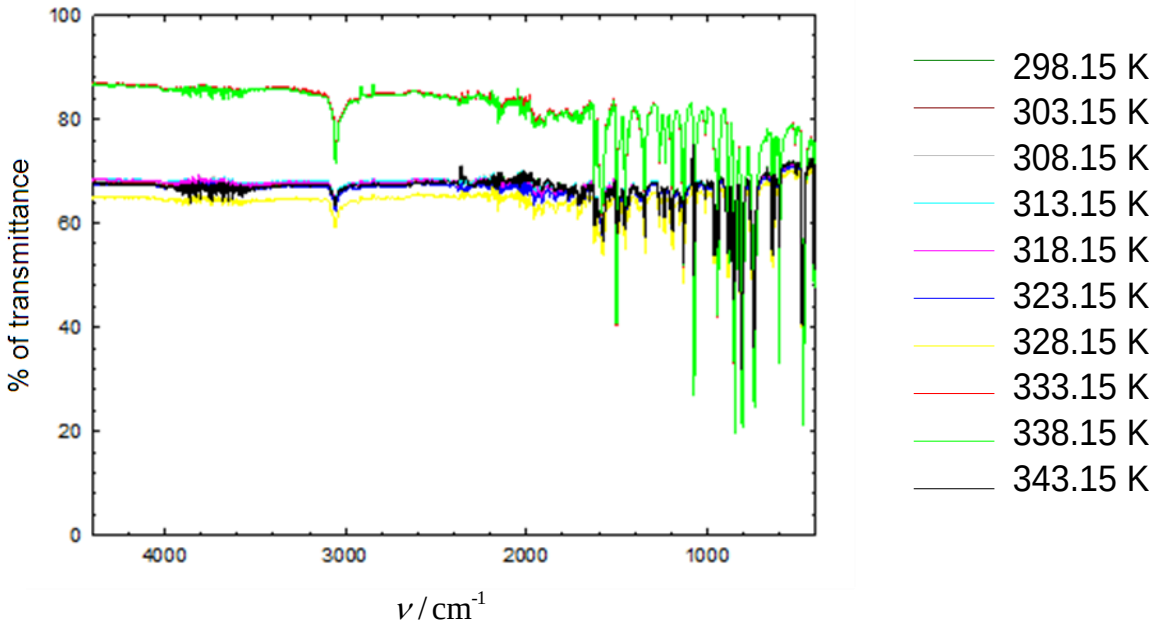

Figure 6.5. FTIR spectra for 2-chloronaphthalene at different temperatures.

$$298.15 \leq T(K) \leq 343.15$$

2-Bromonaphthalene

Table 6.5. Experimental IR spectral data and fundamental vibrational mode assignment, at T = 298.15 K, for 2-bromonaphthalene.

mode description (assignment)	Exp	B3LYP/6-311++G(d,p)		
	ω_{exp} /cm^{-1}	ω_{calc} /cm^{-1}	intensity	ω_{scaled} /cm^{-1}
C-Br stretching	473	482	20.5	467
C-Br stretching	579	586	12.4	568
Aromatic C-H bending	741	756	24.8	732
Aromatic C-H bending	764	773	7.5	749
Aromatic C-H bending	810	823	42.8	797
Aromatic C-H bending	856	869	21.9	842
Aromatic C-H bending	932	951	22.1	921
Aromatic C-H in-plane bending	1061	1079	22.4	1045
Aromatic C-H in-plane bending	1128	1154	11.9	1118
C=C-C Aromatic ring stretching	1343	1387	7.5	1344
C=C-C Aromatic ring stretching	1455	1484	14.4	1438
C=C-C Aromatic ring stretching	1584	1624	35.2	1573
Aromatic C-H stretching	3053	3177	23.2	3078

Note: - the results were obtained using a Spectrum BX apparatus equipped with a GladiATR.
The used scaling factor for this model/basis set was 0.9688.

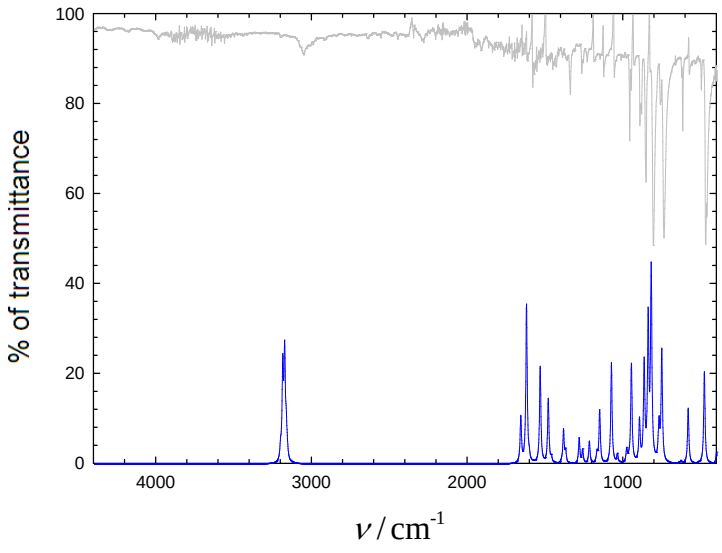

Figure 6.6. Experimental and Theoretical IR spectral data, at T = 298.15 K, for 2-bromonaphthalene.

Note: - the used model/basis set was B3LYP/6-311++G(d,p) using a scaling factor of 0.9688.

2-Iodonaphthalene

Table 6.6. Experimental IR spectral data and fundamental vibrational mode assignment, at *T* = 298.15 K, for 2-iodonaphthalene.

mode description (assignment)	Exp	B3LYP/6-311++G(d,p)		
	ω_{exp} /cm^{-1}	ω_{calc} /cm^{-1}	intensity	ω_{scaled} /cm^{-1}
C-I stretching	466	481	21.8	466
C-I stretching	565	568	10.1	550
Aromatic C-H bending	737	753	24.5	730
Aromatic C-H bending	810	819	49.4	793
Aromatic C-H bending	815	829	34.6	803
Aromatic C-H bending	855	866	17.0	839
Aromatic C-H bending	885	897	7.3	869
Aromatic C-H bending	934	947	25.5	917
Aromatic C-H bending	961	977	3.3	947
Aromatic C-H in-plane bending	1056	1072	16.7	1039
Aromatic C-H in-plane bending	1128	1155	13.1	1119
Aromatic C-H in-plane bending	1268	1287	6.0	1247
C=C-C Aromatic ring stretching	1338	1384	7.4	1341
C=C-C Aromatic ring stretching	1452	1483	13.5	1437
C=C-C Aromatic ring stretching	1496	1534	21.4	1486
C=C-C Aromatic ring stretching	1577	1621	40.8	1570
C=C-C Aromatic ring stretching	1619	1660	9.8	1608
Aromatic C-H stretching	3048	3178	22.6	3079

Note: - the results were obtained using a Spectrum BX apparatus equipped with a GladiATR.

The used scaling factor for this model/basis set was 0.9688.

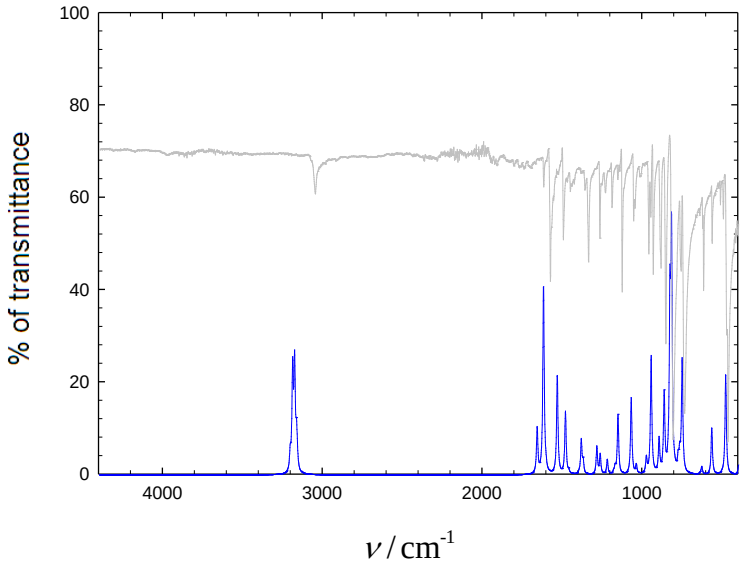

Figure 6.7. Experimental and Theoretical IR spectral data, at *T* = 298.15 K, for 2-iodonaphthalene.

Note: - the used model/basis set was B3LYP/6-311++g(dp) using a scaling factor of 0.9688.

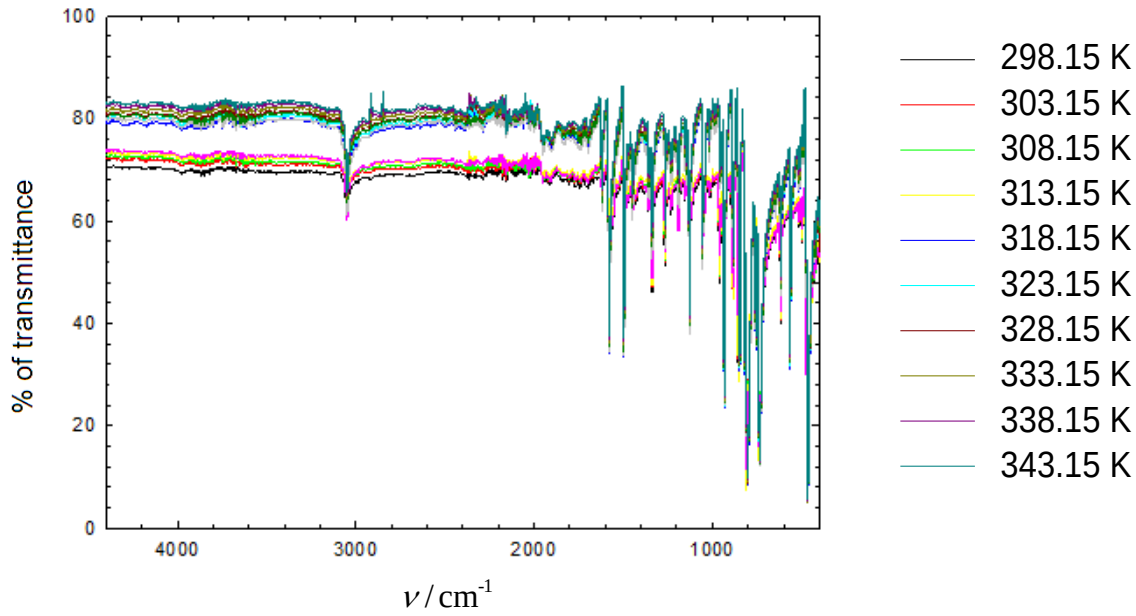

Figure 6.8. FTIR spectra for 2-iodonaphthalene at different temperatures.

$$298.15 \leq T(K) \leq 343.15$$

Attachment B – Ethermo.xls, Worksheet file

The results of ideal-gas thermodynamic functions such as entropy, heat capacity and enthalpy obtained by statistical thermodynamics calculations were done using an Excel worksheet file “ETHERMO.xls” that was developed and tested as part of this MSc Thesis. The rigid-rotor/harmonic-oscillator (RRHO) approximation was adopted. The theoretical background and some details are described in detail in Chapter 4. The necessary information used as input in Excel worksheet file is typically obtained from the output results of any quantum chemical software application (e.g. moments of inertia, harmonic vibration frequencies). The capabilities and calculation functionality of the developed Excel worksheet file “ETHERMO.xls” are similar than the Perl script 'thermo.pl' developed by Karl Irikura. [1] However “ETHERMO.xls” is a more user friendly application and integrates some additional functionalities that were useful for the study done in this thesis.

The main functionalities of the “ETHERMO.xls” are the followings:

1. User-friendly application to compute translational, rotational, vibrational and electronic partition functions;
2. Analysis of the temperature effect on the contribution of the thermodynamic functions;
3. Output of the partial contributions of each vibrational frequency to the thermodynamic functions;
4. Integrate data organization and result analysis based on the Excel functionalities.

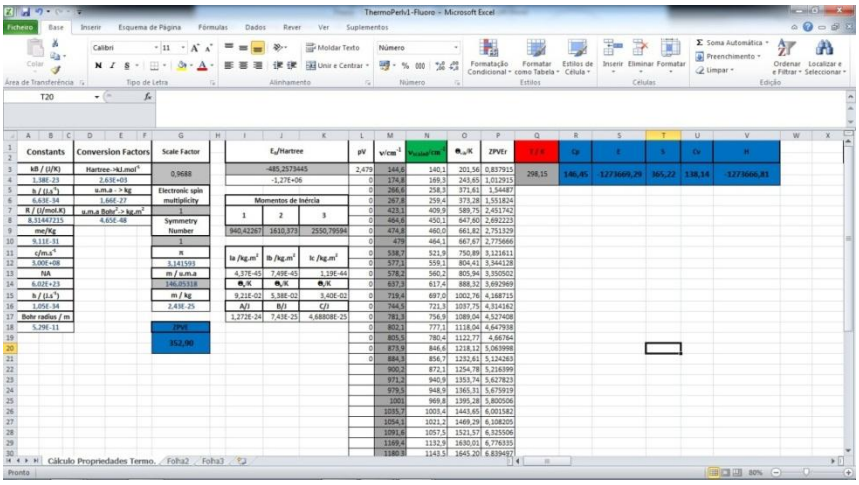

Figure 6.9. EThermo file.

[1] http://www.nist.gov/mml/csd/informatics_research/thermochemistry_cgi.cfm

Attachment C - Computational results

Table 6.7. Results of $C^{0}_{v,\mathrm{m}}$ translational and rotational contributions fractions, using B3LYP/6-311++G(d,p) for the studied mono-halogenated naphthalenes at several temperatures.

$\frac{T}{K}$	1FNaph	1ClNaph	1BrNaph	1INaph	2FNaph	2ClNaph	2BrNaph	2INaph
100	0.2766	0.2560	0.2398	0.2305	0.2786	0.2566	0.2403	0.2300
200	0.1415	0.1352	0.1313	0.1294	0.1410	0.1350	0.1312	0.1290
298.15	**0.0903**	**0.0881**	**0.0869**	**0.0863**	**0.0899**	**0.0880**	**0.0868**	**0.0861**
300	0.0897	0.0875	0.0863	0.0858	0.0893	0.0874	0.0862	0.0855
400	0.0669	0.0659	0.0654	0.0652	0.0667	0.0659	0.0654	0.0651
500	0.0554	0.0548	0.0546	0.0545	0.0553	0.0548	0.0546	0.0544
600	0.0488	0.0484	0.0482	0.0482	0.0487	0.0484	0.0482	0.0481
700	0.0445	0.0443	0.0442	0.0441	0.0445	0.0443	0.0442	0.0441
800	0.0416	0.0414	0.0414	0.0413	0.0416	0.0414	0.0414	0.0413
900	0.0395	0.0394	0.0393	0.0393	0.0395	0.0393	0.0393	0.0393
1000	0.0379	0.0378	0.0377	0.0377	0.0379	0.0378	0.0377	0.0377

Table 6.8. Results of $C_{v,m}^{0}$ vibrational contribution fraction, using B3LYP/6-311++G(d,p) for the studied mono-halogenated naphthalenes at several temperatures.

$\frac{T}{K}$	1FNaph	1ClNaph	1BrNaph	1INaph	2FNaph	2ClNaph	2BrNaph	2INaph
100	0.4467	0.4880	0.5204	0.5390	0.4428	0.4868	0.5194	0.5400
200	0.7170	0.7296	0.7374	0.7412	0.7180	0.7300	0.7376	0.7420
298.15	**0.8194**	**0.8238**	**0.8262**	**0.8274**	**0.8202**	**0.8240**	**0.8264**	**0.8278**
300	0.8206	0.8250	0.8274	0.8284	0.8214	0.8252	0.8276	0.8290
400	0.8662	0.8682	0.8692	0.8696	0.8666	0.8682	0.8692	0.8698
500	0.8892	0.8904	0.8908	0.8910	0.8894	0.8904	0.8908	0.8912
600	0.9024	0.9032	0.9036	0.9036	0.9026	0.9032	0.9036	0.9038
700	0.9110	0.9114	0.9116	0.9118	0.9110	0.9114	0.9116	0.9118
800	0.9168	0.9172	0.9173	0.9174	0.9168	0.9172	0.9172	0.9174
900	0.9210	0.9212	0.9214	0.9214	0.9210	0.9214	0.9214	0.9214
1000	0.9242	0.9244	0.9246	0.9246	0.9242	0.9244	0.9246	0.9246

Table 6.9. Results of S_m^0 rotational contribution fraction, using B3LYP/6-311++G(d,p) for the studied mono-halogenated naphthalenes at several temperatures.

T / K	1FNaph	1ClNaph	1BrNaph	1INaph	2FNaph	2ClNaph	2BrNaph	2INaph
100	0.4134	0.4130	0.4116	0.4096	0.4137	0.4132	0.4118	0.4091
200	0.3763	0.3736	0.3709	0.3687	0.3766	0.3737	0.3711	0.3683
298.15	**0.3407**	**0.3378**	**0.3358**	**0.3342**	**0.3408**	**0.3379**	**0.3360**	**0.3338**
300	0.3400	0.3372	0.3351	0.3336	0.3402	0.3373	0.3354	0.3331
400	0.3085	0.3062	0.3049	0.3039	0.3086	0.3063	0.3051	0.3036
500	0.2827	0.2809	0.2802	0.2797	0.2828	0.2811	0.2805	0.2795
600	0.2619	0.2606	0.2604	0.2602	0.2620	0.2607	0.2606	0.2600
700	0.2452	0.2442	0.2443	0.2444	0.2452	0.2444	0.2445	0.2442
800	0.2315	0.2308	0.2311	0.2314	0.2315	0.2309	0.2314	0.2312
900	0.2201	0.2196	0.2202	0.2206	0.2201	0.2197	0.2204	0.2204
1000	0.2105	0.2102	0.2109	0.2114	0.2106	0.2104	0.2112	0.2113

Table 6.10. Results of S_m^0 translational contribution fraction, using B3LYP/6-311++G(d,p) for the studied mono-halogenated naphthalenes at several temperatures.

T / K	1FNaph	1ClNaph	1BrNaph	1INaph	2FNaph	2ClNaph	2BrNaph	2INaph
100	0.5529	0.5438	0.5373	0.5336	0.5517	0.5426	0.5360	0.5317
200	0.5123	0.5011	0.4935	0.4895	0.5114	0.5001	0.4925	0.4878
298.15	**0.4680**	**0.4575**	**0.4510**	**0.4479**	**0.4670**	**0.4567**	**0.4501**	**0.4463**
300	0.4671	0.4567	0.4503	0.4471	0.4662	0.4559	0.4494	0.4456
400	0.4264	0.4173	0.4122	0.4100	0.4254	0.4166	0.4115	0.4086
500	0.3924	0.3846	0.3807	0.3791	0.3915	0.3840	0.3800	0.3779
600	0.3648	0.3581	0.3551	0.3540	0.3640	0.3576	0.3545	0.3529
700	0.3424	0.3366	0.3342	0.3335	0.3417	0.3361	0.3337	0.3325
800	0.3240	0.3189	0.3170	0.3165	0.3234	0.3185	0.3165	0.3157
900	0.3087	0.3041	0.3026	0.3024	0.3081	0.3038	0.3022	0.3016
1000	0.2958	0.2917	0.2904	0.2904	0.2952	0.2913	0.2900	0.2896

Table 6.11. Results of S_m^0 vibrational contribution fraction, using B3LYP/6-311++G(d,p) for the studied mono-halogenated naphthalenes at several temperatures.

T / K	1FNaph	1ClNaph	1BrNaph	1INaph	2FNaph	2ClNaph	2BrNaph	2INaph
100	0.0337	0.0432	0.0511	0.0568	0.0346	0.0442	0.0522	0.0592
200	0.1114	0.1253	0.1356	0.1418	0.1120	0.1262	0.1364	0.1439
298.15	**0.1913**	**0.2047**	**0.2132**	**0.2179**	**0.1922**	**0.2054**	**0.2139**	**0.2199**
300	0.1929	0.2061	0.2146	0.2193	0.1936	0.2068	0.2152	0.2213
400	0.2651	0.2765	0.2829	0.2861	0.2660	0.2771	0.2834	0.2878
500	0.3249	0.3345	0.3391	0.3412	0.3257	0.3349	0.3395	0.3426
600	0.3733	0.3813	0.3845	0.3858	0.3740	0.3817	0.3849	0.3871
700	0.4124	0.4192	0.4215	0.4221	0.4131	0.4195	0.4218	0.4233
800	0.4445	0.4503	0.4519	0.4521	0.4451	0.4506	0.4521	0.4531
900	0.4712	0.4763	0.4772	0.4770	0.4718	0.4765	0.4774	0.4780
1000	0.4937	0.4981	0.4987	0.4982	0.4942	0.4983	0.4988	0.4991

1-halogenated naphthalenes

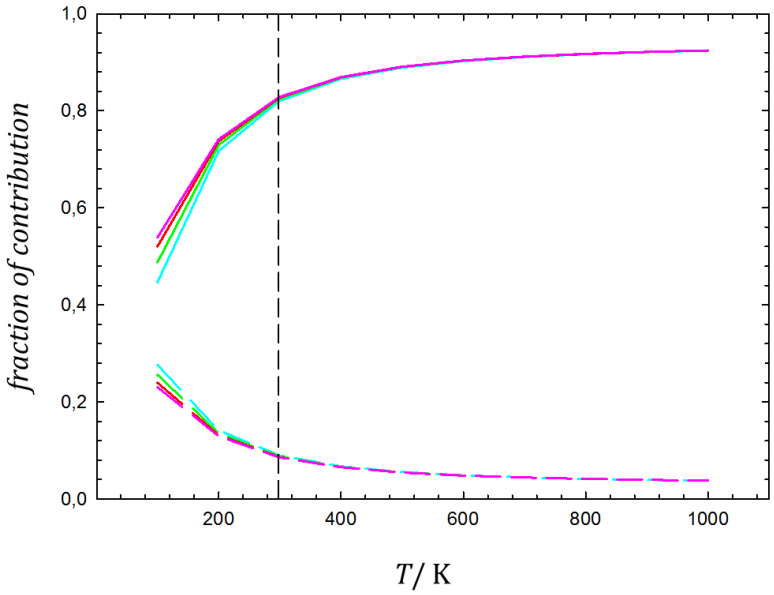

Figure 6.10. Vibrational, rotational and translational fraction contributions for total $C^0_{v,\mathrm{m}}$ in function of T / K using B3LYP/6-311++G(d,p). Scaling factor: 0.9688. ——- vibrational fraction contribution; – – – - rotational and translational fraction contribution (have the same contribution).

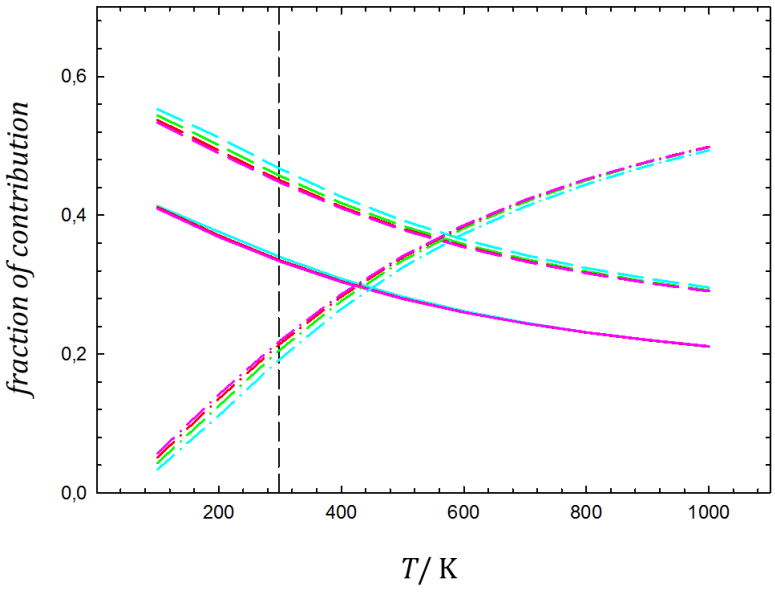

Figure 6.11. Vibrational, rotational and translational fraction contributions for total S^0_{m} in function of T / K using B3LYP/6-311++G(d,p). Scaling factor: 0.9688.
– ● –- vibrational fraction contribution; ——- rotational fraction contribution; – – – - translational fraction contribution.

2-halogenated naphthalenes

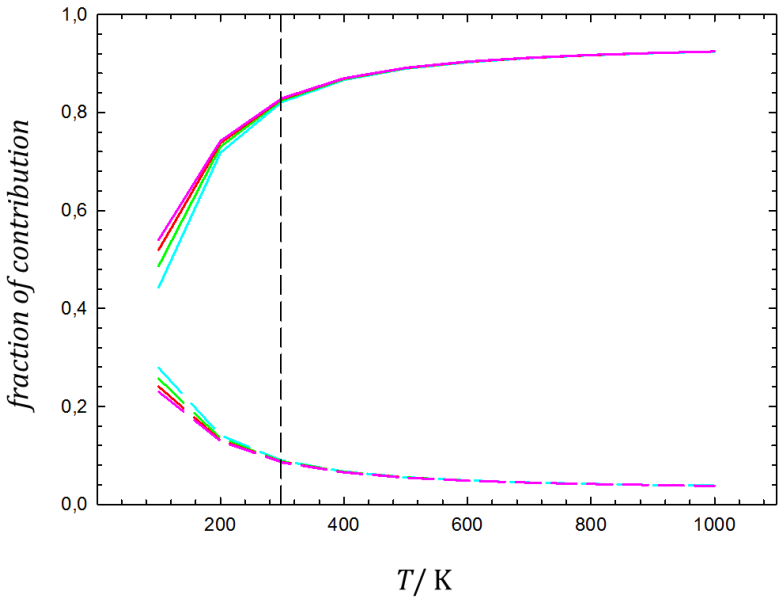

Figure 6.12. Vibrational, rotational and translational fraction contributions for total $C^0_{v,\mathrm{m}}$ in function of T / K using B3LYP/6-311++G(d,p). Scaling factor: 0.9688. ——— - vibrational fraction contribution; – – – - rotational and translational fraction contribution (have the same contribution).

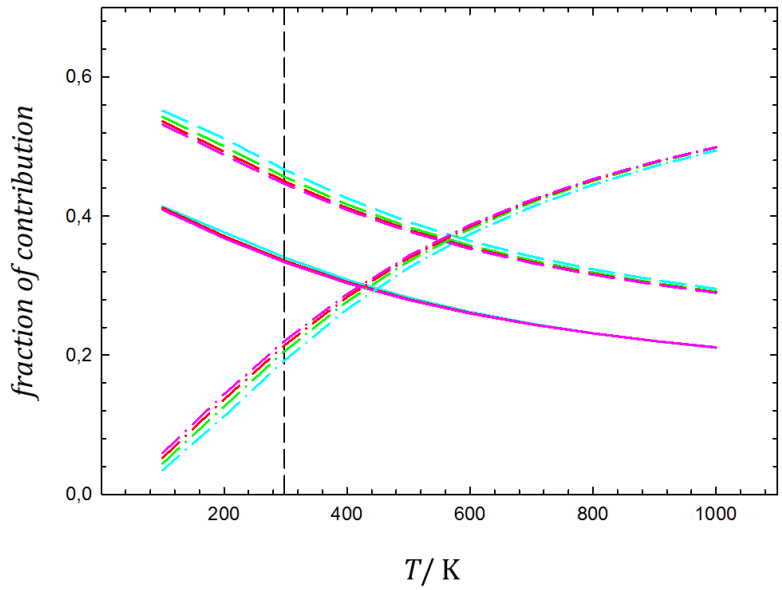

Figure 6.13. Vibrational, rotational and translational fraction contributions for total S^0_{m} in function of T / K using B3LYP/6-311++G(d,p). Scaling factor: 0.9688.
– ● – - vibrational fraction contribution; ——— - rotational fraction contribution; – – – - translational fraction contribution.

Table 6.12. Results of $C^0_{p,\mathrm{m}}$ using B3LYP/6-311++G(d,p) for the studied mono-halogenated naphthalenes at several temperatures.

$\frac{T}{K}$	1FNaph	1ClNaph	1BrNaph	1INaph	2FNaph	2ClNaph	2BrNaph	2INaph
100	53.40	57.04	60.33	62.41	53.08	56.92	60.22	62.54
200	96.47	100.53	103.29	104.66	96.80	100.69	103.40	105.03
298.15	**146.45**	**149.94**	**151.89**	**152.79**	**147.02**	**150.12**	**152.02**	**153.21**
300	147.39	150.86	152.80	153.69	147.96	151.04	152.93	154.12
400	194.61	197.49	198.90	199.52	195.19	197.65	199.01	199.88
500	233.41	235.78	236.84	237.30	233.92	235.91	236.92	237.59
600	264.09	266.03	266.86	267.20	264.52	266.15	266.93	267.44
700	288.42	290.02	290.67	290.95	288.79	290.12	290.74	291.14
800	308.03	309.36	309.89	310.11	308.35	309.46	309.95	310.28
900	324.11	325.22	325.66	325.84	324.39	325.32	325.72	325.99
1000	337.48	338.42	338.78	338.94	337.72	338.51	338.85	339.07

Table 6.13. Results of S^0_{m} using B3LYP/6-311++G(d,p) for the studied mono-halogenated naphthalenes at several temperatures.

$\frac{T}{K}$	1FNaph	1ClNaph	1BrNaph	1INaph	2FNaph	2ClNaph	2BrNaph	2INaph
100	268.04	274.90	283.79	290.65	268.62	275.49	284.49	291.71
200	317.43	327.08	338.18	346.28	317.99	327.71	338.90	347.51
298.15	**365.22**	**376.39**	**388.44**	**396.99**	**365.97**	**377.09**	**389.20**	**398.38**
300	366.13	377.33	389.38	397.94	366.88	378.02	390.14	399.33
400	415.17	427.29	439.82	448.59	416.10	428.03	440.62	450.10
500	462.93	475.63	488.44	497.33	463.98	476.41	489.26	498.91
600	508.31	521.40	534.38	543.34	509.44	522.20	535.22	544.97
700	550.92	564.28	577.37	586.38	552.11	565.10	578.22	588.04
800	590.75	604.31	617.48	626.53	591.99	605.14	618.34	628.21
900	627.99	641.70	654.92	663.99	629.27	642.54	655.79	665.70
1000	662.85	676.66	689.94	699.02	664.16	677.52	690.80	700.74